ACETYLENE BY ELECTRIC ARC

A report on the feasibility of producing acetylene gas by a high intensity arc process

Clive E. Davies

Department of Chemical Engineering
University of Canterbury
Christchurch
New Zealand

21 December 1978

THE FEASIBILITY OF PRODUCING ACETYLENE GAS BY A HIGH INTENSITY ARC PROCESS

SUMMARY OF RESEARCH AND PRINCIPAL FINDINGS

by

C.E. DAVIES

Department of Chemical Engineering,
University of Canterbury,
Christchurch,
New Zealand

21 December 1978

1. SCOPE OF REPORT

In examining the feasibility of acetylene production from coal by a high intensity arc process, many different aspects of the problem have been investigated. This report briefly notes the work done in different areas, and finally offers an opinion on process feasibility based on the results of this research.

2. PRELIMINARY ECONOMIC APPRAISAL

At the outset of the program a very simple analysis was made to estimate the capital costs and running costs associated with acetylene manufacturing plant, and the ability of proven reserves of coal and gas to supply an acetylene plant producing 25,000 tonnes per year (1). This exercise, though somewhat naive in places, unearthed useful capital cost data, and established that the reserves of Stockton No. 2 (low ash) coal would be sufficient for many years beyond a projected plant life of 20 years. In the same analysis the economics of a small scale plant for the manufacture of welding acetylene were probed and because of encouraging indications, the design of a small plant was assigned as one of the 1978 3rd professional design projects.

The work described above necessarily assumed that the process under development would be technically feasible on a large scale. However the author was very concious of the possibility of technical limitations, and in the practical and theoretical research that followed, sought to place the scale-up of the process on a sound footing.

3. EXTRUSION OF COAL

All previous work at Canterbury University on the manufacture of acetylene from a solid carbon feedstock has been carried out with graphite

anodes. A successful process would require a practical mechanism to feed the coal to the arc, and it was considered that a leading candidate for this would be some form of extruder. The extrusion of coal into a rod can be effected by using a reciprocating ram or by a screw extruder. A project of research into the rheological properties of coal was initiated, and at the same time efforts were made to acquire a screw extruder. Preliminary experiments with a ram extruder were encouraging (2), and a more sophisticated deadweight press was constructed. Control gear was also designed and made up, and the apparatus was developed to working condition. A program of research was outlined and offered as a 3rd professional research project (3). The work is being continued by the same student who has been engaged as a research assistant until the end of February 1979.

Efforts to secure a screw extruder were successful thanks to the generosity of Reese Bros. Ltd. A small injection moulding machine was being scrapped by this company and the screw, barrel, hydraulic motor and several other components were offered to us for use on coal extrusion. A screw extruder was assembled from these parts.

Progress in this area has been slow, mainly because of the demands of other aspects of the project. However, liquid coal has been successfully extruded by the screw extruder, and further runs are planned under the continuing investigation of the rheological properties of coal.

An alternative to the screw extruder is extrusion by reciprocating ram. A short visit was made to the Coal Research Association in September 1977 to examine their reciprocating press (4) but this line of research was not pursued.

4. INVESTIGATIONS OF ANODE PHENOMENA

A comprehensive practical study was made of the behaviour of carbon anodes in the high intensity arc. The main emphasis of the work was on the

collection of data on the ablation rate of the carbon anodes. A report is attached (5).

Possibly the most important result was the enhanced understanding of the arc process afforded by sustained contact with the working system. This led to the development of a mathematical model to describe the carbon vaporisation process, and provided insight into the constraints on scale-up.

5. MATHEMATICAL MODELLING

A mathematical model has been derived to describe the process of ablation of carbon from an anode in a high intensity arc, and this has been shown to be in excellent agreement with experimental data. The behaviour of arc systems when scaled up for use with anodes of larger diameter than previously used was also considered, and it was shown that there are some limits to the extent to which the system can be scaled up. Some of the results are used in the next section where project feasibility is discussed. The modelling work is described in the attached report (6).

6. PROCESS FEASIBILITY

The work carried out in this department over the past ten years has demonstrated that acetylene can be made from graphite anodes, and recent work has shown that it is possible to process coal in a high intensity arc reactor. However, the scale up of the process does not look encouraging. The production of suitable anode material from coal is likely to be difficult and costly, but coal based carbons are marketed, and have a relatively low resistivity (circa 0.007 Ωcm). The manufacture of such anodes is by a complex process involving much heat treatment of the coal feedstock, which is finally extruded into rod form. Some idea of the cost of pretreatment can be gauged from the unit cost of extrusion equipment alone. A price of $45,000 (1977) for a plastics extruder rated at 430 tonnes per year was quoted by a local engineering and importing company.

The design philosophy of a process plant will not be discussed, but would either entail the use of preformed rods or would employ a continuous feeder presumably extruding and heat treating the raw coal feed into the arc.

The theoretical analysis of the behaviour of carbon anodes carrying large currents revealed several points relevant to plant scale up and these are repeated below:

(i) The energy requirement for anodes of zero length for the vaporisation unit mass of carbon, $(SER)_c$, is lowest for anodes of small diameter when the anode is carrying the maximum permissible current, being about 25-30 kWh kg^{-1}.

(ii) For material of specified resistivity and thermal conductivity there is a maximum rate of carbon vaporisation for a specified background temperature†.

(iii) $(SER)_c$ increases as anode diameter is increased, and at the maximum ablation rate is approximately double the minimum value.

As a consequence of the above, the minimum number of producing units for a specified rate of acetylene production is dictated by the maximum ablation rate per unit (and to a lesser extent by carbon conversion). For a plant operating the minimum number of reactors, $(SER)_c$ will be greater than the minimum value. If $(SER)_c$ is kept low by operating with anodes of diameter

---

† In reference 6, a background temperature of 2000 K was used in all calculations, as this was believed to be close to the prevailing wall temperature in the reactor. It would be possible of course to increase this slightly or to lower it, though doing this would have little effect on the discussion of the process feasibility that follows.

smaller than the maximum, unit throughput is reduced, and a number of reactors greater than the minimum is required for the same total production.

We will first consider two simple analyses for a 400 tonne per annum plant producing welding acetylene, as plant costs for this are available.

Dakin and Stevens (7) have designed a 400 tonne per year plant for their 3rd professional design project, but unfortunately the limitations on reactor scale up were not available to them at the time they did their design. Their plant design is still valid however, and the following analyses are based on their costs with revisions to the capital cost of process plant and energy costs being made where necessary. It is assumed that a single reactor and its feed system costs $20,000. In case 1 a plant with the minimum number of reactors is considered, i.e. all reactors operate at their maximum capacity, and in case 2, a plant with reactors operating close to maximum efficiency are considered. Both analyses follow Dakin and Stevens in every respect except for the revised estimates of capital cost and power costs. Dakin and Stevens quote a process equipment cost of $445,704. Included in this cost is $104,416 for coal extrusion equipment, and $20,000 for arc reactors. These costs have been deleted to leave a residual plant cost of $321,288. To this was added a total reactor cost obtained as the product of the number of reactors and unit reactor cost ($20,000). (N.B. The thermal conductivity of coal derived carbons is much lower than for graphite, and reference to equation 16 in reference 6 shows that the permissible current for an anode of specified diameter will be lower than for graphite. We would therefore expect that the maximum ablation rate for a material of specified resistivity but having a thermal conductivity lower than for graphite would be lower than for graphite. This is important as the number of units for the given production rate would be even greater than specified below with consequent increased costs.)

In each analysis, the power dissipated by ohmic heating in the vaporising electrode is included. Electrode length is assumed to be ~15 cm.

Case 1

Production rate of Acetylene	400 tonnes per year
Resistivity of Anode	0.007 Ωcm
Maximum ablation rate (Fig. 13 in reference 6)	1.2 g s^{-1}
Current (Fig. 14 in reference 6)	3500 amps
Anode diameter (Fig. 14 in reference 6)	70 mm
Number of reactors (70% carbon conversion, 8000 h/yr, 3on standby)	20
$(SER)_c$	50 kWh kg^{-1}
Power dissipation by ohmic heating	
33.4 kW per working reactor	561 kW
Power dissipation for carbon vaporisation	3571 kW
Total reactor power dissipation	4132 kW

Cost Estimate

	$
Process plant equipment (including reactors)	721,288
Piping and services	44,600
Instrumentation	47,691
Total Plant	813,579
Lighting (2% Plant)	16,272
Design (10% Plant)	81,358
Civil work	26,899
Land (¼ hectare)	50,000
FIXED CAPITAL	988,108
Working Capital (3 mnths production costs)	368,765
TOTAL CAPITAL	1,356,873

Production Cost Estimate (1 year of 8000 hrs)

		$
Coal @ 520 tonnes @ $40 per tonne		20,800
Hydrogen, 8 tonnes @ $0.115 per tonne		924
Electricity @ $0.03 per kW		
Reactors	4132 kW	
Motors	498 kW	
Lighting	3 kW	
Total	4633 kW	1,111,920
Labour - 3 men per shift @ $7 per man per hour (4 shifts, 12 men)		168,000
Office Staff (15% labour)		25,200
Overheads		
Depreciation (10% fixed capital)		98,811
Maintenance (5% fixed capital)		49,405
		1,475,060

Revenue

Price of Acetylene	$\$4.34\ kg^{-1}$
Cost of bottling	$\$1.40\ kg^{-1}$
Nett value of acetylene	$\$2.94\ kg^{-1}$
Revenue per annum	$1,176,000

CASE 2

Production rate of Acetylene	400 tonnes per year
Resistivity of Anode	0.007 Ωcm
Ablation rate (Fig. 3 in reference 6)	$0.35\ g\ s^{-1}$
Current (eq. 16 in reference 6)	760 amps
Anode diameter (Fig. 18 in reference 6)	~15 mm
Number of reactors	65

(70% carbon conversion, 8000 h/yr, 8 on standby)

$(SER)_c$	30 kWh kg^{-1}
Power dissipation by ohmic heating	
34 kw per working reactor	1938 kW
Power dissipation for carbon vaporisation	2142 kW
Total reactor power dissipation	4080 kW

Cost Estimate

	$
Process plant equipment (including reactors)	1,621,288
Piping and services	44,600
Instrumentation	47,691
Total Plant	1,713,579
Lighting (2% Plant)	34,271
Design (10% Plant)	171,358
Civil work	26,899
Land (¼ hectare)	50,000
FIXED CAPITAL	1,996,107
Working Capital (3 mnths production costs)	403,450
TOTAL CAPITAL	2,399,556

Production Cost Estimate (1 year)

Coal @ 520 tonnes @ $40 per tonne		20,800
Hydrogen (8 tonnes @ $0.115 per tonne)		924
Electricity @ $0.03 per kWh		
Reactors	4080 kW	
Motors	498 kW	
Lighting	3 kW	
Total	4581 kW	1,099,440
Labour - 3 men per shift @ $7 per man per hour (4 shifts, 7 men)		168,000
Office Staff (15% labour)		25,200
Overheads		
Depreciation (10% fixed capital)		199,610
Maintenance (5% fixed capital		99,805
		1,613,799

Revenue

Price of Acetylene	\$4.34 kg^{-1}
Cost of bottling	\$1.40 kg^{-1}
Net value of Acetylene	\$2.94 kg^{-1}
Revenue per annum	\$1,176,000

The foregoing cost estimates dramatically demonstrate the consequences of a high energy consumption and a large number of reactors. In each case, the running costs exceed revenue.

A plant for the manufacture of acetylene for use in PVC production, say 25,000 tonnes per year would require ~1200 reactors to operate as in case 1, and ~3700 as in case 2. The cost of reactors alone could thus exceed \$25 million. At 1976 prices, a complete plant using existing technology was estimated to cost \$25 million.

7. SUMMARY

It has been shown that the high intensity arc process for the manufacture of acetylene from a solid feedstock can only be scaled up to a limited extent, and that the throughput of a reactor operating at maximum capacity would be quite small. Because of this a large number of reactors would be required for the production of acetylene in commercial quantities, and using only the crudest figures for reactor costs, it is clear that economics alone forbid further consideration of this arc process as a candidate for the commercial production of acetylene.

It has not been necessary to discuss the practicability of such plant, but it should be recorded that there are still gross technical problems to be overcome before the laboratory scale plant operated at Canterbury University could be run on a continuous basis under conditions approaching maximum efficiency or maximum output.

8. A NOTE FOR THE FUTURE

In the attached report Abrahamson (8) notes that it may be possible to produce acetylene by reacting hydrogen with solid carbon at temperatures below the sublimation temperature of graphite. He calculates that energy requirements would be low, and infers from his analysis that a single unit of 1 MW capacity would be possible. In that case, the cost estimates of Dakin and Stevens could possibly stand unchanged and a small plant might be a viable proposition.

References

1. Davies, C.E. 1976 "The Capital Cost, Running Costs and Raw Material Consumption of a plant producing 25,000 tonnes/year of Acetylene from Coal or Coal and Methane", Progress report, Dept of Chemical Engineering, University of Canterbury.

2. Davies, C.E., 1977 "An Investigation of the Feasibility of Extruding Stockton No. 2 Coal in a Ram Extruder", Progress report, Dept. of Chemical Engineering, University of Canterbury.

3. Pemberton, S., 1978 "Rheology and Extrusion of Liquid Coal" B.E. Project Report, Dept. of Chemical Engineering, University of Canterbury.

4. Davies, C.E., 1977 "Visit to Coal Research Association 19, 20, 21 Sept. 1977", Visit Summary, Dept. of Chemical Engineering, University of Canterbury.

5. Davies, C.E., and Wiles, P.G., 1978 "The Vaporisation of Carbon in a High Intensity Electric Arc: Part I, Experimental", research report, Dept. of Chemical Engineering, University of Canterbury.

6. Davies, C.E., 1978 "The Vaporisation of Carbon in a High Intensity Arc: Part II, Theoretical", research report, Dept. of Chemical Engineering University of Canterbury.

7. Dakin, L.M. and Stevens, R.B., 1978 "Acetylene from Coal Ex 1 MW Arc Reactor", Engineering Design III (Chemical), Dept. of Chemical Engineering, University of Canterbury.

8. Abrahamson, J., 1978 "Acetylene from N.Z. Coke - Anode via the Canterbury University Electric Arc Process", research note, Dept. of Chemical Engineering, University of Canterbury.

ACETYLENE FROM N.Z. COKE - ANODE VIA THE CANTERBURY UNIVERSITY ELECTRIC ARC PROCESS.

DR. J. ABRAHAMSON,
CHEMICAL ENGINEERING DEPARTMENT,
UNIVERSITY OF CANTERBURY,
DECEMBER, 1978.

ABSTRACT:

The severe limitations of using a coke anode with the electric arc reactor are discussed. The only way to achieve a reasonable size for a single unit is to use a porous electrode, and for a 1 MW unit, 22 kW g^{-1} or 6.1 kWh kg^{-1} would be used for carbon reaction, and a little above this for acetylene production. A new simpler approach, avoiding complicated solids handling, is proposed.

INTRODUCTION:

The major part of the experimental work done with the arc reactor has ablated graphite electrodes in an atmosphere of hydrogen. As has been shown by the report by Dr. C.E. Davies (attached), and a forthcoming publication, the physics of this reaction is now fairly well understood, and we are confident of scaling up results on the graphite electrode to much larger reactors. Dr. Davies correctly takes into account the temperature rise within the cylindrical electrode, and limits the current so that the electrode is not split open by high carbon vapour pressures at the centre. This severely limits the size of electrode and hence reactor, which can be built commercially. Also Dr. Davies has a sound description of the energy cost of carbon vaporisation (the minimum turns out to be double that for the carbide route, based on the acetylene which would be produced).

However, all our thinking on this project has been restricted to evaporation at the tip of the electrode. When we consider using realistic values of thermal and electrical conductivity for coke, as opposed to graphite, two features become important:

(1) Internal heating of the electrode becomes much more important, with more restrictive limits than Dr. Davies gives.

(2) Evaporation from the electrode shank becomes important, and even dominating.

A COKE ANODE:

Below, the properties

density $\rho = 600$ kg m^{-3}

electrical resistivity $\eta = 10^{-4}$ Ω m

thermal conductivity $k = 0.75$ W m^{-1} K^{-1}

will be used for a coke electrode made from extruded coal. (Note our present extruded coal has a density of 700 kg m^{-3}, an electrical conductivity of 10^{-4} Ω m was found with coked coal subjected to anode tip temperatures, and a drop of 50% in thermal conductivity from that at 1300 K to 3000-4000 K, similar to graphite, was assumed. Values of 1.5 W m^{-1} K^{-1} were found for cokes at 1300 K by Terres (1928), reported in "Chemistry of Coal Utilization" Vol.1, p.321, Chapman and Hall, 1945.)

Using these properties, the temperature predicted at the centre of a 45 mm dia. rod carrying 2500 A (C.E. Davies' size at which a maximum allowable ablation rate occurs, for $\eta = 10^{-4}$ Ω m, but for a graphite conductivity) is calculated to be 42000 K! Well before reaching this temperature, the rod will have split. Obviously the maximum distance between surfaces must be much less than 45 mm for a coke carrying appreciable current.

Carbon surfaces can lose energy by radiation, convection and ablation. A study of convection in hydrogen, using some of the early work of Langmuir with tungsten filaments in hydrogen, shows that convection losses can rise to 50% of the radiative losses near 4000 K, mainly because of the chemical-transport-enhanced conductivity of hydrogen. Ablation cooling also increases in importance faster than radiation. One can use this ablation heat sink at the surface to cool the electrode, even if the surface is internal, provided

it is being swept out with hydrogen. Figure 1 shows an electrode with holes along its length, which can be used to control the "internal" temperature of the carbon.

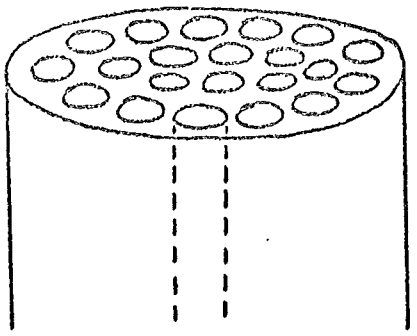

Figure 1. Electrode extruded with holes.

A simplified analysis which gives the important characteristic lengths is as follows:

Consider a slab of carbon 2 ℓ thick, ablating into hydrogen from both surfaces, as in Figure 2. The question to be asked is - what temperature and ablation rate will the surfaces have, when the current density i has been increased to the level where the midpoint is at 4000 K, near the sublimation temperature of cargon? Or conversely, what is the allowed i for a given slab thickness?

Let $\dot{m}_s$ = mass rate of ablation
kg m^{-2} s^{-1}

λ = enthalpy of reaction J g^{-1}

g = energy release rate W m^{-3} = $i^2 \rho$

x = distance through slab

Figure 2. Slab approximation.

Then using the differential conduction equation

$$-k \frac{\delta^2 T}{\delta x^2} = g, \text{ together with limits } k \frac{\delta T}{\delta x}\Big|_{\text{surface}} = \dot{m}_s \lambda$$

$$\text{and } k \frac{\delta T}{\delta x}\Big|_{\text{centre}} = 0,$$

one can derive the energy balance over one half-slab

$$\dot{m}_s \lambda = g\ell = i^2 \rho \ell$$

and $$k(T_{max} - T_s) = \tfrac{1}{2} \dot{m}_s \lambda \ell$$

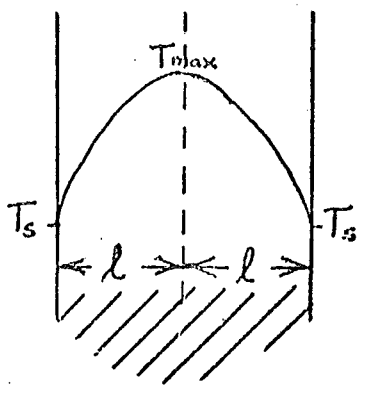

If we now have $\dot{m}_s \lambda$ as a function of temperature, it is an easy matter

to solve for T_s and hence i, for a given ℓ and T_{max}.

Table 1 gives values for $\dot{m}_s$ (from experiment), λ (assuming an equilibrium H/C gas at T_s) and $\dot{m}_s\lambda$. Details will be given in a forthcoming paper.

TABLE 1: Graphite ablation rates (independent of atmospheric pressure or type of gas) and enthalpy of reaction (assuming the formation of an H/C composition in equilibrium with solid carbon) for surface temperature T_s.

T_s/K	$\dot{m}_s$/g m^{-2} s^{-1}	λ/kJ g^{-1}	$\dot{m}_s\lambda$/MW m^{-2}
3200	8	14	.13
3300	17	15	.3
3400	40	15	.6
3500	80	16	1.3
3600	150	17	2.6
3700	300	18	5.4
3800	600	20	12
3900	1200	22	26
4000	2200	23	51

Based on the above ζ, k, the characteristic lengths and maximum current densities are given below as a function of T_s (with T_{max} an arbitrary 3950 K).

T_s/K	ℓ/mm	i/A m^{-2}
3200	8.6	3.9×10^5
3300	3.5	9.0×10^5
3400	1.4	2.1×10^6
3600	0.2	
3800	0.02	

The interesting temperatures are 3200 and 3300 K, as it is feasible to make holes with 17 and 7 mm separation respectively. It would be desirable in a commercial process to make the anode as large as was

manageable, say 100 mm dia, with 80 - 6 mm dia. holes in it. Thus the current for 3200-3300 K will be 2200 A - 5000 A. A 1 m unsupported (vertical) length of anode seems structurally feasible. If we use 5000 A, the base of the anode will operate with internal surfaces at about 3300 K. As the coke ablates, the holes will enalrge, the distance between surfaces will diminish, the current density will increase, and the voltage drop per unit length along the anode will increase. The rate of feed will determine how much carbon is ablated before reaching the arc, and this rate of feed is determined in turn by the energy balance at the tip.

Assuming a constant current intensity along the anode, and operating T_s = 3300 K, a feed of 10 mm s^{-1} will result in a total ablation rate of 33 g s^{-1}, with only 2.5 g s^{-1} of this ablated at the tip. The voltage drop along the anode would be about 100 V, and together with a 60 V arc drop, the energy use is about 22 kJ g^{-1} (allowing for 55 kW radiated from the side). The current density will not be constant, and at this current, the anode will be shorter than 1 m. A single reactor of this size, using 0.8 MW, will be expected to produce 900 tonnes per year of acetylene if used for the normal 8000 hours. The 22 kJ g^{-1} is equivalent to 6.1 kWh kg^{-1}, or about half that used in carbide furnaces.

FUTURE WORK:

The above analysis shows that a single 1 MW arc reactor is possible, and would give an energy use well within the economic range for the supply of acetylene for the Christchurch district, as considered in a 1978 design study done in this department. However, the extrusion of such an anode still relies on careful temperature control and some expensive and complicated machinery. All of the advantages of the porous anode may be obtained by using a simple bed of coke, contained and fed in the right way, and heated by a heavy current, without the presence of an arc at all. Work is in progress along these lines, to devise and operate a carbon evaporator with a much simpler feed.

THE VAPORISATION OF CARBON IN A HIGH INTENSITY ELECTRIC ARC

PART I: EXPERIMENTAL

by

C.E. DAVIES

and

P. WILES

Department of Chemical Engineering,
University of Canterbury,
Christchurch,
New Zealand.

8 December 1978

CONTENTS

ACKNOWLEDGEMENT

We would like to thank the entire technical staff of the Department of Chemical Engineering, as all members have at various times worked on modifications and repairs to the high intensity arc reactor.

Mr Trevor Berry has been of great assistance in photographic experiments, and this is gratefully acknowledged.

SYMBOLS

Symbol	Meaning
E	Arc voltage drop
E_a	Anode voltage drop
f	correction factor
k,k'	calibration constant
I	current
R	radiation intensity
$(SER)_a$	specific energy requirement for acetylene formation
$(SER)_c$	specific energy requirement for carbon vaporisation
T	temperature
ϕ	work function of graphite
λ	wave length

Subscripts and Superscripts

cal	calibration
f	refers to value at the anode face
meas	measured
true	true

LIST OF FIGURES

LIST OF PLATES

Fore more detailed description of plates 7-12, refer to the text of Section 6.

ABSTRACT

A comprehensive study of the high intensity arc has been undertaken. The main emphasis was on the rate of vaporisation of the anode in a D.C. arc. Anodes of several grades of carbon were used including some having a central coal core. The diameter of the anodes in most experiments was 7.94 mm or 9.53 mm, and currents varied between 120 and 400 amps.

A program of experiments was completed on the premises of a local steelmaker, and alternating currents up to 5000 amps were reached with anodes up to 25.4 mm in diameter.

The temperature profile along an anode has been measured, and the temperature of the anode tip found to be ~3950 K.

The cores of the composite graphite/coal anodes were examined by Scanning Electron Microscope, and the electrical resistivity of the core measured. Core resistivity was approximately 0.01 Ω cm.

1. INTRODUCTION

The work described in this report is critical to the development of a process for the production of acetylene gas from a solid carbon feedstock. For the sake of overall clarity the background and incentives for the work are outlined, and a brief description given of the general principles used in acetylene manufacture.

1.1 Background

By virtue of the ease with which it can take part in addition reactions acetylene is a very attractive building block from which many of the vast number of organic chemicals produced by the global chemical industry can be made, but in practice it is not used in large quantities because of its high cost. The most important alternative feedstock is ethylene and though reaction schemes for the production of a given chemical from ethylene are often more complex and difficult than for acetylene, this complexity is offset by the lower cost of the feedstock. Ethylene is produced from oil, but with the continual escalation of oil prices, and the growing awareness of the finite nature of the world's oil reserves, the long-term future of an oil-based chemical industry does not look good. The world's reserves of coal on the other hand, though finite are much more extensive, and a coal based chemical industry will one day become an economic necessity. From the New Zealand point of view, the incentives for utilizing coal as a chemical feedstock are, if anything, greater than for most other countries, and have been extensively and lucidly detailed by Abrahamson and Stott (1), Abrahamson (2), and later Ward (3). Briefly, the case for a coal-based chemical industry in this country is as follows.

New Zealand has no oil reserves, and only relatively small proven reserves of natural gas (4), though there are significant, but NOT large reserves of coal. The major domestic outlet for hydrocarbon based organic chemicals is in plastics, and plastics consumption is rapidly increasing (5). Polyvinyl chloride (PVC) demands particular attention as its monomer, vinyl chloride, is a simple chlorinated acetylene, easily and conveniently made from acetylene gas. Alternative routes to vinyl chloride, e.g. via ethylene, have been developed but do not have the inherent simplicity of the direct route from acetylene. At present nearly all the resins used by the plastics industry in this country are imported, and unless these can be replaced by resins made from indigenous raw materials, demand will only be met at considerable and ever increasing cost in overseas funds.

1.2 Acetylene manufacture

Acetylene is made directly from hydrocarbon feedstocks by a number of similar but distinct processes†. Each process shares two common features, a high temperature and a system for rapidly quenching the reactor product gases. The reason for this is easy to see when Free Energy of Formation is plotted vs Temperature for various hydrocarbon species. For Temperatures greater than 1500 K, acetylene is the most stable species (see Fig. 1), but at the temperatures at which acetylene formation becomes feasible the decomposition reaction is highly favoured as the free energy change for this reaction is negative. Thus, every acetylene manufacturing process must ensure that any acetylene formed is 'frozen' before decomposition can occur. This is done by careful reactor design to control residence time, and by rapidly quenching the product gas when it leaves the reactor.

All direct processes currently in commercial use for acetylene production take gaseous or liquid feedstocks. The feed is vaporised and heated to a temperature above 1500 K and the acetylene produced 'frozen' by rapid quenching.

1.2.1 Acetylene from a solid feedstock

In making acetylene from a solid feedstock, the same approach, viz. the rapid quenching of a gas phase $^{C}/_{H}$ mixture, must be followed. A severe problem immediately becomes apparent, as it is necessary to effect the phase change of the solid carbon feedstock. Volatiles in the feed are readily utilized, but temperatures circa 4000 K are required to vaporise solid carbon.

The high temperatures needed are found in the plasmas provided in electric arcs, and two distinct approaches to the use of arc plasmas in acetylene production from solids have emerged. In so-called "plasmatron" devices, a powdered feedstock is introduced to an arc, hydrogen added if required and the products quenched. An alternative is to utilise the feedstock

---

† The carbide process which uses coal as its feedstock is an indirect route to acetylene in that calcium carbide is first formed, and this is then reacted with water.

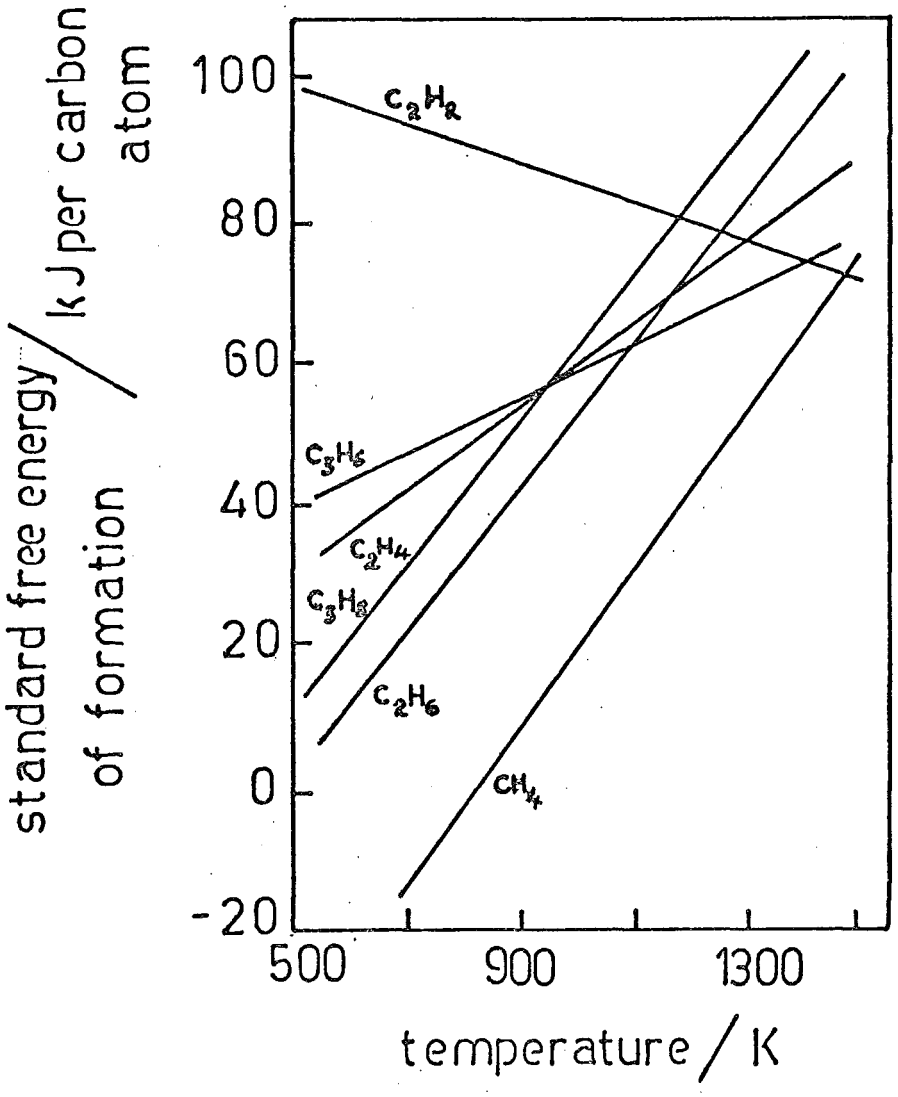

FIG 1: STANDARD FREE ENERGY OF FORMATION OF HYDROCARBONS AS A FUNCTION OF TEMPERATURE

in the form of a conducting rod. This rod is the anode and an arc is struck between this and another electrode. The tip of the anode is vaporised, and the addition of molecular or chemically bound hydrogen, e.g. H_2 gas, natural gas, etc. enables a suitable gas phase $^{C}/_{H}$ mixture to be produced.

1.3 Consumable anode devices

The manufacture of acetylene by vaporising a solid carbon anode in a hydrogen atmosphere and subsequently quenching the gases produced was pioneered by Raymond Baddour of Massachussets Institute of Technology (6)(7) in the early 1960s. He used a 6.35 mm (¼ inch) diameter graphite anode and struck an arc between this and a cylindrical graphite cathode. The gases leaving the arc were sampled by a water cooled probe, and subsequently analysed. Acetylene concentrations of up to 18.6% by volume were reported, but the specific energy requirement $(SER)_a$, i.e. the energy required to make unit mass of acetylene, was substantially higher than that usual in industrial practice (circa 10 kWh/kg), the smallest value obtained being about 66 kWh/kg.

In spite of its high energy consumption, the process was recognised as having potential as a method for the direct conversion of coal to acetylene, and with this in mind, Abrahamson (2), and later Ward (3), caried out experimental investigations of consumable anode arc reactors. Both authors adopted a reactor configuration somewhat different from that used by Baddour, and struck an arc between two opposing cylindrical electrodes housed in a graphite shell. All the gases leaving the arc were quenched, and the acetylene concentration of the quenched products measured. Graphite anodes were used in both studies.

Abrahamson's work was carried out with 3.3 mm diameter anodes at arc powers up to 3 kW, while Ward worked with a larger system, dissipating up to 30 kW in a reactor fed by anodes 7.95 mm in diameter. Some improvement in $(SER)_a$ was observed when the larger reactor was used, as Abrahamson reported a minimum $(SER)_a$ of 130 kWh kg^{-1} while Ward claimed a figure of 45 kWh kg^{-1}. Though the apparent improvement is significant, a reactor producing acetylene at 45 kWh kg^{-1} is unlikely to form the basis of a competitive commercial process.

1.4 Objectives of study

Our knowledge of the behaviour of consumable anode systems is substantial as a result of the work cited above, and the thermodynamics and kinetics of the carbon-hydrogen-hydrocarbon system are fairly well understood (see for

example ref. 8). However, we are not yet in a position to design, scale up or evaluate the potential of a consumable anode process, as vital quantitative information on the interaction of the process variables is lacking.

The direct production of acetylene from a solid carbon feedstock may be thought of as taking place in three steps.

(i) the carbon is vaporised
(ii) carbon vapour and hydrogen are mixed in the reactor and acetylene is formed
(iii) the gases leaving the reactor are quenched to preserve the acetylene.

Thus three distinct sequential operations must be performed, vaporisation, mixing (and reaction) and quenching.

High temperature reactors for acetylene production are used in a number of commercial processes, e.g. Hüls, Hoechst, Wulff, and all employ a quenching system. It is inferred from this, and also our own experience that quench capacity will not be a limiting factor in a process design. For this reason, no further attention will be given to quench design in this research program.

Throughout all stages of this work the design of the high temperature arc reactor has been under constant scrutiny, and it is considered that no real fundamental improvement could be made to the designs pioneered by Abrahamson and Ward.

The vaporisation of the carbon anode is accomplished by the action of the electric arc, and while it appears that the current density at the anode tip is an important variable in the determination of ablation rate, the relationship between the parameters affecting the rate of ablation is not well defined. Since a knowledge and understanding of the ablation process is of vital importance to the design and evaluation of the technical and economic feasibility of the consumable anode process, a study of the vaporisation of the carbon anode has been singled out for particular attention. Thus a program of experiments was designed to supplement previous experience and to attempt to clarify the manner in which anode ablation rate is linked to the operating variables.

1.4.1 Outline of scope of investigation

This study has as its ultimate objective the manufacture of acetylene from coal. Accordingly, attempts were made to examine the behaviour of coal in the high intensity arc by using composite carbon/coal anodes as well as graphite and two other grades of carbon. Several different categories of experiment were performed and these are outlined below.

(i) Composite anodes were made by drilling holes in 7.94 mm carbon rods, and packing them with powdered coal. These were run at fairly low currents ~40 amps, in a small arc reactor prior to the commencement of the work described in (ii).

(ii) Extensive observations and measurements were made of the rate of vaporisation of anodes made of different grades of carbon (including composite graphite/coal anodes) and diameters ranging from 5.08 mm to 9.53 mm. Currents from 120-380 amps were used, and arc power dissipation reached 24 kW. The effect of methane addition to the reactor was investigated, and an attempt was made to improve acetylene yield by adding hydrogen directly to the carbon jet via a hole drilled in the anode.

(iii) Temperature profile along the anode was measured.

(iv) A study of ablation at very high (alternating) currents was undertaken using an electric arc furnace on the premises of a local steel maker.

(v) In a study of the cores taken from the composite graphite/coal anodes, their resistivity was measured, and an examination made of their micro-structure, using a scanning electron microscope.

2. COMPOSITE ANODES AT LOW CURRENT

It was pointed out above that all previous work with consumable anodes has been carried out with graphite. Graphite can be purchased in the form of uniform rods of high conductivity, where as coal in its raw state is an amorphous semi-conductor. Clearly the step from a graphite to a coal feed is a large one and ultimately would involve complex pretreatment of the feedstock to make a rod suitable for the arc reactor.

Attempts have been made to produce carbon rods from coal (9) (10) (11) (12) and work with this objective is continuing (13) (14), but no such rods are at present available. However, it was considered that much valuable information on the behaviour of coal in an electric arc could be obtained from studies with composite anodes, made by packing a hollow carbon rod with powdered coal. The first experiments were carried out in a small arc reactor designed by Wiles (15), for spectrographic studies. The reactor was very simple to operate, and a low current density at the anode tip ensured that vaporisation rates were small, allowing plenty of time for observation of the arc attachment. Relatively short bores which were easy to drill and pack were adequate for most experiments.

2.1 Apparatus

The reaction chamber was a water-cooled brass cylinder mounted with its central axis horixontal. Anode and cathode were located at right angles to each other. The anode was fed axially, by turning a brass screw and the position of the vertical cathode could also be adjusted if required. Quartz observation windows were located in the end and sides of the reactor. The gases produced by the arc left via a duct in the top and gas to provide the desired atmosphere could be admitted through a pipe in the underside of the reactor. A photograph of the reactor is shown in Plate 1.

2.2 Experimental method

Anodes were prepared by drilling a hole of 3.2 mm ($^1/_8$ inch), 4.8 mm ($^3/_{16}$ inch) or 6.35 mm (¼ inch) diameter in the selected carbon rod, and packing this with coal. Small quantities of -72 B.S. mesh Stockton No. 2 coal were introduced to the central hole, and a vacuum applied to settle the powder. The rod was then removed from the vacuum and the base gently tapped against a hard surface. This process was repeated until the central hole was full. Three types of carbon rod were used, all obtained from Union Carbide Inc., U.S.A.: graphite, grade AGSR; carbon-graphite, grade CMG; and an extruded petroleum coke, grade GA. The swelling number of the coal

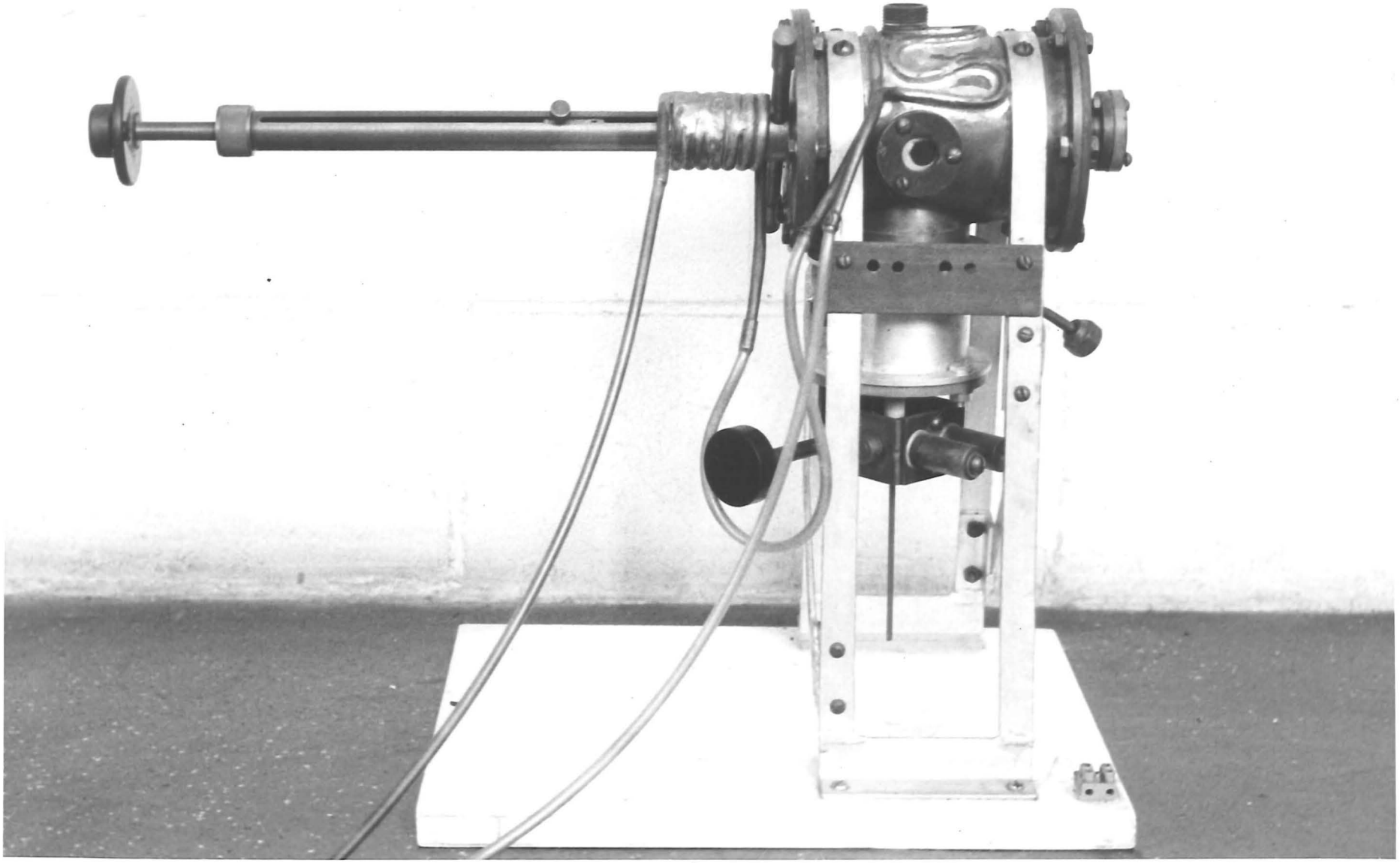

PLATE 1

was 8½-9. The packed anode was placed in the anode holder of the reactor and the gas for the required atmosphere (nitrogen in all experiments) turned on, and the experiment commenced by gently touching the cathode against the anode tip.

2.3 Observations

In a typical experiment, a small portion of the coal core had fallen out of the anode during the setting up, and on start up, the arc attached itself to the outer carbon shell only. When the shell had vaporised sufficiently for the coal core to be presented to the arc, the arc did attach itself to the core. The attachment wandered over the anode tip, and it appeared that the time spent attached to the carbon shell was longer than the ratio of the crossectional areas of core and shell would have suggested. The profile of an anode shows the shell to have been vaporised to a greater extent than the coal core. Anodes were sectioned so that the internal structure could be examined, and typical examples are shown in Plates 2 and 3. In each case, the tip shape with the preferential erosion of the shell can be clearly seen.

One experiment (No. 3) carried out with a rod of extruded petroleum coke having a 3.2 mm ($^1/_8$ inch diameter) central bore packed to a depth of 264 mm, had to be abandoned when the entire anode shattered. The smell of volatile matter was strong, and it was noticed that the anode fragments and brass anode guide were hot. It is thought that ohmic heating prior to the arc caused the release of volatiles from the coal. The bore was plugged by the plastic mass of the coal, and the volatiles could not escape. Pressure built up until the rod shattered.

Observations and experimental conditions are summarised in Table 1.

2.3.1 Appearance of core

After the anodes had been run in the arc, they were sectioned in a Lagun ML3 milling machine using a $^1/_{64}$ inch thick circular cutter. The effects of heat conducted from the anode tip were clearly visible, and extended backwards to the point of entry to the reactor, after which the anode had the benefit of the reactor water cooling system.

PLATE 2

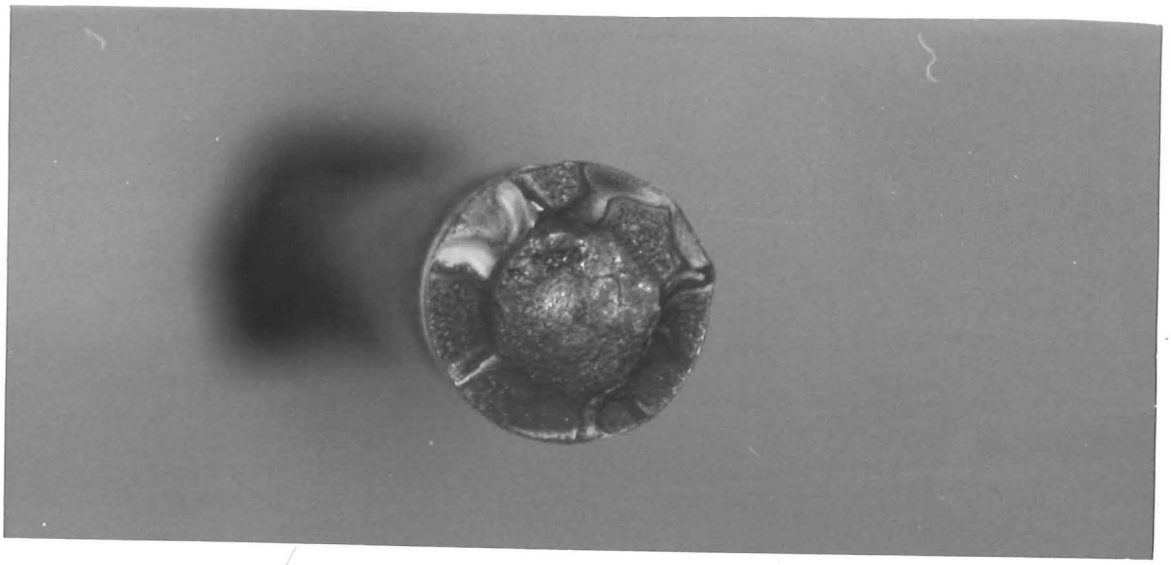

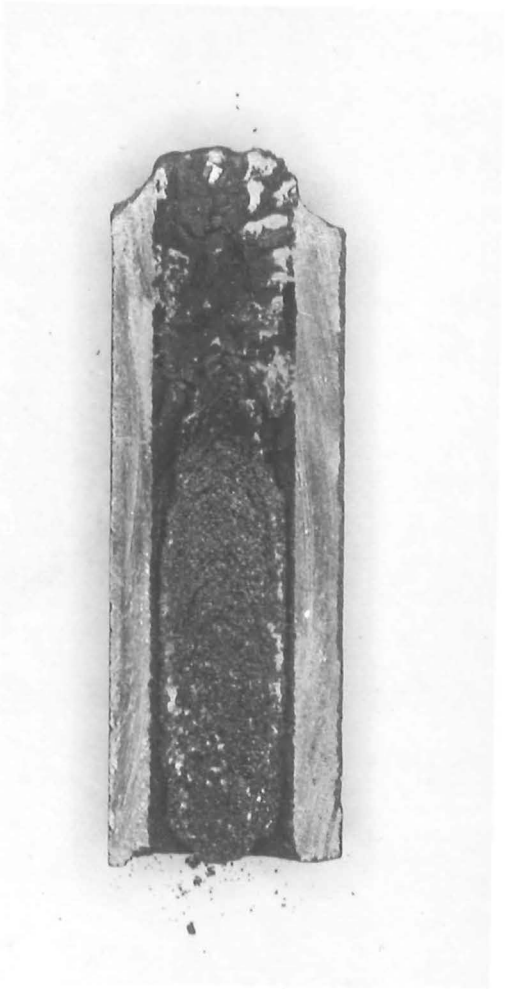

PLATE 3

Table 1: Observation on behaviour of composite anodes in electric arc

In all cases arc voltage approximately 50 V.

Expt. No.	Carbon Grade	Bore Diameter (mm)	Current (Amps)	Observations
1	AGSR	3.2	30 - 40	Coal cokes without swelling past tip and arc readily attaches to coke core, but attachment to outer shell appears to dominate. Shape of tip approximates conical Frustum.
2	CMG	3.2	40+	As above
3	GA	3.2	40	Appearance of arc and attachment same as for AGSR and GA. After 3 minutes rod shattered.
4	AGSR	4.8	30+	Stable arc with good attachment to coal. Shell preferentially ablated.
5	AGSR	6.35	30+	Stable arc, attachment wandering over whole face of anode. Tip flat, but still evidence of preferential erosion of graphite shell.
6	CMG	4.8	30+	Considerable movement over tip, but stable.
7	CMG	6.35	30+	Evidence of coal swelling at start up, but once hot, same dense core as in other experiments. Arc and attachment stable.

Several distinct regions were visible, each associated with an increasing temperature. First of all, the packed powder melted to form a black glassy solid. After this, the volatiles were released, and this region appeared as a fragile frothy char, again black in colour. This was followed by a brittle greyish coke, which was apparently denser than the previous region. Following this and extending to the tip was a dark dense plug. The coked core was not strongly bonded to the carbon shell, and black deposits of 'soot' were observed at the carbon/coke interface. The appearance of the tip suggested that soot had been deposited there as well, and samples examined by scanning electron microscope confirmed this. (See Section 6).

2.4 Summary

The most important results to emerge from this simple study were:-

(i) The coal, in spite of its high swelling number, did not swell past the anode tip.

(ii) The arc readily attached itself to the coke surface.

(iii) The composite anodes "burnt" stably in all experiments.

Thus, certainly at low current, the composite anodes did not exhibit any characteristics which would make their use difficult or impossible, and the program was continued by using similar, but larger anodes ($^3/_8$ inch O.D., $\frac{1}{4}$ inch bore) in the 30 kW reactor designed by Ward. The arc experiment in which the anode shattered drew attention to this potential hazard, and in subsequent experiments with anodes with long bores, holes were drilled radially in the carbon shell to allow volatile matter to escape.

3. VAPORISATION OF CARBON IN THE HIGH INTENSITY ARC

3.1 Previous Work

There is only scanty published information on the rate of vaporisation of carbon electrodes in electric arcs, and the results given by different authors are not at first sight entirely consistent.

3.1.1 Influence of arc parameters

Finkelnburg (16) in his comprehensive work on the high current arc gave some attention to the consumption of electrodes. He established that mass loss from the anode is due to evaporation and found an apparent linear relationship between this and arc wattage. Likewise, Baddour and Iwasyk (6), considering vaporisation in a hydrogen atmosphere, reported a linear variation of the rate of vaporisation with arc wattage and a small dependence on hydrogen flow rate. At constant power, the vaporisation rate of carbon increased as the hydrogen flow rate decreased.

In their studies of the high intensity electric arc, both Abrahamson (2) and Ward (3) examined the relationship between the arc variables, (in their work, current, voltage and hydrogen flow rate), and found that the rate of carbon vaporisation varied with current only. Abrahamson observed a linear dependence with current, while Ward's results were definitely non-linear as ablation rate appeared to increase exponentially with current.

There is an apparent conflict in the published results, in that some authors note that ablation rate varies with arc power, while others record that it varies with arc current. However, Finkelnburg's data were most probably obtained at a constant or nearly constant voltage, and Baddour and Iwasyk report very stable arc voltages for all their experiments. Finkelnburg does not give voltages for his ablation experiments, but does present a characteristic voltage/current curve for the high intensity arc. For currents greater than 80 amps, arc voltage was between 40 and 45 volts for three different types of anode carbon, and over the range 25-100 amps, arc voltage varied only 16%. Baddour and Iwasyk note an average voltage of 50 volts and a variation of only 5 volts from run to run. Baddour and Blanchet (7) found a linear variation of carbon vaporisation rate with power for vaporisation in hydrogen and methane, while at the same time recording significantly fluctuating voltages. There is considerable scatter about their lines of best fit, and the individual voltages and currents are not available, so it is not possible in this case to test whether the plot

could be equally well presented as a function of current. From the above discussion, we can see that the available experimental evidence supports a linear relationship between carbon vaporisation rate and arc current, although the work of Ward does not show this trend. The results of other authors are again discussed in section 3.5.2.

At this point it is significant to note certain quantitative differences between Ward's results and those of the other authors studied, in particular, Abrahamson. Both these authors used equipment of the same type, but of different scale. Abrahamson used anodes 3.3 mm in diameter and achieved ablation rates up to 55 g h^{-1} at a current of 50 amps. Ward used 7.95 mm diameter anodes, and currents up to 220 amps, and reports ablation rates up to 576 g h^{-1} at 220 amps. These results are obviously not directly comparable, but a cautious comparison can be made by expressing vaporisation rate as a mass per unit area per unit time, and current as current density at the anode face. (The reader is advised to read Part II Section 4.1 as it is shown that great caution should be exercised in comparing results obtained for anodes of different diameter.) For 7.95 and 3.3 mm anodes, a difference of ~20% in the ablation rate at a specified current intensity is expected. At 4.4 A mm^{-2} Ward gives carbon vaporisation rates circa 11.6 g h^{-1} mm^{-2} while Abrahamson's curve shows 6.4 g h^{-1} mm^{-2}. This is an enormous discrepancy, and it is shown in section 3.5 that Abrahamson's data are in accord with the findings of other authors. It is clear then that Ward's results must be suspect, both qualitatively and quantitatively, and as it was considered important that the uncertainties surrounding the vaporisation rate of carbon in an electric arc be removed, our research program repeated much of Ward's work.

3.2 Apparatus

All carbon vaporisation experiments were carried out using the electric arc reactor designed by Ward. This consisted of a conical graphite shell 65 mm in diameter and 60 mm high mounted vertically and located in a shallow graphite dish ~30 mm deep. This inner graphite lining was surrounded by alumina insulation to reduce heat loss. The lining and its insulation were contained in a water cooled copper jacket which was flanged to provide access to the reactor interior. The anode was fed vertically through a hole in the reactor floor, and the horizontal cathode was admitted at the junction of the upper and lower parts of the graphite lining. Product gases left via a central hole in the reactor top. Windows in the same place as the cathode allowed observation of the arc. Anodes up to 9.53 mm diameter were

fed by a hydraulically driven piston in a sealed magazine. The cathodes were made of graphite, and designed so that they were cooled by part of the hydrogen flow to the reactor. Hydrogen was also admitted at the anode. The hydrogen flow rate was measured by rotameters. In some experiments the feed magazine was modified to allow hydrogen or methane to be fed up a central hole in the anode. The cooling water flow rate wasmetered and its temperature change measured by thermocouples on the inlet and outlet lines.

Power was supplied by three Phillips welding reactors connected to give an open circuit voltage of 150 volts, and currents in excess of 400 amps. The maximum current for a given experiment was fixed by altering the position of the reactor cores.

The principal features of the arc reactor are shown in Fig. 2, and details of the design and the criteria used for it are given in reference 3.

3.2.1 Preparation of anodes

Graphite anodes were only available in short lengths (30 cm) and it was necessary to join several of these to obtain an anode long enough for an experimental test. The rods were drilled and tapped and screwed together to form a continuous length up to 1.8 m long. In most experiments rods 9.53 mm or 7.94 mm diameter were used, though in some cases the anode tip was turned down on a lathe to 5.08 mm (0.2 inch) or 6.35 mm (¼ inch) for a length of several centimetres. This enabled readings at current intensities higher than was otherwise possible to be obtained.

Composite graphite/coal anodes were prepared from 9.53 mm diameter rods with a 6.35 mm hole drilled centrally down most of their length. Stockton No. 2 coal ground to -72 B.S. mesh (211 μm) was introduced to the hollow rod in small quantities (~1 gm) and the base of the rod tapped gently but firmly about 30 times on a hard surface. Plastic floor tiles gave the most satisfactory core. The density of the core was reproducible to within ±2%, the mean value being 900 kg m^{-3}.

3.2.2 Mass per unit length of anodes

A mean value of the mass per unit length (m.p.l.) of the different anodes used was obtained by measuring the length of a number of rods. The 9.53 mm diameter rods weighed 1.24 g cm^{-1} ± 1.5%, and the 7.94 mm diameter rods 0.796 g cm^{-1} ± 1%. Measurements were made on composite anodes that had passed through the arc, and the m.p.l. found to be 0.85 g cm^{-1}.

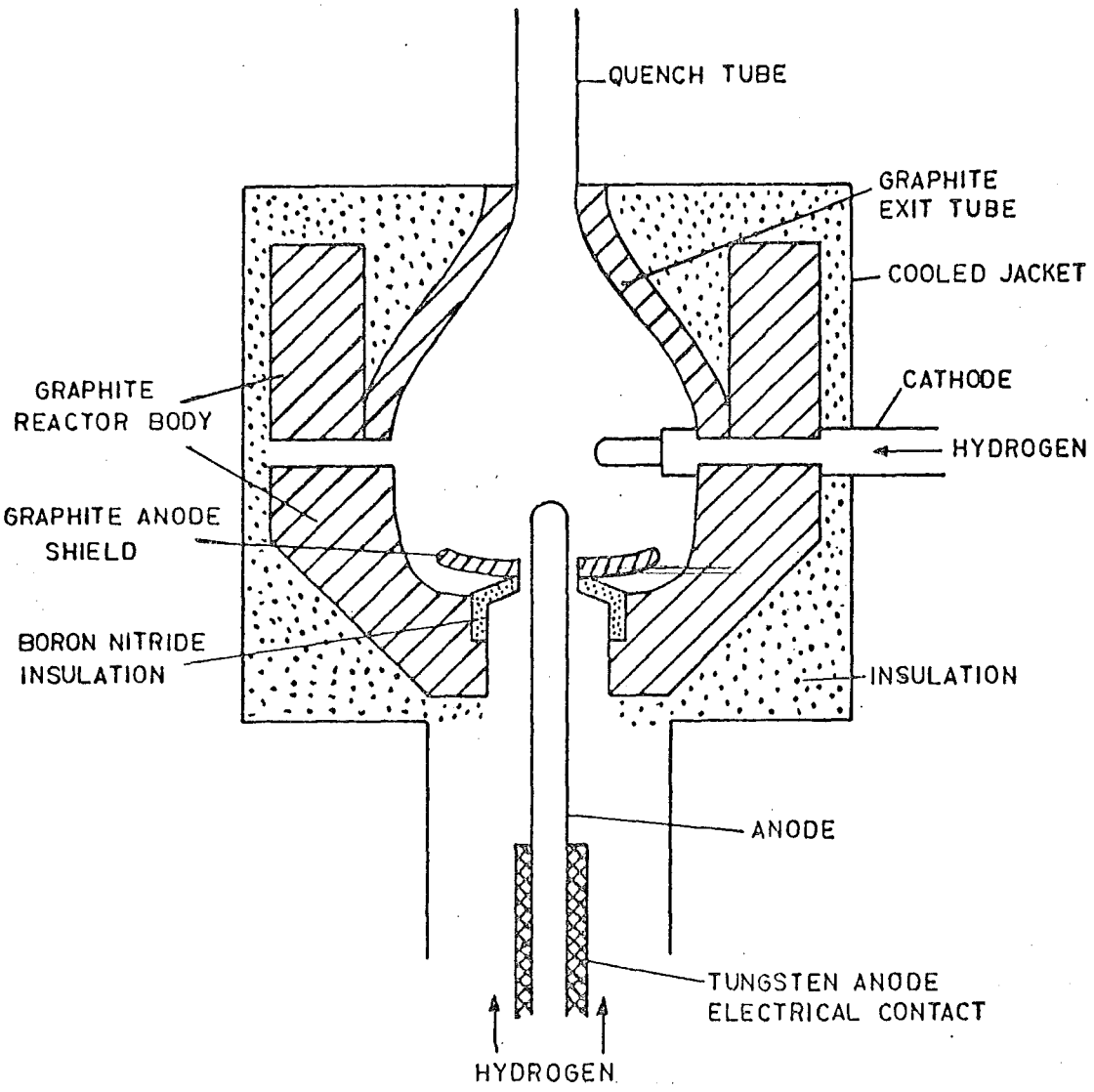

FIG. 2: PRINCIPAL FEATURES OF REACTOR

This figure refers to graphite + coke as the volatiles had all been released by the high temperatures experienced in the arc.

A density of 1670 kg m^{-3} was used to calculate the m.p.l. of the 6.35 mm, 5.08 mm, and annular anodes.

3.3 Experimental method

The rate of carbon vaporisation was measured by a direct method so that some of the errors and uncertainties introduced by calibrations and indirect techniques were avoided. (The current and power records were still potential sources of error).

Shallow grooves were machined at regular intervals (2 cm, 3 cm or 4 cm) in the anodes, and an image of the anode was focussed onto a screen placed at the side of the reactor. The instant at which a groove passed a fixed point on the screen was noted on a chart recorder by the pen of an externally activated event marker. Separate traces were taken of arc current and arc wattage, and acetylene concentration was continuously monitored by infra-red spectrometer.

In a typical test, the anode magazine was loaded, the cathode, anode and the graphite reactor lining weighed, and the reactor assembled. The hydrogen flows to the anode and cathode were set and the maximum current fixed by adjusting the cores of the welding reactor. The experiment was started by gently touching the cathode or the anode, and maintaining the position of the anode tip by varying the oil flow to a hydraulically driven piston that moved the anode forwards. The rate of consumption of the anode was recorded as described above by noting the time taken for (images of) grooves on the anode to pass a fixed point on a screen. Samples of quenched reactor products were taken during each run, and analysed by gas chromatography. A hypodermic syringe was used to withdraw the samples of product gas through a serum cap located in the exhaust line.

After a run, the remainder of the anode, the cathode and the graphite shell were reweighed to find the mass of carbon deposited in the reactor.

3.4 General observations

3.4.1 Graphite anodes of solid crossection

Most runs with solid graphite anodes were stable and generally uneventful. Fluctuations in current and voltage did occur but were small, and it was obvious to the eye without recourse to recorded results that the

vaporisation rate was steady. Stable runs were always associated with a characteristic hum and with experience this alone was sufficient to identify periods of arc stability. On several occasions excessive amounts of carbon were deposited on the cathode, but this only occurred when the cathode projected far into the arc jet.

Observations of the image of the arc focussed onto a screen at the side of the reactor showed that the arc attached to the end face of the anode only†. Both observation during and inspection of an anode after a run suggested that the vaporisation of carbon occurred only from the anode tip, as the anode remained parallel along all of its length. Measurements made with a micrometer screw gauge along the anode right up to the tip confirmed that there was no change in diameter.

3.4.2 Graphite anodes of annular crossection

These runs were characterised by the same phenomena as anodes of solid crossection. It is particularly interesting to note that again, carbon vaporisation took place off the end of the anode only, i.e. no vaporisation occurred from any surface internal or external that was at right angles to the longitudinal axis of the anode. Measured vaporisation rates confirmed the above observation, as the specific vaporisation rate based on the annular area (area of solid carbon) varied with current density in the same way as the anodes of solid crossection.

3.4.3 Composite graphite/coal anodes

Stable runs were achieved without difficulty, and the arc was observed to attach to the coal core without any bias for the graphite shell. This observation is of great importance as it testifies to the technical possibility of running coal derived anodes in an electric arc.

In most experiments, small fragments of the core material were seen to detach from the core, and on a number of occasions, short lengths (up to 4 cm) of the coked core were found on the reactor floor. There was also strong evidence of the thermal softening undergone by the coal as it approached the arc. Devolatalized spirals of frothy coke extruded through the vent holes in the carbon shell by the pressure of the escaping volatiles were also found on the reactor floor after each run.

---

† By taking high speed movies of the arc, Wiles (17) has found that this is not strictly true, as the arc root does fleetingly wander out of the crater at the anode tip, to the side of the anode.

Composite anodes were preceded by anodes of solid graphite. In many experiments, the approach of a composite anode was heralded by a very small increase in the concentration of acetylene (continuously measured by infra-red spectrometer), which was maintained throughout the vaporisation of the coal/graphite anodes.

3.4.4 Carbon anodes: non-graphite

As well as the graphite anodes used in most of our experiments, Union Carbide supplied two other grades of carbon rod. Grade CMG is a dense fine grained extruded carbon-graphite material containing a high percentage of graphite, and grade GA is an ungraphitized extruded petroleum-coke based carbon.

These materials behaved in the same way as graphite in the high current electric arc, though there is evidence of a higher ablation rate for grade GA (see section 3.5.2)

3.4.5 Methane addition

The energy consumption per unit mass of acetylene produced by the arc process is very high, and much has been spoken of the economies that could accrue from the introduction of methane (natural gas) to the reactor or the product stream. The methane would be cracked by energy not available for the vaporisation of carbon. The idea is attractive and some commercial installations employ a liquid hydrocarbon spray to quench reactor product gases, at the same time cracking a portion of the spray to acetylene. The addition of methane to the hot reactor products, viz. a methane quench, would undoubtedly be effective, but it must be noted that the major losses from the system are through the reactor walls. Heat balances have shown that at least 70% of the energy input to the reactor is lost via the reactor walls to the cooling water, while the quench load is only about 15% of the input. In this study, attention was directed to the problem of reducing reactor losses by direct injection of methane, and two types of experiment were performed. Methane was admitted via the cathode, and in later experiments, it was passed up a hole drilled up the centre of the anode. The possibility of passing methane into the reactor through holes in the reactor wall was not investigated. This would have entailed extensive, expensive (and time consuming) modification of the reactor, and the results obtained after preliminary tests were so discouraging that there was little incentive to pursue this line of investigation any further.

Two experiments were conducted. In the first, the methane flowrate was ~3.1 gmin^{-1} and in the second the flowrate was 2.1 g min^{-1}.

At the higher flowrate, the effect of methane addition was immediate and obvious, the anode dimmed and a massive soot deposit was laid down on the cathode. A plug of soot formed in the top of the reactor and the experiment was abandoned. In the other test (methane rate = 2.1 g min^{-1}), the concentration of acetylene in the product gas rose slightly (~4% cf. 3%) and was maintained for a significant period.

A 9.53 mm graphite anode with a 6.35 mm bore was used to investigate the effect of methane addition via the anode. The experiment was first run without any added methane and a total hydrogen flowrate of ~3.75 g min^{-1}. This gave a carbon to hydrogen ratio of ~1.1. The absolute ablation rate was ~4 g min^{-1} which at 100% carbon conversion would produce ~4 g min^{-1} acetylene. Methane was added first at a rate of ~4 g min^{-1} viz. a similar potential acetylene production rate, and later at ~8 g min^{-1}. The hydrogen flowrate was lowered to 2.85 g min^{-1} to keep the C/H ratio down. With no hydrogen addition, an ablation rate of 5.4 - 6 g h^{-1} mm^{-2} was recorded at a current intensity of ~5.2 Amps. Methane at 4.1 g min^{-1} lowered the ablation rate to 3.6 g h^{-1} mm^{-2} at 4.2 A min^{-2} and at 8 g min^{-1} the ablation rate dropped even further. At the end of the experiment (after a period of continuous methane addition for 1 3/4 minutes) the ablation rate and acetylene concentration fell to zero.

The effect of methane addition on ablation rate is also discussed in section 3.5.2 and some experimental results are plotted in Fig. 7.

The observable effects of adding methane via the anode were the same as for cathode addition. The ablation rate fell (the current also dropped), the anode dimmed, and a spectacular soot deposit (which finally halted the experiment) was laid down within the reactor and in the quench tubes. Photographs of this deposit are shown in plate 4.

A gas sample taken when the methane flow was 8.2 g min^{-1} contained C_2H_2, C_2H_4 and CH_4 at 6%, 0.5% and 0.2% by volume. C_2H_6 was negligible. It is interesting to note that this gas composition is typical of a run with no methane addition (see Table 4). Another gas sample taken at the end of an extended (4½ min) period of methane addition was of rather different composition, containing 4.5% C_2H_2, 0.8% C_2H_4, and 3% CH_4.

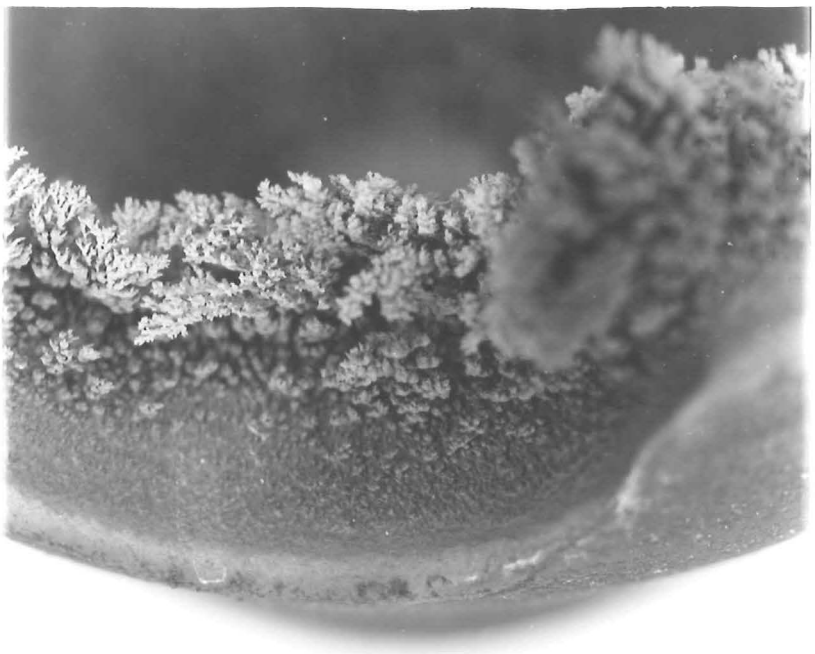

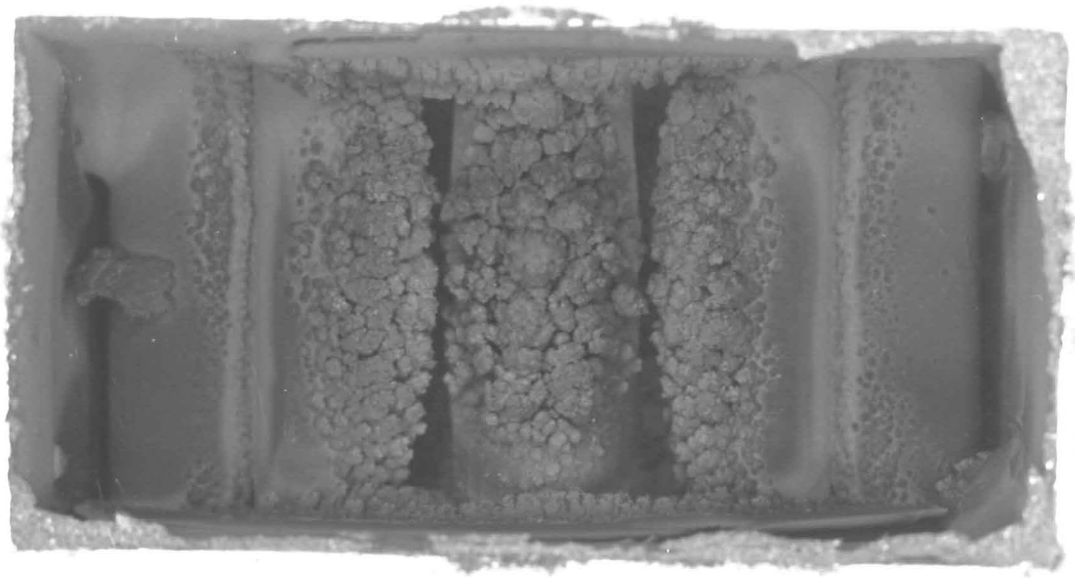

PLATE 4

3.4.6 Hydrogen addition

In most of the work done with Ward's reactor, the hydrogen required for the reaction with carbon to form acetylene, was admitted at the cathode and anode where it also acted as a necessary coolant. Impressive acetylene concentrationsin the product gas have indicated that adequate mixing is occurring in the reactor, but nevertheless, the possibility of obtaining improved yields by introducing hydrogen directly to the carbon vapour, viz. up a hole in the anode, led to several experiments with this objective.

A 9.53 mm diameter anode with a 6.35 mm bore was prepared and ablation rates were measured for several different hydrogen flows. The anode visibly dimmed and the rate of ablation was noticably lower than for no hydrogen flow up the anode centre. The current was also lower than for the period with no hydrogen addition, and it seems that the current:ablation relationship is unaffected. See Section 3.5.2 and Fig. 7. Acetylene concentration as indicated by the infra-red spectrometer actually decreased where hydrogen was passed up the hole in the anode.

3.5 Quantitative results

The major emphasis of this work has been in the measurement of the rate of ablation of carbon anodes. Samples of product gas were also taken in some runs and carbon deposition within the reactor noted so that material balances could be made.

3.5.1 Reduction of data

During the course of one experiment the rate of vaporisation of the anode was measured over several distinct time intervals. It was necessary therefore to find a time averaged value of the current and power during any interval in which measurements were taken. This was done as follows. The current or power trace was photostated and mean values of current or power over intervals of approximately 90 seconds duration were found by cutting and weighing and appropriately scaling the photostat of the chart record. A histogram was then produced showing current and power on the same time base. The required values of current and power were then selected and used in the calculation of the current density and voltage associated with each ablation measurement. Since voltage was not separately measured, it was obtained by dividing arc power by arc current, and ranged from a minimum of about 50 volts to about 100 volts. Arc power varied from about 9 kW - 24 kW. In most runs, both current and power were fairly steady.

A complete summary of all numerical data collected is given in the appendix.

No attempt has been made to present any sort of empirical correlation for ablation rates and arc current, as the complexity of the phenomenom is greater than might first be expected. The model derived in Part II, which appears to provide a very satisfactory quantitative description of the vaporisation process, points out some of the dangers in comparing data from anodes of different diameter.

3.5.2 Ablation rate

Fig. 3 has been prepared to compare the results obtained with a 7.94 mm anodes in this study with the results obtained by Ward using identical anodes. In spite of considerable scatter in both sets of data, the trends are obvious, and it is clear that Ward's results do not agree with the findings of this work. Our results support a linear relationship between current and vaporisation rate for an anode of specified diameter and this is in keeping with theoretical arguments advanced in Part II of this report.

Fig. 3 includes data points for three grades of carbon. Most of the results are for graphite, but ablation values for experiments with grade CMG and grade GA are also shown. It is interesting to note that at a specified current intensity the ablation rate of carbon GA appears to be higher than for graphite or grade CMG, and an explanation for this is given in the supplement to Part II.

Two very good examples of the linearity of ablation rate as a function of current are those due to Abrahamson and Finkelnburg. Both authors have plotted numerous data points over a wide range of current (power in the case of Finkelnburg, but see section 3.1.1) and there is very little scatter.

Fig. 4 is reproduced from ref. 2 and shows ablation rate as a function of current for a 3.3 mm anode.

Finkelnburg expressed the rate of vaporisation of an anode in mm s^{-1} and the original line of best fit is reproduced in Fig. 5 which retains the original units (mm s^{-1}, kW) on the ordinate and abscissa. The diameter of the anode was not specified, but is thought to be 11 mm since anodes of this size are known to have been used by Finkelnburg in some of his experimental work, and also give mass rates of ablation compatible with our experience (note that g s^{-1} = mm s^{-1} x density x crossectional area).

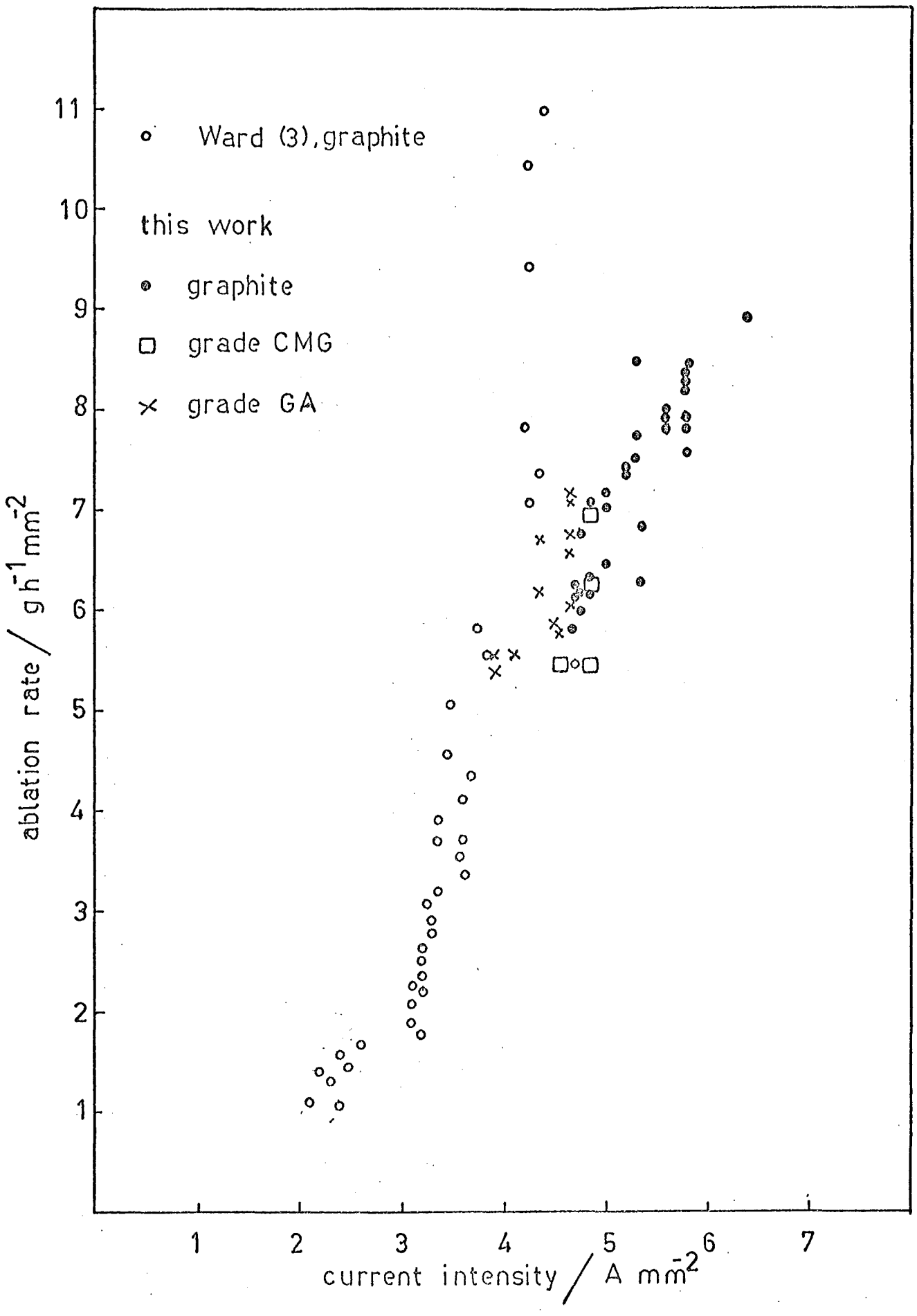

FIG 3: ABLATION RATE AS A FUNCTION OF CURRENT INTENSITY

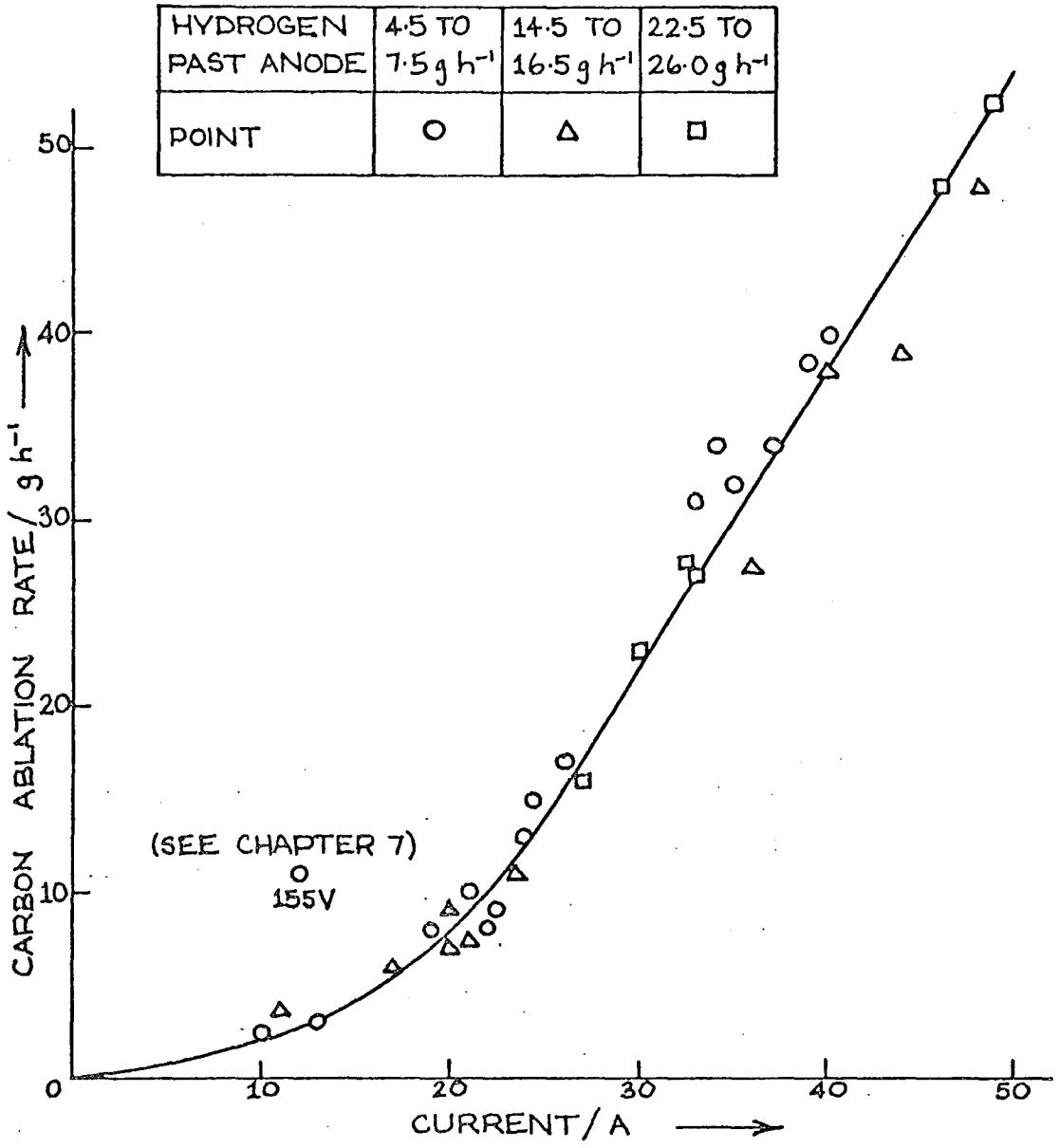

FIG 4: ABLATION RATE FOR A 3.3 MM DIAMETER ANODE

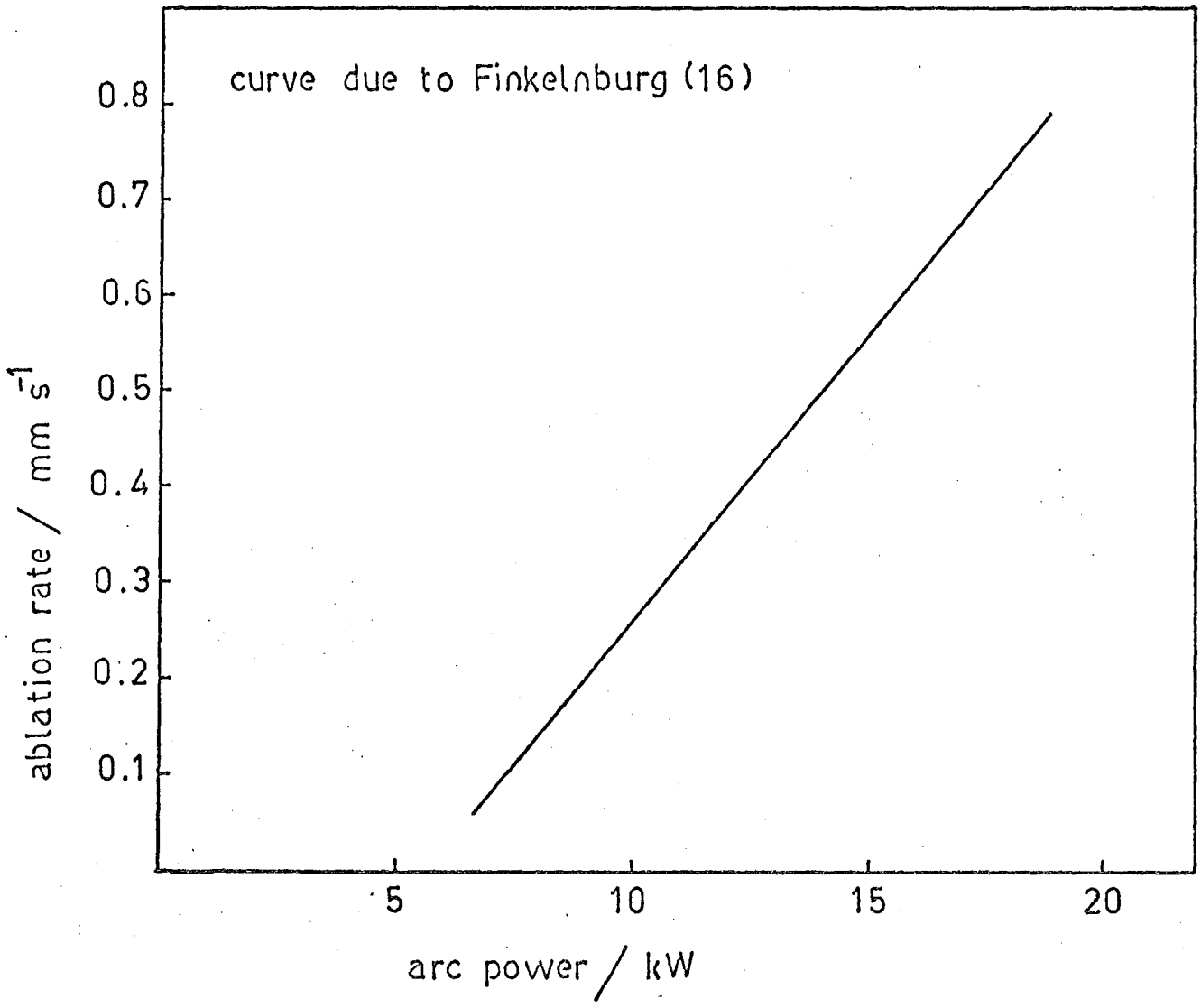

FIG 5: ABLATION RATE AS FUNCTION OF ARC POWER FOR AIR ARC

As noted earlier, comparison of ablation rates of anodes of different diameter can be misleading, because at a specified current intensity the rate of ablation increases slightly with increasing anode diameter. Bearing this in mind, and noting that the expected (theoretical) vaporisation rate for a 3.3 mm anode at a specified current intensity is ~20% smaller than for a 9.53 mm anode (see Part II, Fig. 3), the data from the different sources quoted above, have been plotted on the same graph. Fig. 6 shows, with the exception of Ward's results, these data support each other quantitatively. The results for composite anodes tend to show a higher rate of ablation than solid graphite. No significance is given to this as it can probably be attributed to the tendency of the core to produce solid fragments as well as a carbon vapour. For ablation rates see Appendix.

Fig. 7 shows the ablation rates obtained for annular anodes used in experiments with hydrogen and methane addition. Unfortunately there is very little data available, and no firm conclusions can be drawn from the plot. During the experiment, the ablation rate appeared to fall, but on inspection of the current record, it was apparent that current had also dropped during the periods of gas addition, and it would seem that the current:ablation rate characteristic is unaffected by the addition of hydrogen or methane via a hole in the anode.

3.5.3 Carbon balance

Carbon enters the reactor as a solid cylindrical anode. The tip of the anode is continuously vaporised by the arc, and some of the carbon vapour reacts with hydrogen to form acetylene as well as other hydrocarbons. Most of the unreacted carbon vapour is deposited in the reactor or in the quenching system.

It often proved difficult to get accurate quantitative analyses of the reactor off gases, the major problem being contamination of the sample by air. However, reliable analyses were obtained for 7 experiments and using these a carbon balance was taken over the whole duration of the run which varied from 4 to 11 minutes. Instantaneous gas composition and instantaneous ablation rate were measured, and it was assumed that the instantaneous deposition rate of carbon in the reactor was the same as the (measured) mean value for the whole run.

Table 2 shows the carbon balances for seven experiments.

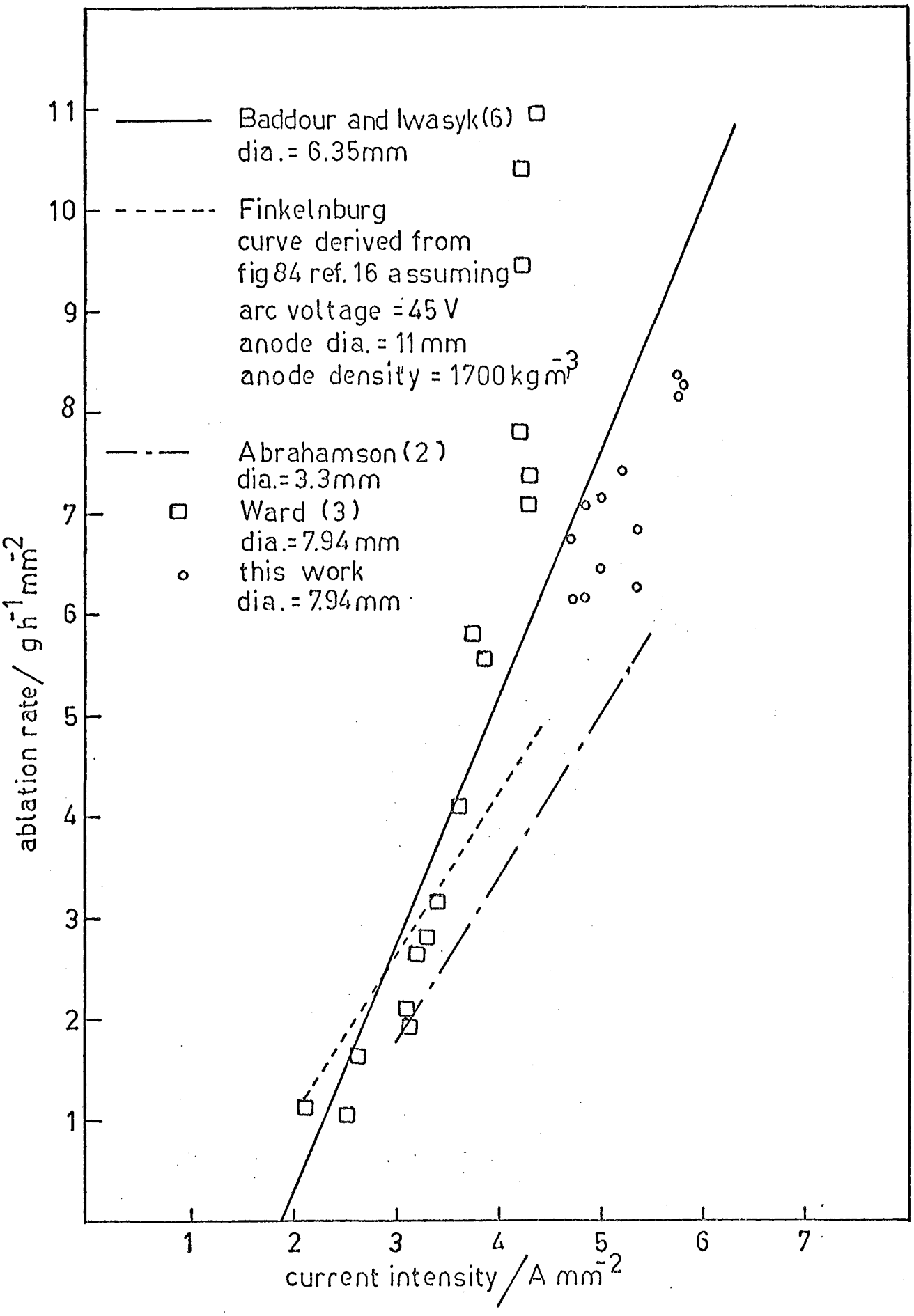

FIG 6: ABLATION RATE AS A FUNCTION OF CURRENT DENSITY

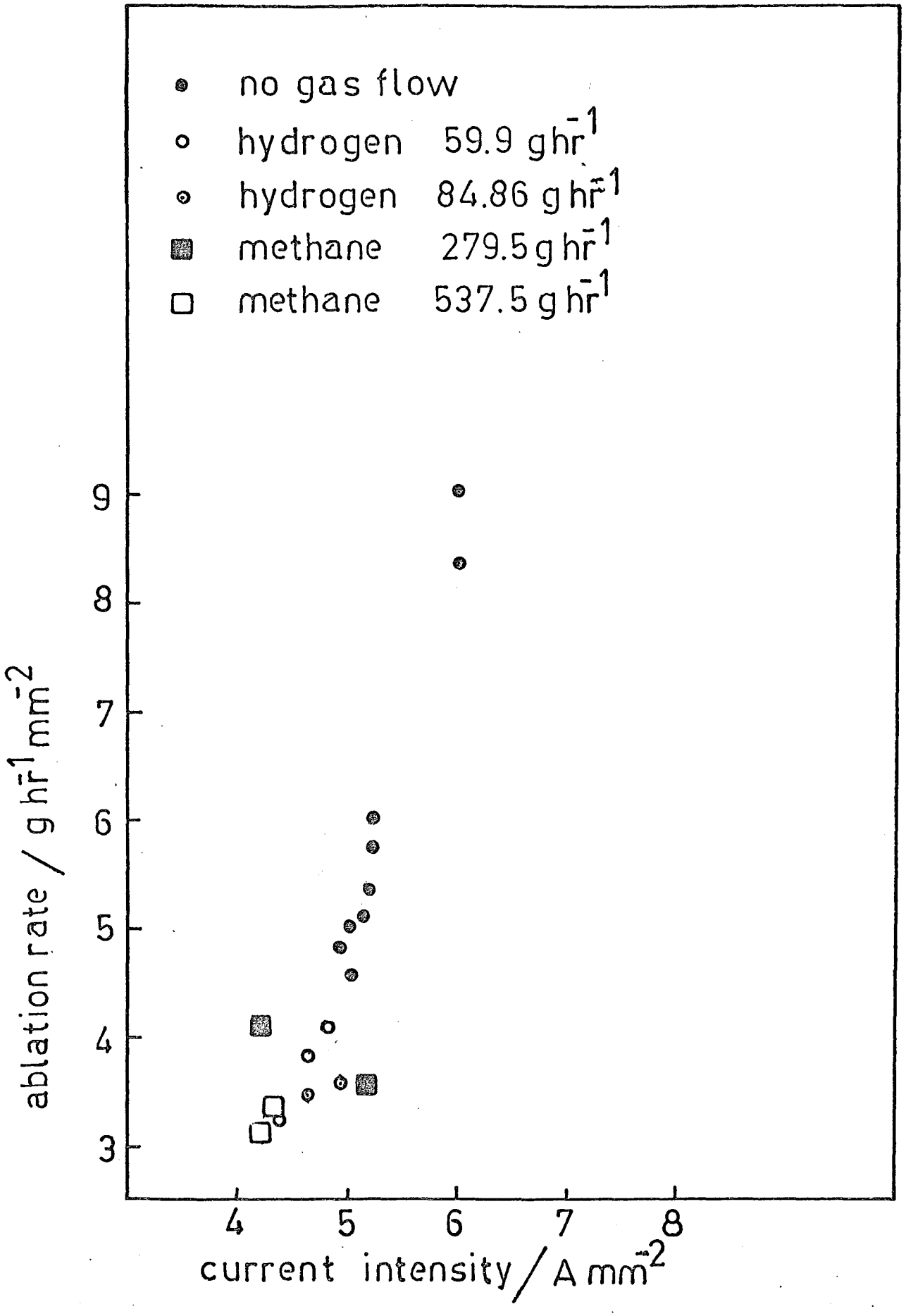

FIG 7: ABLATION RATE OF ANNULAR ANODES (9.53 MM OD, 6.35 MM ID)

Table 2 Carbon Balances

Run No.	Duration of run	Instantaneous anode ablation rate	Mean % of total carbon vaporised deposited in reactor	Rate of carbon deposition	Rate of Carbon loss in gases leaving reactor	% carbon vaporised converted to acetylene	Carbon unaccounted for as % carbon vaporised	Carbon to hydrogen mass ratio based on carbon vaporised	Energy to produce unit mass acetylene $(SER)_a$	Energy to vaporise unit mass of carbon
	Min.	$g\ h^{-1}$	%	$g\ h^{-1}$	$g\ h^{-1}$	%	%	-	$kWh\ kg^{-1}$	
1	6	384	28	107	216	51.5	16	1.7	116	65.1
2	4	419	31	130	282	60.76	1.6	1.86	78.4	57.2
3	4½	343	35	120	207	53.4	4.5	1.55	121	69.97
4	11	292	27	79	211	61.9	0.8	1.45	71.4	47.94
5	9½	240	26	62	206	70	-12	1.08	76.9	58.3
6	8	205	20.5	42	157	70.1	3	0.92	121.9	92.68
7	11	175	27*	47	112	41.6	9	1.6	131.3	79.86

* estimated

Six of the seven balances show a carbon deficit, and as carbon deposited in parts of the system outside the reactor cannot be measured, it is probable that a small quantity of solid carbon is leaving the system in the product gas. Of course the gas analyses are also subject to error and could contribute to the carbon deficit, particularly when even trace quantities of the high hydrocarbon products are overlooked. It is also possible that some of the higher hydrocarbons, even if present in the product gas, are lost by condensation to the walls during sampling.

Table 3 shows the percentage of carbon redeposited within the reactor for a number of runs for which gas analyses were not available. The runs were of longer duration than those considered in table 2, but the percentage of carbon redeposited remains much the same.

Table 3: Redeposition of carbon in reactor; supplementary data

Duration of Run	Mean Percentage of Total Carbon Vaporised Redeposited in Reactor
Min	%
15	25
22	19
23	20
13	28
17	27

The analysis of the reactor product gas and the total hydrogen flow rate to the reactor for each of the 7 carbon balances are given in table 4.

3.5.4 Energy requirements

Energy is an expensive commodity, and the amount of energy required to produce unit mass of acetylene will probably influence the economic viability of the process. The arc process for acetylene manufacture from a solid feedstock uses electrical energy to vaporise the solid (anode) feed, so that the gas phase reactions for acetylene formation can proceed. Unfortunately, only a portion of the energy supplied to the reactor is available for vaporising the anode. There is a voltage drop at the anode, E_a, a drop across the arc, and a voltage drop at the cathode. The sum of these gives the measured arc voltage E, and the product of this and the arc current I, gives the energy supplied to the reactor. The energy transfered to the anode surface by the condensation of electrons, is given by $I(E_a + \phi)$ where

Table 4: Gas Analyses for Carbon Balances

Gas Species/% v/v

Run No.	CH_4	C_2H_2	C_2H_4	C_2H_6	C_3C_4	C_6H_6	CO	CO_2	H_2 by difference	Total hydrogen flow to reactor/g h^{-1}
1	0.16	7.4	0.53	-	0.05	trace	-	trace	91.86	225
2	0.2	6.4	0.66	trace	0.1	-	-	trace	92.64	225
3	~0.15	6.9	0.54	-	~0.15	-	~0.15	-	92.11	222
4	0.28	7.5	0.75	trace	~0.054	-	~0.54	~0.01	90.876	202
5	0.21	6.35	0.69	0.105	-	-	1.06	0.021	92.52	222.6
6	-	5.4	0.43	trace	-	-	0.11	trace	94.06	222.6
7	-	5.6	0.5	-	-	-	-	-	93.9	158.7

ϕ is the work function of the anode material (carbon). $E_a \simeq 11$ volts and $\phi = 4.5$ volts. So, only a fraction of the energy input to the reactor, $\sim(\frac{11 + 4.5}{E})$, can be used to vaporise the anode. For $E \simeq 60V$, approximately 25% of the energy input to the reactor is available for vaporisation of the anode, and some of this will be lost by radiation. Because of this, the specific energy requirement for carbon vaporisation $(SER)_c$ for an electric arc reactor is much greater than the latent heat of vaporisation of carbon (6.47 kWh kg^{-1}).

Not all the carbon vapour is converted to acetylene, as some is deposited in the reactor, and some is converted to methane, ethylene and higher hydrocarbons. The energy requirements for acetylene formation in an electric arc reactor will thus always be higher than for carbon vaporisation. (See table 2).

Fig. 8 is a plot of $(SER)_c$ vs current. Data points for both 7.94 mm and 9.53 mm anodes are shown as only few data are available for 9.53 mm anodes at the higher currents. Note the rapid decrease in $(SER)_c$ as current increases, and the good agreement with Fig. 16 in section 7, Part II. (Strictly speaking, data for anodes of different diameter should not be included on the same plot, because it has been shown that there will be a small difference in the ablation rate at a specified current intensity. See fig. 3, Part II. However, the ablation rate curves for anodes of 9.53 mm and 7.94 mm only differ by about 4%, and as the % fluctuation in arc voltage is much larger than this, the trends illustrated by Fig. 8 will not be noticably influenced).

3.5.5 Carbon conversion

The desired product from the reactor is acetylene, but as seen above, only part of the carbon that is vaporised forms acetylene. Some is deposited in the system as solid carbon, and some appears in other gaseous species such as methane, ethylene and higher hydrocarbons. Ward and Abrahamson have examined carbon conversion over a range of carbon to hydrogen ratios, and the conversions found in this work, though showing considerable scatter, are in keeping with earlier findings. Defined as $\frac{\text{(carbon in acetylene)}}{\text{(carbon vaporised)}}$ carbon conversion is greatest when the carbon to hydrogen ratio (C/H) is close to 1, being about 70%. As C/H increases, conversion falls, and is about 55% at C/H = 1.7.

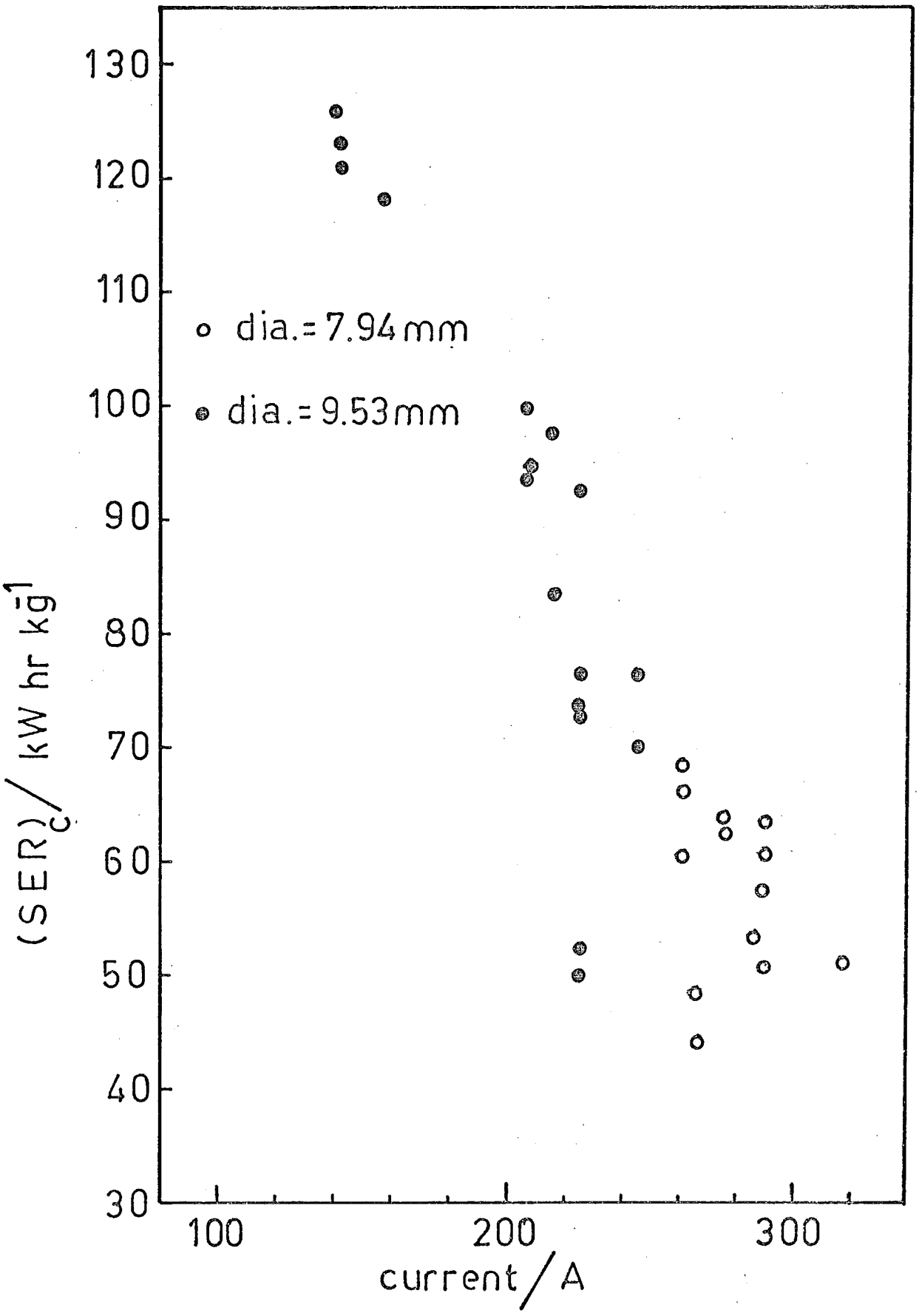

8: SPECIFIC ENERGY REQUIREMENT AS A FUNCTION OF CURRENT

3.5.6 Product gas

In all analyses many different hydrocarbon species were detected, though as expected, the most abundant gas was acetylene. Acetylene was present at concentrations between 5% and 8% by volume, and contained between 80% and 92% of the carbon leaving the reactor in the product gas stream. Ethylene was the next most abundant gas, at about 0.8% by volume in most analyses. Methane was found at about 0.2% by volume. The higher hydrocarbons, though only detected in small volume concentrations are significant as they contain, on a mass basis, as much carbon as the methane fraction.

The ratio of acetylene to methane and ethane is surprisingly low when the analyses given in table 4 are compared with the analysis of the product gas from an arc process cracking a crude oil. In a review (18) of papers presented at the Eighth World Petroleum Congress held in 1971 in Moscow, the analysis was given of the product gas of a process described by representatives of Fabwerke Hoechst A.G. and Chemische Werke Hüls. Acetylene concentration was high at 14.5% by volume, but so were the concentrations of ethylene and methane, at 6.51% and 6.04%. The volume ratio of acetylene to ethylene is thus 2.22, and of acetylene to methane is 2.4. The weight selectivity (conversion to specified product) for the conversion of the feedstock to acetylene and ethylene is given as 56%. In our work, the ratios of acetylene to ethylene and methane respectively are ~8.75 and ~35, and acetylene yields (selectivity) up to 70% are usual.

3.6 Summary

Apart from providing useful data, the program of experiments outlined in the preceeding pages has provided the stimulus and background for the theoretical developments presented in Part II. The appendix lists all experimental data.

As has already been pointed out, no empirical correlations have been produced, because it is believed that a realistic model to describe the process has been developed, and in the light of our current understanding of the system, it is apparent that extrapolation of results is difficult and likely to be unreliable. On the other hand, the model (see Part II) should be entirely satisfactory for engineering purposes, and all indications are that it is capable of an extremely accurate description of the vaporising anode. The principal findings of the program are listed below:

(i) Measurements on the rate of ablation of anodes made of different types of carbon and graphite confirm that it is a linear function of arc current, and provide data that is supported quantitatively by the results of other authors.

(ii) The addition of methane to the reactor in any but the smallest amount causes very heavy deposits of soot to be laid down in the reactor walls and quench tubes.

(iii) The addition of hydrogen directly to the carbon vapour via a hole drilled up the centre of the anode did not increase acetylene concentrations in the product gas.

(iv) Carbon balances have been successfully completed for a number of experiments.

(v) Composite coal/graphite anodes have been run in the reactor, though the coal cores of such anodes have shown a tendency to fragment. Acetylene concentration was very slightly higher than when solid anodes were used.

4. TEMPERATURE PROFILE

In anticipation of the development of a model that would allow the temperature profile along an anode to be computed, measurements were made of the temperature along an anode so that experimental data would be available for comparison with the model.

4.1 Apparatus and method

A white screen was placed in front of a Moll compensated thermopile made by Kipp and Zonen, Delft, Holland, and a small hole made in the screen to allow free passage of radiation to the detector which had an apeture of ~4 mm. The position of the hole was marked by a black cross drawn on the screen. The thermopile and screen were mounted on a bench jack, allowing the thermopile to be raised or lowered relative to the fixed arc reactor. Radiation from the arc was focussed onto the screen, and by manually adjusting the jack, radiation from any part of the anode could be made incident on the detector. The output of the thermopile was fed to a Yokogawa chart recorder. A camera was positioned on a tripod, so that photographs could be taken of the image on the screen, and the flash attachment of the camera was used to trigger an event market on the recorder. The thermopile output was recorded as a continuous trace on the Yokogawa. A photograph of the image of the anode on the screen in front of the thermopile recorded the position of the anode tip relative to the point of measurement, viz. the point marked by the cross, and the event marker indicated the value of the thermopile output at the instant the photograph was taken.

A standard carbon arc (19) was used to calibrate the output of the thermopile. To ensure that the optical system was identical to that used in the main experiment the window from the arc reactor and the focussing lens from the main experiment were also used in the calibration run.

4.2 Results

It was necessary to apply a correction factor to the radiation intensities measured by the thermopile, because a certain proportion of the arc radiation was always cut off by the window in the reactor, and the focussing lens. Data supplied by the manufacturers for the lens (and window) gave a cut off point at a wavelength of 3 μm.

In Principles of Heat Transfer, Kreith (20), there is a plot of the fraction of the total emissive power in the spectral region between $\lambda = 0$

and λ, as a function of λT, and this was used to determine an appropriate correction factor.

The fraction of the total emissive power in the region 0 - λ (in this case 0 - 3 μm) is expressed as a function of λT, so strictly speaking the correct value of the radiation intensity can only be found by iteration. In this work, it was considered that sufficient accuracy could be obtained in one iteration, and a single correction factor was applied to the radiation intensity measured by the thermopile.

Let us call the reading on the chart recorder R (arbitrary units). R_{cal}^{meas} corresponds to a black body temperature of 3792 K, the temperature of the standard arc, so we can write:

$$kT_{cal}^4 = R_{cal}^{true} \doteqdot f_{cal} \times R_{cal}^{meas} \tag{1}$$

$$k \doteqdot \frac{f_{cal} \times R_{cal}^{meas}}{T_{cal}^4} \tag{2}$$

The correction factor f is found using the value of T obtained from the uncorrected value of the radiation intensity measured by the thermopile.

In an iterative calculation the value of T, found from the corrected value of the radiation intensity, can be used to recalculate T until the required degree of convergence is obtained.

Considering the temperature of the anode face:

$$kT_f^4 = R_f^{true} \doteqdot f_f \times R_f^{meas} \tag{3}$$

$$T_f^4 \doteqdot \frac{f_f \times R_f^{meas} T_{cal}^4}{f_{cal} \times R_{cal}^{meas}} \tag{4}$$

$$f_f \doteqdot f_{cal} \tag{5}$$

So,

$$T_f^4 = \frac{R_f^{meas} \times T_4^{cal}}{R_{cal}^{meas}} \tag{6}$$

Temperatures along the anode were found (relative to the tip temperature) as follows.

$$k' T_f^4 = R_f^{true} \doteqdot f_f R_f^{meas} \tag{7}$$

$$k' \doteq \frac{f_f \times R_f^{meas}}{T_f^4} \tag{8}$$

$$k' T^4 = R^{true} = f \times R^{meas} \tag{9}$$

$$T^4 = \frac{f \times R^{meas}}{k'} \tag{10}$$

The corrected temperatures obtained for a 7.94 mm anode, run at 220 amps, are listed in table 5. It is seen that the tip temperature is ~3950 K.

In Part II, section 4.2, the temperature profile along an anode is discussed, and in Fig. 12 Part II, both measured and computed profiles are compared.

Table 5: Temperature Profile on Graphite Anodes
Current = 220 amps

Distance from anode tip mm	Temperature K
0.77	3950
1.15	3777
1.15	3887
1.25	3693
1.35	3920
1.54	3884
1.73	3758
1.83	3831
3.27	3481
3.27	3526
5.00	3184
5.58	3029
5.67	2837
5.96	2792
6.15	2767
7.12	2720
7.79	2561
8.08	2591
10.77	2265

5. VAPORISATION OF GRAPHITE ELECTRODES AT VERY HIGH ALTERNATING CURRENTS

Experiments conducted at the University of Canterbury were limited in their scope. If high current intensities were to be achieved, anodes of small diameter had to be used; and all experiments were confined to absolute values of current less than 400 amps.

Alloy Steel N.Z. Ltd, operates two three-phase arc furnaces, each capable of drawing up to 6000 amps per phase. One of these furnaces is in operation at all times, and the other kept on stand by. The use of the standby furnace was offered to our group for experiments on the vaporisation of carbon electrodes at high currents.

5.1 Experimental method

A piece of old furnace electrode was flattened at one end, and drilled and tapped to receive experimental electrodes, 15.9 mm, 19.05 mm and 25.4 mm (5/8", 3/4", 1") in diameter. Thus mounted, the experimental electrode was positioned beneath one of the furnace electrodes, and the mounting block, viz. the piece of furnace electrode, pinned to the furnace floor by another of the furnace electrodes. The third electrode was not required, and was raised out of the region of the floorof the furnace. In this way, a circuit could be completed between two of the furnace electrodes via an arc stuck to the experimental electrode. A schematic diagram of the circuit is shown in Fig. 9.

An experimental test was started by lowering the furnace electrode until it touched the experimental electrode. An arc was struck, and the operator then endeavoured to maintain a constant current by matching the rate of recession of the experimental electrode to the rate at which the furnace electrode was lowered. At first current was found to fluctuate over wide limits, but after a number of tests, technique was refined and steadier readings were maintained. Instantaneous values of current were noted every five seconds (when conditions permitted) and the duration of the test was measured by stop watch. There was no voltmeter built into the system, but arc voltage drop was measured with our own portable digital voltmeter. Grooves were machined and holes drilled across the diamter at 30 mm intervals in the experimental electrodes to enable the amount of material consumed to be determined. Observations of the experiments were made by John Abrahamson, P. Wiles, and C. Davies, and these and the data collected are presented in the following sections.

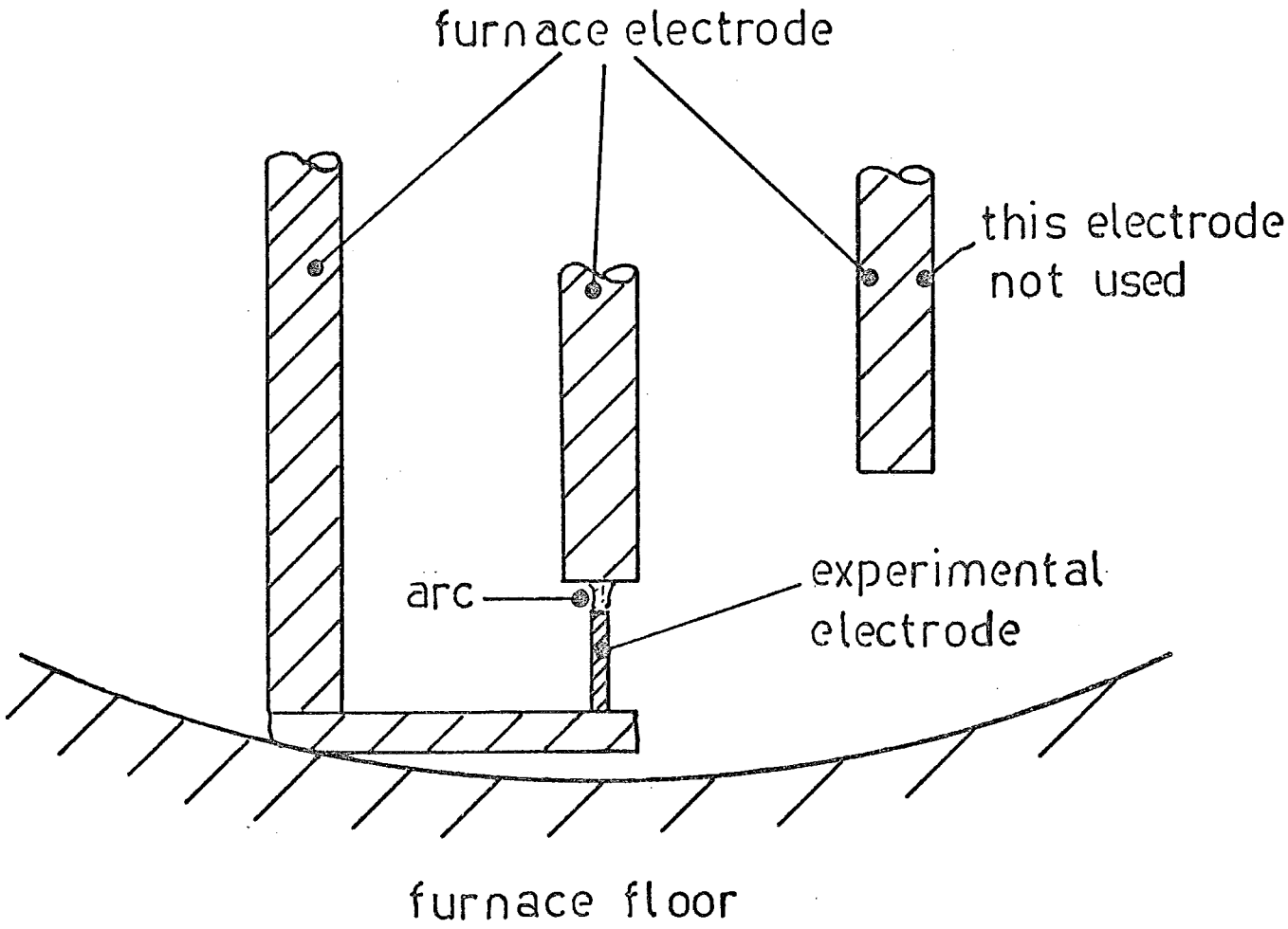

FIG 9: SCHEMATIC DIAGRAM OF EXPERIMENTAL ARRANGEMENT AT ALLOY STEEL LTD

5.2 Observations and Results

Test date - 9.6.78

Diameter	25.4 mm
Test duration	20 s
Current	approx. 4000 amps
Length ablated	approx. 30 mm

Comment: Viewed via a welding visor, the whole electrode glowed "white" hot. The test ended when the electrode abruptly snapped at its base.

Test date - 14.6.78

(1)	Diameter	25.4 mm
	Test duration	45 s
	Current	t = 0 - 10 s I = 4000-5000 amps
		t > 10 s I ≒ 3500 amps
	Length ablated	approx. 60 mm
(2)	Diameter	25.4 mm
	Test duration	25 s
	Current	approx. 5000 amps

Comment: Electrode white hot and clouds of carbon observed round it.

(3)	Diameter	19.05 mm

Comment: Electrode broke immediately circuit was completed.

(4)	Diameter	15.875 mm
	Test duration	9.2 s
	Current	2000 amps
	Length ablated	approx. 15 mm
(5)	Diameter	15.875 mm
	Test duration	105
	Current	3500 amps falling to
		2000 amps after 7 s
(6)	Diameter	15.875 mm

Comment: 4 short 'burns' of approximately 1½ second duration each, caused fragments to fly off the anode.

Test date - 16.6.78

(1)	Diameter	25.4 mm					
	Test duration	approx. 20 s					
	Current	t/s	0	5	10	15	~20
		I/amp	5500	5100	4800	4500	?
	Length ablated	approx. 55 mm					

Comment: Test stopped by violent explosion. Pieces of the white hot anode were hurled 15 yards and fused the foundry sand on landing. Examination of the pieces showed that material was missing from the centre of the electrode, apparently vaporised. A photograph of the fragments is shown in plate 5. A reading by optical pyrometer gave the surface temperature of the electrode as well in excess of 3000 K prior to the explosion.

(2)	Diameter	25.4 mm	
	Test duration	82 s	
	Current	t = 0	I ≒ 5000 amps
		5s < t < 20 s	I ≒ 3000 amps
		t = 25 s	I ≒ 3400 amps
		t > 30 s	I ≒ 3000 amps
	Length ablated	approx. 60 mm	

Comment: Test very stable.

(3)	Diameter	25.4 mm
	Test duration	55 s
	Current	almost constant at 4000 amps
	Voltage	100 volts
	Length ablated	approx. 150 mm
(4)	Diameter	19.05 mm
	Test duration	23 s
	Current	almost constant at 3200 amps
	Length ablated	approx. 20 mm

Comment: Violent explosion split anode down middle and halted test. A hole was observed in the furnace electrode showing that this too had been vaporising in this test

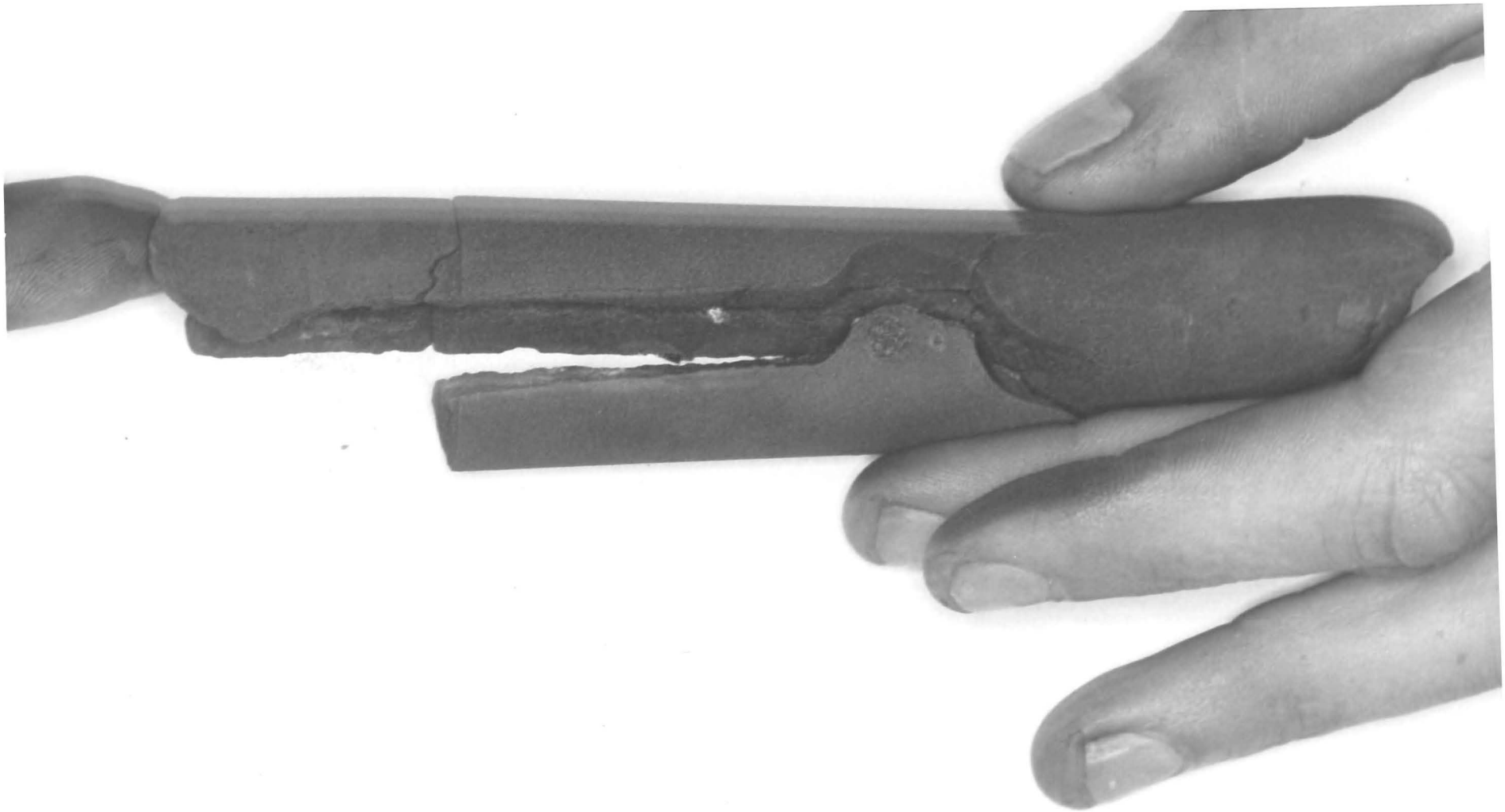

PLATE 5

5.3 Discussion

The accuracy of the current record and the uncertainties surrounding the actual amount of material vaporised combine to devalue the usefulness of the ablation rates that can be computed from the results presented above. It is encouraging to note however, that the apparent ablation rates are of the expected order. For instance, for experiment 3 of 16.6.78, ablation is approximately 16.4 g h^{-1} mm^{-2} at a current density of 7.9 A mm^{-2}, which is close to the value of 11-13 g h^{-1} mm^{-2} expected from extrapolation of results obtained on 7.94 mm electrodes with direct current. Experiment 2 of 16.6.78 gave an ablation rate of approximately 4.4 g h^{-1} mm^{-2} at a current density of 5.9 A mm^{-2}, while the value expected for a 7.94 mm electrode at the same direct current intensity is about 8 g h^{-1} mm^{-2}.

Rather more interesting than the ablation rate measurements were the dramatic demonstrations of the effects of ohmic heating at high current. The electrodes became white hot, and after sustained values of high current, exploded. The shattering of the electrode, and loss of material from the anode centre is the direct result of a radial temperature gradient, the temperature at the electrode centre, being greater than at the surface. If the current is sufficiently high, ohmic heating raises the electrode to the sublimation temperature of graphite, which is first reached at its centre. Vaporisation into the pores ensues, and where sufficient pressure builds up, the electrode explodes. This phenomenon is discussed in more detail in Part II, section 5.

6. AN INVESTIGATION OF THE CORES OF THE COMPOSITE COAL/GRAPHITE ANODES

A number of composite anodes were sectioned longitudinally with a 1/64 inch circular cutter in a Lagun ML3 milling machine, and the cores investigated. Visual observations were recorded, and electron micrographic examination was made of samples removed at different distances from the anode tip. Measurements of electrical resistivity were also made on a number of cores extracted intact from the graphite shell.

6.1 Appearance of Core

When anodes were sectioned longitudinally, the gradual metamorphosis of the coal from a packed powder to a hard coke could be observed, and several seemingly distinct regions could be identified.

The effects of exposure to high temperatures extended to a distance about 80 mm back from the tip, and at this point the closely packed powder of the unheated anode gave way to a shiny fused solid. Stockton No. 2 coal is known to exhibit plasticity when heated, first softening at about 370 K; the coal begins to decompose at ~400 K. Closer to the tip, bubbles were apparent in the solid black coal mass which became more and more frothy, and silver grey in colour. The core became brittle, and was very fragile, and showed several cracks across its diameter. Nearer the tip, the core was stronger, and its colour became a dark grey. Black soot deposits were observed at the graphite/core interface. The central portions of the core appeared less dense than the outside, and this was more closely seen on examination of plugs of core material that had been sectioned across the diameter. Two regions were visible; an inner area about 3 mm in diameter was distinct from an outer annulus. The inner region was fragile, and could be easily removed by a small twist drill. The outer annulus was relatively hard. Plate 6 is a photograph of a sectioned anode.

6.2 Electron micrographs

Two different cores were examined and proved to have essentially the same microstructure. A trend, apparent to the unaided eye, for a grouping of larger pores at the core centre was confirmed, and two unusual features were noted among the cells of the honeycomb structure that comprised the core. Encrustations identified as soot growths were observed coating many of the smooth cell surfaces, and a number of long regular smooth surfaced whiskers were found at seemingly random locations near the core tip.

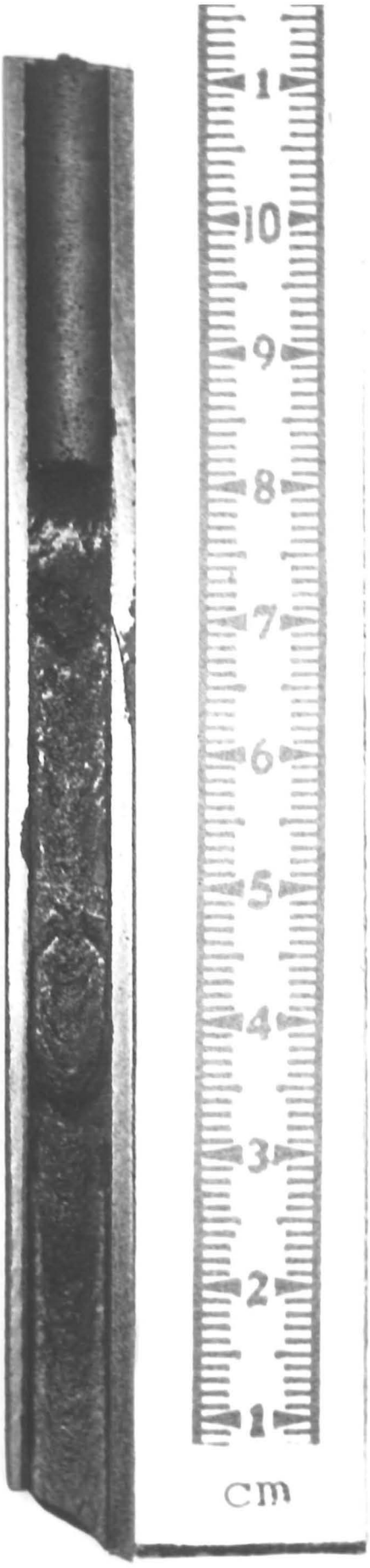

PLATE 6

Fig. 10 shows schematically the regions of the core from which samples were taken, and Table 6 gives the magnification of the photographs of the core samples which are presented as plates 7 - 12.

Table 6: Magnification of Plates

Plate 7	Magnification
7a	55
7b	550
7c	25
7d	21800
Plate 8	
8a	4500
8b	370
8c	25
8d	370
Plate 9	
9a	1200
9b	2000
9c	11000
9d	7900
Plate 10	
10a	1700
10b	17
10c	25
10d	4500
Plate 11	
11a	17
11b	550
11c	550
11d	550
Plate 12	
12a	17
12b	5500
12c	550
12d	550

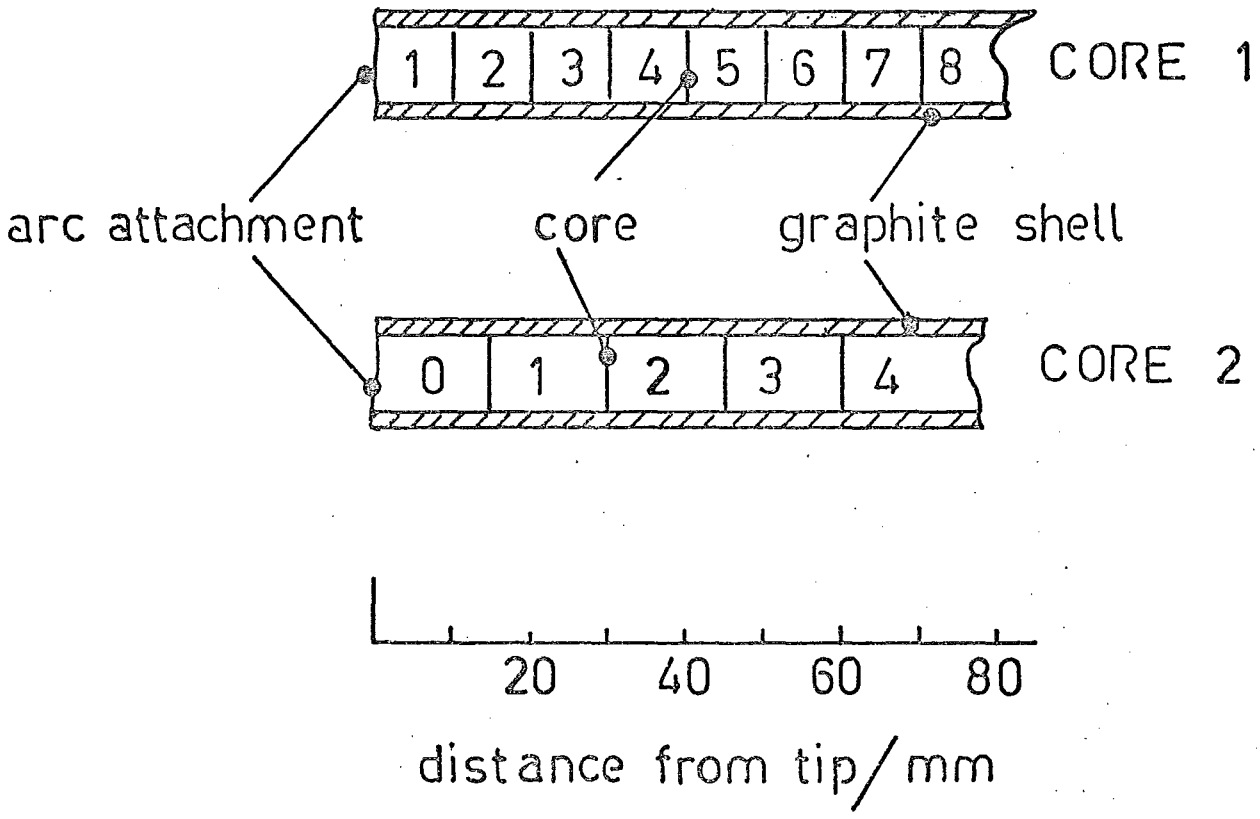

FIG 10: DIAGRAM TO SHOW LOCATION OF CORE SAMPLES RELATIVE TO ANODE TIP

6.2.1 Core No. 1

Sample 1: Plate 7a shows the surface of the graphite casing to which the arc had been attached. There are no unusual features, and the crystallites of graphite are clearly visible. The same surface is shown at higher magnification in plate 7b.

Sample 2: This was photographed end on, and is the part of the tip of the coal core to which the arc had attached. Plate 7c shows the porous nature of the core with pore size greater at the centre (lower part of the photograph), than at the outside. A distinct radial crack is also visible seemingly separating the regions of high and lower porosity. Examination of the tip at intermediate and high magnifications revealed several fibres. In some cases these occurred singly, though clusters of several fibres together were also observed. Plate 7a and plate 8a show single fibres that have a very large length to diameter ratio and a very regular smooth surface over most of their length. The fibre in plate 7d exhibits a 'green twig' fracture, and in spite of this must be quite flexible to exhibit the degree of curvature followed by the unbroken portion. The fibre in plate 8a abruptly changes diameter at each end, to much smaller, but apparently constant dimensions. Plate 8b shows part of the inside of the crack visible in plate 7c. The surface of the cells is not smooth but is covered with what seems to be a light encrustation regularly laid down over most of the area visible in the photograph.

Sample 3: This was mounted so that an end on view could be obtained of a piece of region 2 core material, which had been broken rather than cut.

Plate 8c clearly shows the porous structure with larger pores visible towards the centre. A well defined radial crack effectively delineates the central region from the outer annulus. The smooth surface of the cells is shown in plate 8d and at higher magnification in plate 9a. In the course of exploratory examination of the specimen, numerous areas covered with the light matted encrustations previously seen in plate 8b were identified. At high magnifications these were seen to consist of small clusters of small spheres which tended to link together in small chains. Plate 9b, 9c, 9d, 10a show such encrustations at different magnifications.

Sample 4: Plate 10b is a photograph of a longitudinal section of core, and contrasts the large pores observed for the central region with the smaller pores encountered at the edge of the coal core. Also visible are

'parabolic' curves formed when the broken edges of the pores are connected. These could be seen quite clearly by unaided eye, and are also visible in plate 3 and plate 6.

Sample 5: In region 4 there was a crack, and the opposing surfaces opened by this crack appeared to be covered with deposits of soot, i.e. a loose black encrustation. Plate 10c is a general view at low magnification of an inner surface of the crack, and plate 10d shows one of the soot clusters at high magnification. The structural form of the encrustation is the same as the encrustations examined on sample 3 (see plate 9b). The same structure was encountered again when core number 2 was examined, and again sooty growths visible to the eye were found to be composed of clusters and chains of small spheres.

Sample 7: This sample shows the transition from powder to frothy coal mass via an apparently homogeneous fused solid. In plate 11a all three areas are clearly identified. At the top of the photograph is the fused powder with no bubbles visible and a smooth shiny surface. Bubbles begin to appear in the central position of the photograph (especially towards the left), and at the bottom, fairly large pores have been formed. At slightly higher magnification, plate 11b shows the bubble free fused mass, plate 11c shows the beginnings of pore-growth, and in plate 11d, a number of well developed pores have appeared.

6.2.2 Core No. 2

Examination of this core did not reveal any structural features not previously observed in the study of core 1, but did show the presence of fibres and 'soot' encrustations of the same type as previously identified.

Sample 1: This is a piece of the graphite shell on which a black 'sooty' deposit can be seen with the unaided eye. Plate 12a is a low magnification general view of the sample, and plate 12b shows the black deposits to have the same structure as the encrustations seen in core 1.

Sample 2: This piece of core was taken from region 1 about 15 mm from the anode tip. Plate 12c shows in the same photograph, fibres, 'soot' encrustations, and pores. Plate 12d shows a group of fibres in which several very fine whiskers can be observed. Also visible is a 'soot' cluster.

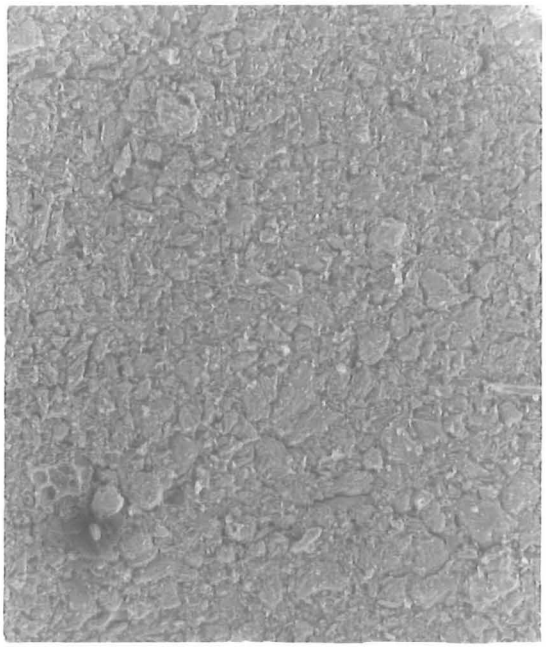

a

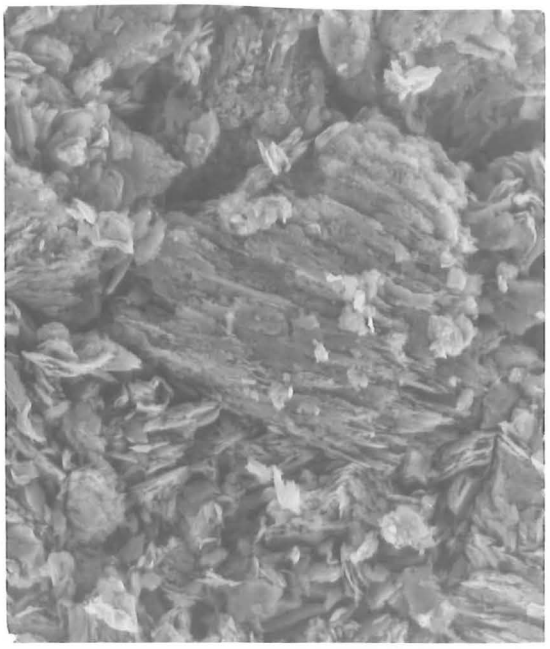

b

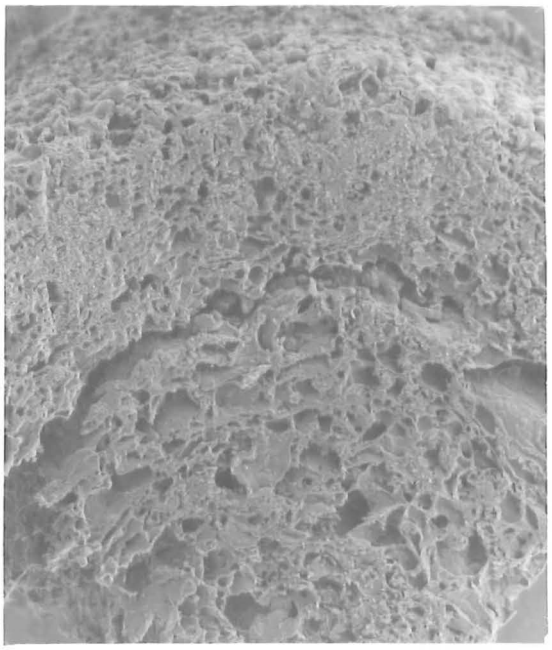

c

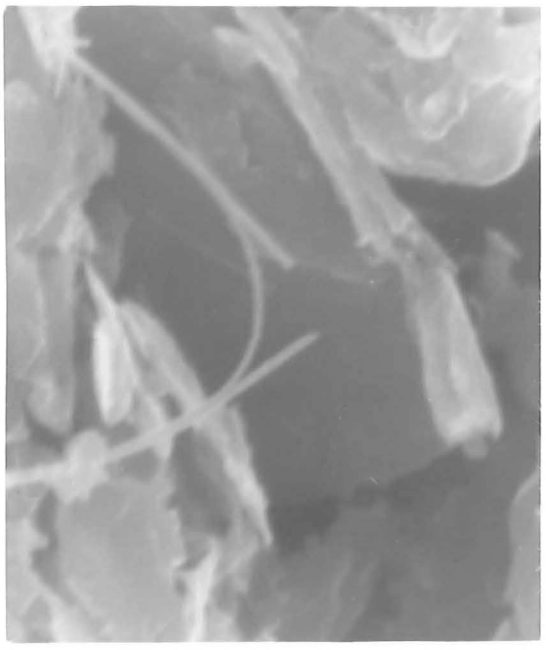

d

PLATE 7

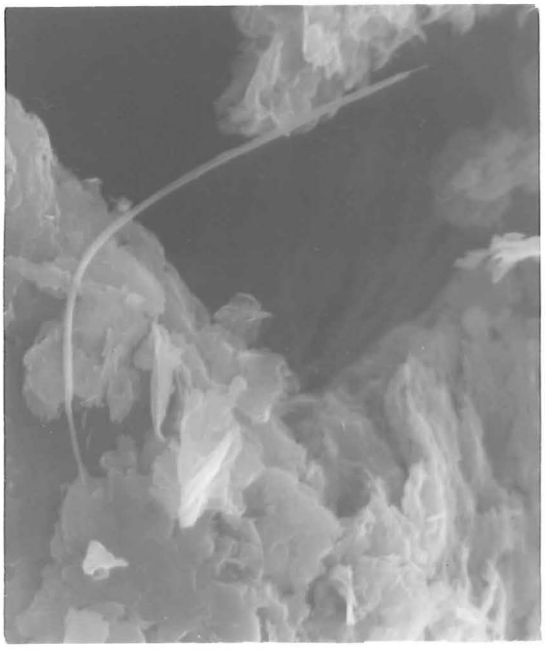

a

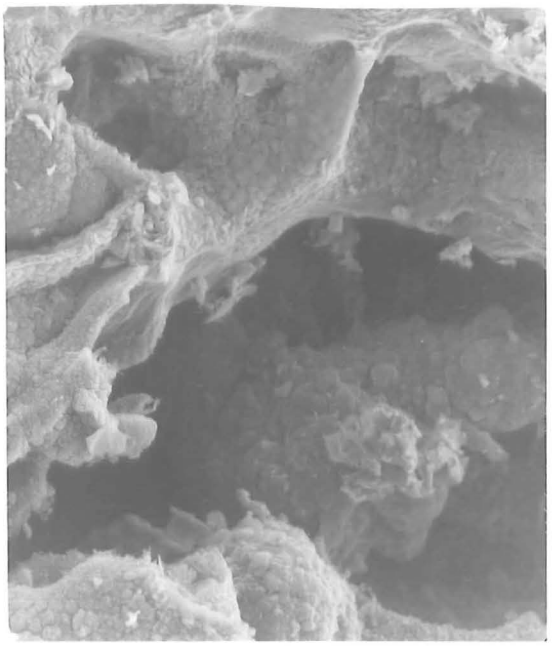

b

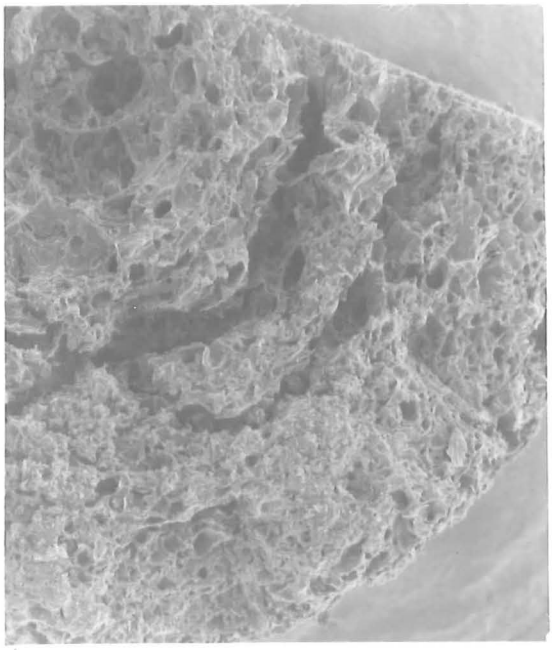

c

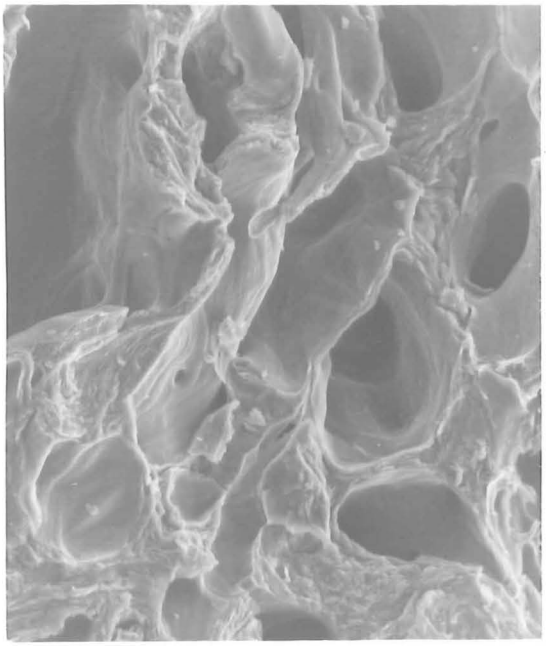

d

PLATE 8

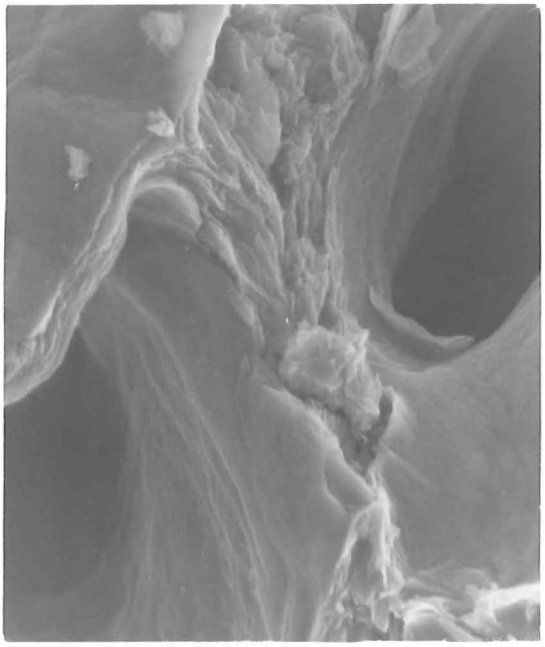

a

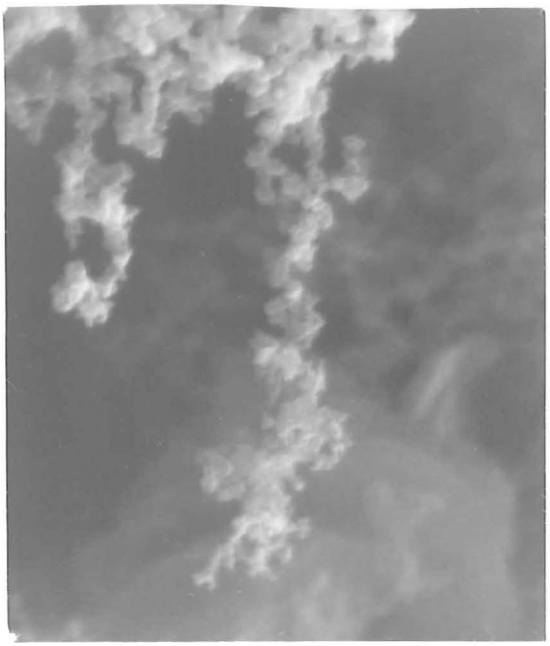

b

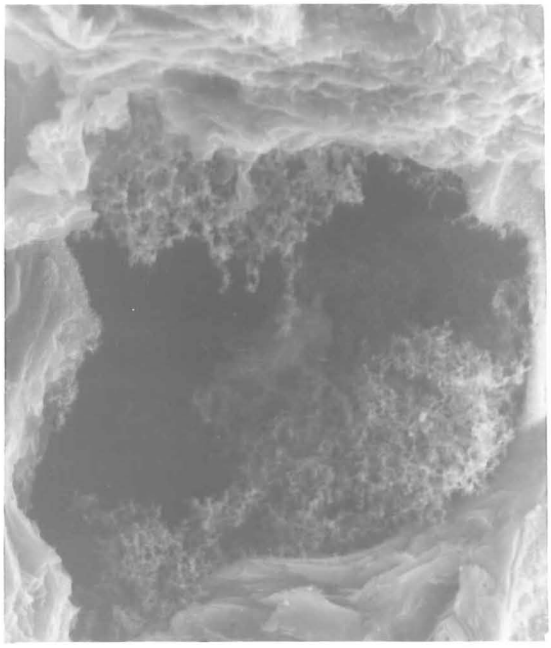

c

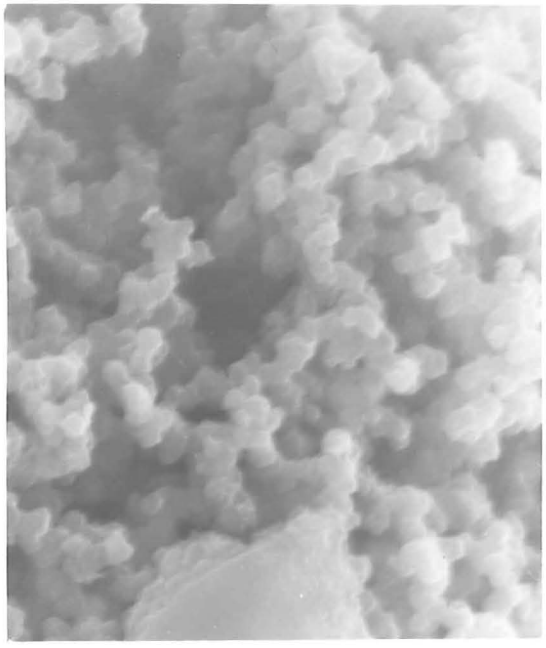

d

PLATE 9

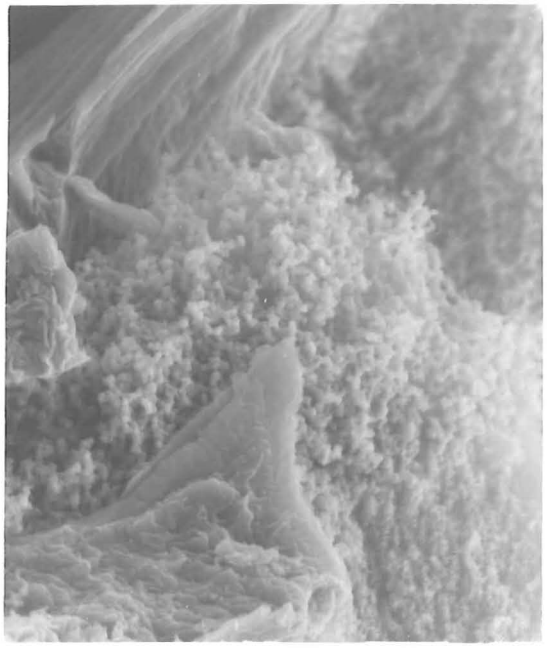

a

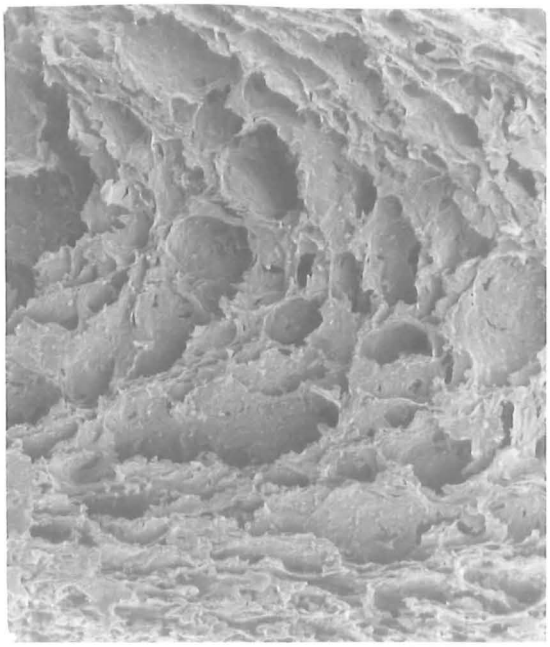

b

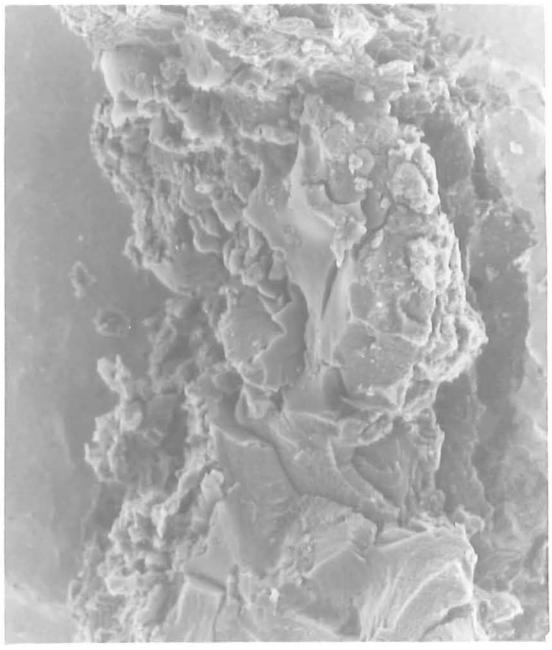

c

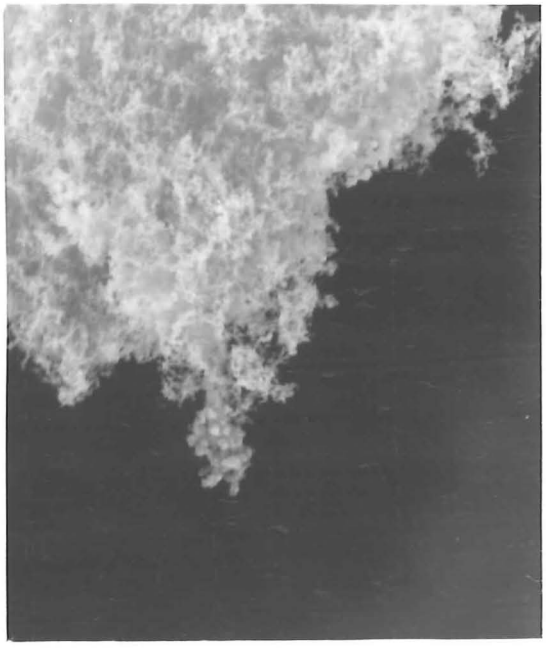

d

PLATE 10

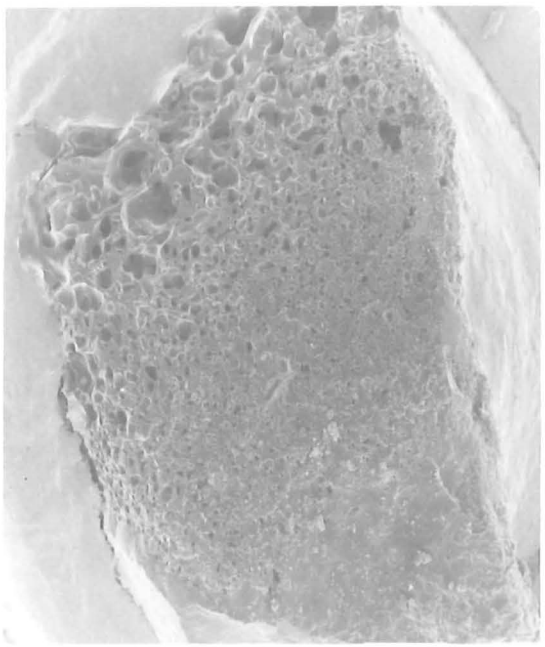

a

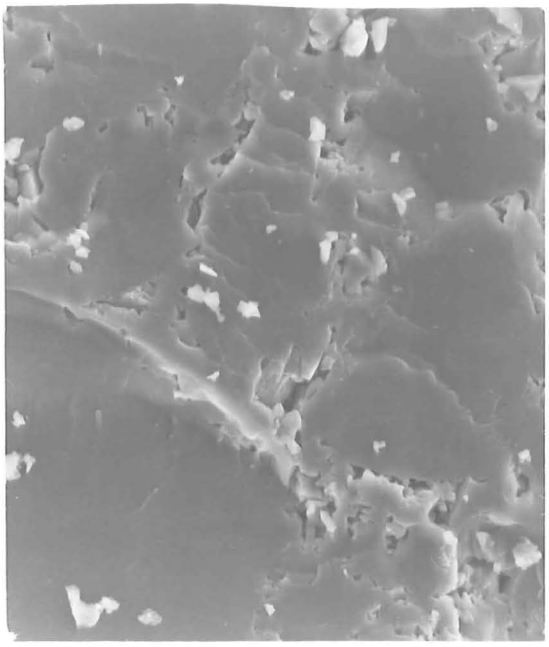

b

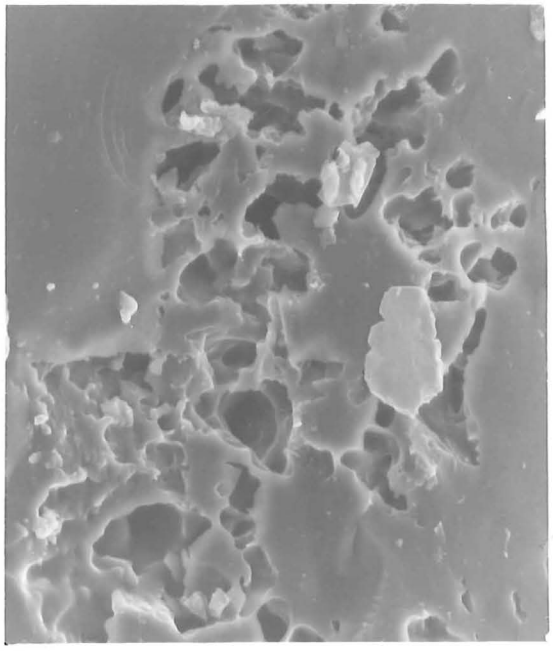

c

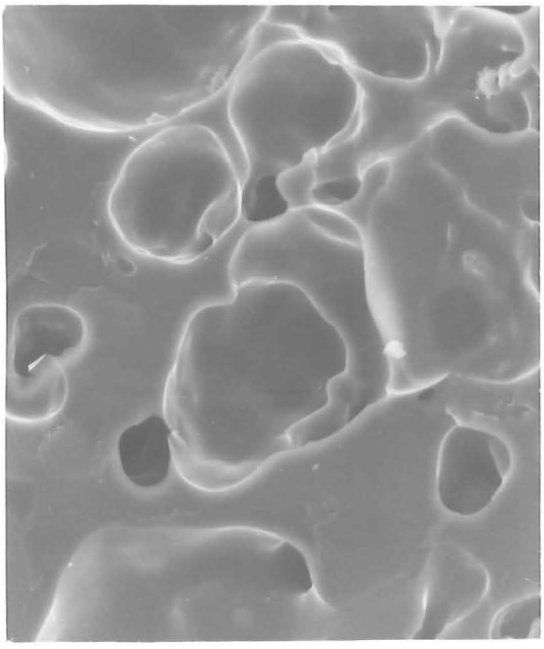

d

PLATE 11

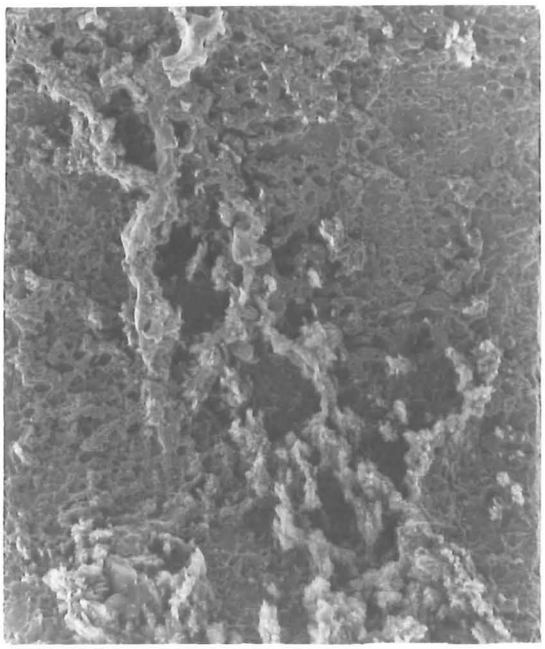

a

b

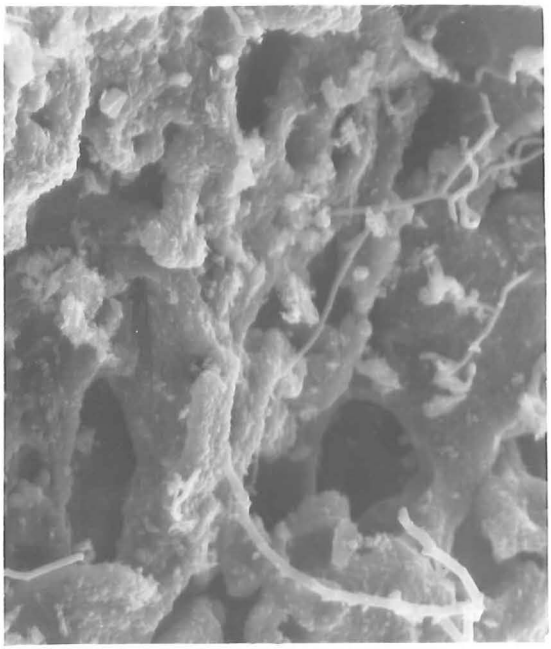

c

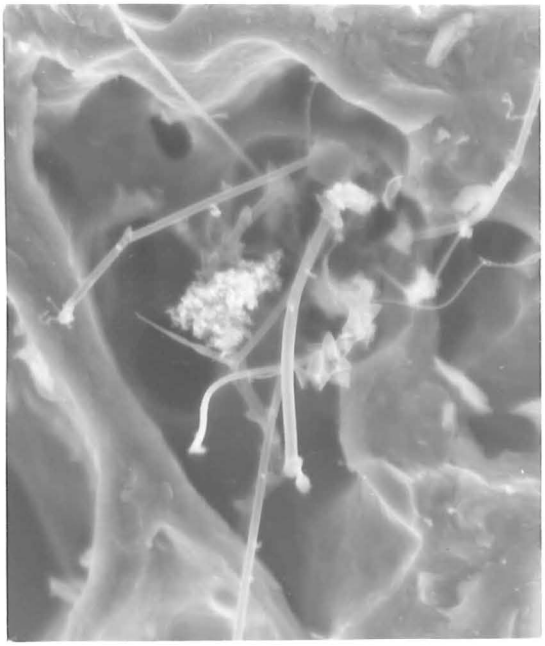

d

PLATE 12

6.3 Discussion of electron micrographs

One of the problems encountered in the tests with composite anodes was the tendency of the core to fragment and fine sections of the core up to 30 mm long to leave the graphite casing, thus bypassing the arc. Many large cracks were observed in the core which appeared to divide naturally into a central porous region and an outer (slightly denser) annulus. This partitioning effect is probably due to the heat treatment of the anode entering the arc chamber, as cores taken from a composite anode that had been plunged into a furnace at 1000 C showed the same type of annulus/core structure. In places, the annulus was very thin, and broke, freeing a plug of core material that could be easily dislodged.

The soot deposits observed in most of the samples examined are probably the result of cracking of the volatiles released when the coal decomposed.

No explanation is offered for the formation of the fibres.

6.4 Resistivity measurements

Measurements of the resistivity of a number of core samples were made using an AVO B.150 universal bridge and a simple tufnol† cell to accommodate the test piece. A 6.35 mm (¼ inch) diameter hole was drilled in a tufnol cylinder 75 mm long and 23 mm in diameter, and a brass terminal screwed into one end. The test piece was located in the cell and covered by the other terminal, also brass. The top terminal could be loaded with different weights up to a maximum of 13.5 kg giving a pressure of ~40 bar on the test piece. The resistance of the terminals and leads was 3 milliohms, and was constant for all experiments. It is known that in measuring the resistance of a solid, the resistance at the point of contact with the terminals of the external circuit can be quite large. Better contact can be promoted by increasing the loading and/or covering the contacts with a highly conductive powder, e.g. copper or graphite. The fragility of the coal core samples used in this work prevented large loads from being used as the samples crushed. Contact resistance was reduced by covering the ends of the test piece with copper powder and in each measurement, a standard load of 4.5 kg was applied. Fig. 11 is a schematic diagram of the apparatus, and Table 7 summarises the data collected from three different test pieces.

† trade name of material

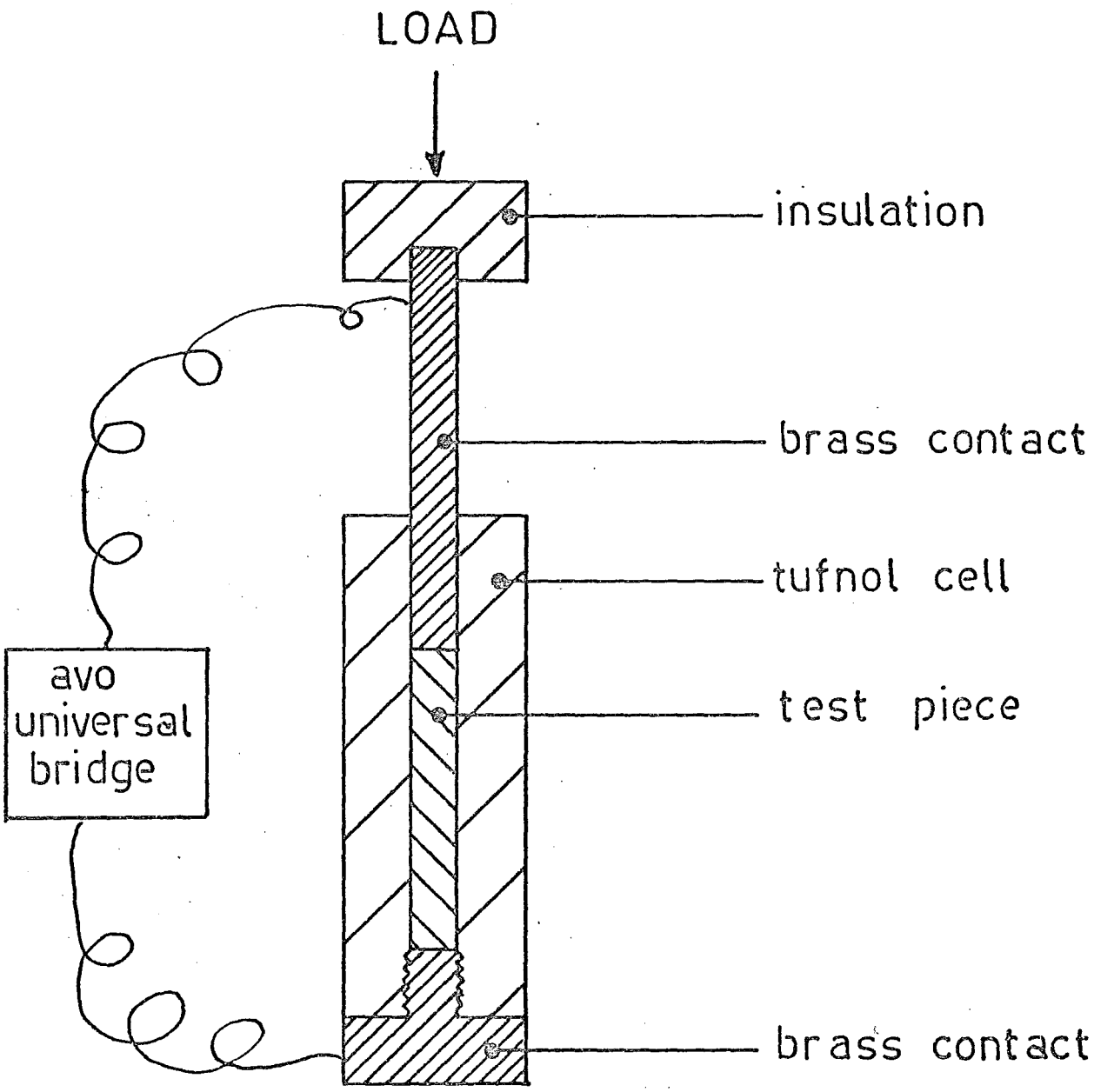

FIG 11: SCHEMATIC DIAGRAM OF RESISTANCE APPARATUS

Table 7: Resistivity of coal cores

Test Piece	Length mm	Diameter mm	Resistance	Resistivity Ωcm	Comment
(1)	25.8	5.715	118	0.01173	Test piece was found on reactor floor after run, and had thus been exposed to high temperature for some minutes.
(2)	14.49	5.69	96	0.0173	
(2a)	6.63	5.69	43	0.0164	Test pieces 2a and 2b were obtained by dividing (2) into two halves. 2a was the tip, and as expected showed the lower resistivity. 2c is 2b with 3 mm central core removed.
(2b)	6.64	5.69	48	0.018	
(2c)	6.64	5.69	58	0.0134	
(3)	5.665	5.55	42	0.01793	

6.4.1 Effect of load

A number of experiments were carried out to examine the effect of load. A piece of GA carbon was subjected to loads up to 13.5 kg in the test cell. The ends were covered with copper powder to promote good contact. Resistance is plotted against load in fig. 12, and it is seen that at about 12 kg, the measured resistance appears to be independent of load. In another experiment, a piece of graphite was tested, again with copper powder at its ends, at loads up to 13.5 kg. Results are also shown for a piece of core material loaded to 5 kg.

These tests are quantitatively inconclusive but they do demonstrate that a significant contact resistance can be expected, and is not eliminated by the standard load (4.5 kg). The manufacturers quote a resistivity for carbon grade GA between .0035 Ωcm and 0.0046 Ωcm (21), and for graphite, between 0.0008 and 0.0013 Ωcm. The calculated resistivities at 13.5 kg are 0.0076 Ωcm and 0.0017 Ωcm. If we assume the upper (manufacturer's) value of resistivity in each case and calculate appropriate sample resistances, the GA test piece is ~34 mΩ and the graphite ~18 mΩ.

This represents additional contact resistance (beyond the standard loading) of 29 mΩ and 16 mΩ respectively. It is to be expected that materials of different microstructure and mechanical properties would show different contact resistance and no firm quantitative conclusions can be drawn from the above discussion. However, it is thought that an allowance of 20 mΩ for the contact resistance beyond the standard load is not unreasonable. Estimates of the core resistivities using resistance values adjusted by this amount

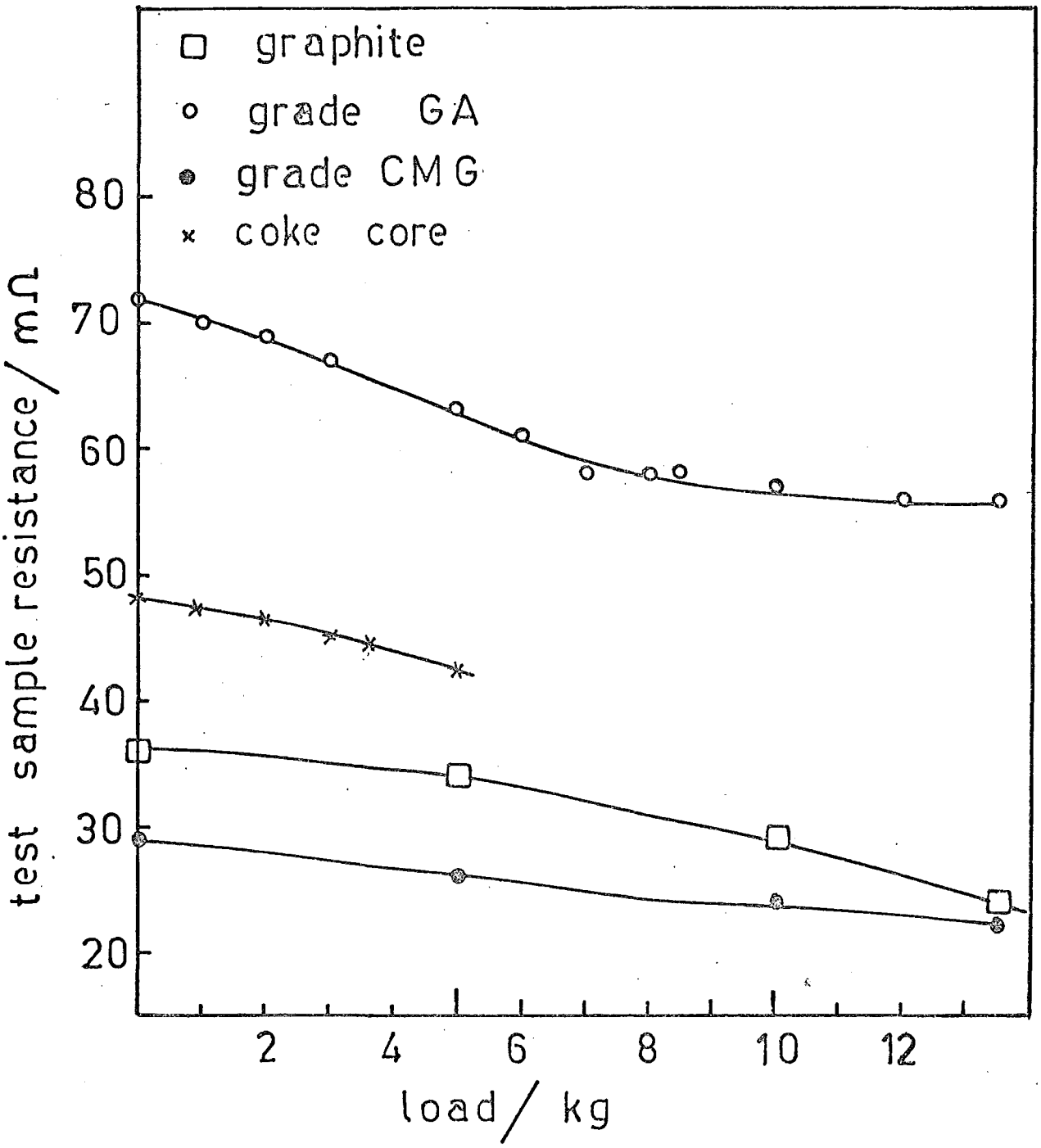

FIG. 12: EFFECT OF LOAD ON SAMPLE RESISTANCE

are presented in Table 8.

Table 8: Revised Resistivities

Test Piece	Resistivity
	Ωcm
1	0.00974
2	0.0133
3	0.00939

APPENDIX

In the following pages, are tabulated the data collected for carbon vaporisation.

Anode Diameter mm	Comment	Arc Current Amps	Arc Power kW	Arc Voltage V	Ablation rate gh^{-1}	Hydrogen rate gh^{-1}	Current density $A\ mm^{-2}$	Ablation rate $gh^{-1}mm^{-2}$	Carbon to hydrogen mass ratio	$(SER)_c$ $kWh\ kg^{-1}$
5.08		290	19.43	67	580.3	227.1	14.31	28.63	2.56	33.47
6.35		240	13.2	55	373.4	222.6	7.57	11.79	1.68	35.3
6.35		245	-	-	352.5	202.2	7.74	11.13	1.74	-
6.35		245	-	-	423.1	202.2	7.74	13.36	2.09	-
6.35		245	-	-	423.1	202.2	7.74	13.36	2.09	-
7.94		233	-	-	287.9	202.2	4.69	5.8	1.42	-
		233	-	-	309.8	202.2	4.69	6.24	1.53	-
		233	-	-	269.0	202.2	4.69	5.42	1.53	-
		235	-	-	303.3	202.2	4.73	6.11	1.50	-
		237	-	-	296.8	202.2	4.77	5.98	1.47	-
		237	-	-	306.3	202.2	4.77	6.17	1.51	-
		237	-	-	335.1	202.2	4.77	6.75	1.66	-
		241	-	-	313.2	202.2	4.85	6.31	1.55	-
		241	-	-	351.5	202.2	4.85	7.08	1.74	-
		241	-	-	306.3	202.2	4.85	6.17	1.51	-
		249	-	-	355.4	222.6	5.02	7.16	1.60	-
		249	-	-	349.0	222.6	5.02	7.03	1.57	-
		249	-	-	320.2	222.6	5.02	6.45	1.44	-
		259	-	-	365.8	222.6	5.22	7.37	1.64	-
		259	-	-	369.3	222.6	5.22	7.44	1.66	-
		261	25.4	97	384.2	225.0	5.26	7.74	1.71	66.1
		261	25.4	97	372.3	225.0	5.26	7.50	1.65	68.2
		261	25.4	97	421.4	225.0	5.26	8.49	1.87	60.3
		266	14.92	56.1	339.0	222.6	5.35	6.83	1.52	44.0
		266	15.02	56.5	311.2	222.6	5.35	6.27	1.40	48.3

contd.

7.94	277	24.7	89.0	388.2	225.0	5.58	7.82	1.73	63.6
	277	24.7	89.0	396.1	225.0	5.58	7.98	1.76	62.3
	277	24.7	89.0	392.6	225.0	5.58	7.91	1.74	62.9
	286	23.91	89.0	405.6	225.0	5.76	8.17	1.80	58.96
	286	23.91	84.0	415.5	225.0	5.76	8.37	1.85	57.6
	287.5	23.67	82.0	411.5	225.0	5.79	8.29	1.83	57.5
	289	23.44	81.0	419.5	225.0	5.82	8.45	1.86	50.8
	290	23.8	82.0	388.2	225.0	5.84	7.82	1.73	61.3
	290	23.8	82.0	392.6	225.0	5.84	7.91	1.74	60.6
	290	23.8	82.0	375.7	225.0	5.84	7.57	1.67	63.4
	318	22.74	71.5	443.2	225.0	6.40	8.93	1.96	51.3
9.53	140	12.1	86.0	95.83	158.7	1.88	1.29	.604	126.3
	141	12.24	87.0	99.55	158.7	1.89	1.34	.627	123.0
	143	12.4	87.0	102.5	158.7	1.91	1.38	.646	120.9
	157	12.17	77.5	102.5	158.7	2.11	1.38	.646	118.8
	167	-	-	109.9	165.7	2.25	1.48	.663	-
	167.5	-	-	116.3	165.7	2.22	1.57	.702	-
	170.5	-	-	112.2	165.7	2.30	1.51	.677	-
	207	19.79	95.6	212.5	222.6	2.79	2.67	.89	99.7
	207	19.79	95.6	198.4	222.6	2.79	2.86	.95	93.1
	209	13.64	65.0	144.9	158.7	2.81	1.95	.91	94.2
	216	13.42	62.0	161.2	158.7	2.91	2.17	1.01	83.3
	216	13.42	62.0	138.2	158.7	2.91	1.86	.87	97.1
	218	-	-	132.5	222.6	2.93	2.67	.60	-
	223	-	-	137.0	222.6	3.00	2.76	.62	-
	223	-	-	142.0	222.6	3.00	2.86	.64	-
	225	11.44	50.8	228.8	171.7	3.03	3.08	1.33	50.0
	225	11.44	50.8	217.7	171.7	3.03	2.93	1.27	52.6

contd.

9.53			225	18.91	84.0	205.0	222.6	3.03	2.76	.92	92.3
			225	18.91	84.0	248.1	222.6	3.03	3.34	1.11	76.2
			226	12.76	56.0	175.3	158.7	3.04	2.36	1.10	72.8
			227	12.86	57.0	175.3	158.7	3.06	2.36	1.10	73.4
			236	-	-	160.3	222.6	3.18	3.23	.72	-
			236	-	-	153.0	222.6	3.18	3.08	.69	-
			245	17.81	73.0	253.3	222.6	3.30	3.41	1.14	70.3
			245	17.81	73.0	253.3	222.6	3.30	3.14	1.05	76.3
7.94	3.2 mm bore		276	22.90	83.0	327.4	222.0	6.66	7.85	1.47	69.9
			278	22.90	82.3	324.5	222.0	6.66	7.78	1.46	70.6
			282	22.90	81.2	343.0	222.0	6.76	8.22	1.55	66.7
			284	22.90	80.6	339.0	222.0	6.80	8.18	1.53	67.6
			288	22.90	79.5	439.2	222.0	6.90	10.53	1.98	52.1
			288	22.90	79.5	369.4	222.0	6.90	8.85	1.66	62.0
9.53	6.35 mm bore		220	15.5	70.4	218.0	225.0	5.16	5.12	.97	71.1
			223	15.5	69.5	228.0	225.0	5.23	5.35	1.0	68.0
			223	15.5	69.5	256.0	225.0	5.23	6.01	1.14	60.5
			223	15.5	69.5	244.0	225.0	5.23	5.73	1.1	63.5
			256	19.46	76.0	357.6	227.1	6.00	8.39	1.57	54.4
			256	19.46	76.0	384.4	227.1	6.00	9.02	1.69	50.6
		Hydrogen rate									
	hydrogen up	ghr^{-1}	210	16.8	80.0	205.0	225.0	4.93	4.81	0.91	82.0
	6.35 mm bore	0	215	16.5	77.0	195.6	225.0	5.04	4.59	0.87	84.4
		0	215	16.6	77.0	213.5	225.0	5.04	5.01	0.95	77.8
		59.9	188	16.8	89.0	137.2	284.9	4.41	3.22	0.48	122.5
		59.9	198	16.8	85.0	162.8	284.9	4.65	3.82	0.57	103.2
		59.9	205	16.7	81.0	173.5	284.9	4.81	4.07	0.61	96.0
		84.86	198	17.3	87.0	146.6	309.86	4.65	3.44	0.47	118.1
		84.86	211	17.0	81.0	152.6	309.86	4.95	3.58	0.49	111.4

contd.

		Methane rate gh^{-1}								
9.53	Methane up	279.5	180	16.5	91.7	174.0	171.0	4.22	4.08	-	-
	6.35 mm bore	279.5	220	15.5	70.4	153.0	225.0	5.16	3.59	-	-
		537.5	180	16.5	91.7	133.0	171.0	4.22	3.12	-	-
		537.5	186	16.5	88.7	142.0	171.0	4.36	3.34	-	-
		537.5	186	16.5	88.7	144.0	171.0	4.36	3.38	-	-
	6.35 mm coal core		158	-	-	152.3	165.7	2.13	2.05	-	-
	(Stockton No. 2)		158	-	-	176.8	165.7	2.13	2.38	-	-
	"		159	-	-	157.5	165.7	2.14	2.12	-	-
	"		187	13.31	70.0	254.8	158.7	2.52	3.43	-	-
	"		187	13.31	70.0	322.4	158.7	2.52	4.34	-	-
	"		196	-	-	165.7	162.2	2.64	2.23	-	-
	"		199	-	-	170.1	162.2	2.68	2.29	-	-
	"		209	-	-	149.3	162.2	2.81	2.01	-	-
	"		214	13.2	62.0	322.4	158.7	2.88	4.34	-	-
	"		225	11.44	50.8	277.8	171.7	3.03	3.74	-	-
	"		225	11.44	50.8	277.8	171.7	3.03	3.74	-	-
	"		242	-	-	322.4	222.6	3.26	4.34	-	-
	"		242	-	-	322.4	222.6	3.26	4.34	-	-
	"		242	-	-	322.4	222.6	3.26	4.34	-	-
	"		249	-	-	340.2	222.6	3.35	4.58	-	-
	Carbon Grade										
7.94	CMG		224	13.7	61.0	267.1	202.0	4.57	5.45	-	51.3
	CMG		238	14.38	60.0	265.1	202.0	4.86	5.41	-	54.2
	CMG		238	14.38	60.0	338.1	202.0	4.86	6.90	-	42.5
	CMG		238	14.38	60.0	305.3	202.0	4.86	6.23	-	47.1
	GA		195	16.10	83.0	275.4	202.0	3.91	5.52	-	58.4

Contd.

7.94	GA	195	16.10	83.0	267.9	202.0	3.91	5.37	-	60.8
	"	206	16.10	78.0	275.4	202.0	4.13	5.52	-	58.4
	"	217	15.74	73.0	318.4	202.0	4.35	6.58	-	49.4
	"	217	15.92	73.0	333.3	202.0	4.35	6.68	-	47.8
	"	221	14.94	68.0	292.4	202.0	4.43	5.86	-	51.1
	"	226	14.72	65.0	286.4	202.0	4.53	5.74	-	51.4
	"	231	14.49	63.0	358.3	202.0	4.63	7.18	-	40.4
	"	231	14.49	63.0	337.3	202.0	4.63	6.76	-	43.1
	"	231	14.49	63.0	353.8	202.0	4.63	7.09	-	41.0
	"	233	14.72	63.0	325.8	202.0	4.67	6.53	-	45.2
	"	233	14.72	63.0	301.4	202.0	4.67	6.04	-	48.8
	"	233	14.72	63.0	358.3	202.0	4.67	7.18	-	41.1

REFERENCES

1. Abrahamson, J. and Stott, J.B., 1970 "N.Z. P.V.C. Proposals", New Zealand Engineering, 15 Sept., p.241.

2. Abrahamson, J. 1971, "The reactions of coal in a high intensity electric arc", Ph.D. thesis, University of Canterbury.

3. Ward, R.A., 1974, "The Production of Acetylene in a High Intensity Arc", Ph.D. thesis, University of Canterbury.

4. Freer, W.W., 1973, "Development of the Maui Gas Field", A.R. Shearer, Government Printer, p.40.

5. Business Indicators, published monthly by Bank of New Zealand.

6. Baddour, Raymond F., and Iwasyk, John M., 1962, "Reactions between elemental carbon and hydrogen at temperatures above 2800 K", Ind. and Eng. Chem. Proc. Des. and Dev., 1, No. 3, p.169.

7. Baddour, Raymond F., and Blanchet, Jean L., 1964, "Reactions of carbon vapour with hydrogen and with methane in a high intensity arc", Ind. and Eng. Chem. Proc. Des. and Dev., 3, No. 3, p.258.

8. Mearns, A.M., 1973, "Multi-step reaction processes", Chapter 6 in "Chemical Engineering Process Analysis", Oliver and Boyd, Edinburgh.

9. Dechayatanapaisan, S., 1970, "Carbon anodes for plasma acetylene generator" B.E. Project Report, Dept. of Chemical Engineering, University of Canterbury.

10. Glass, D.M., 1971, "Carbon anodes for plasma acetylene generator", B.E. Project Report, Dept. of Chemical Engineering, University of Canterbury.

11. Patel, N., 1972, "Carbon anodes for plasma acetylene generator", B.E. Project Report, Dept. of Chemical Engineering, University of Canterbury.

12. Lau L.P., "Experimental production and testing of carbon anodes for plasma arc reactor", B.E. Project Report, Dept. of Chemical Engineering, University of Canterbury.

13. Davies, C.E., 1977, "An investigation of the feasibility of extruding Stockton No. 2 coal in a ram extruder", Progress report, Dept. of Chemical Engineering, University of Canterbury.

14. Pemberton, S.T., 1978, "Rheology and Extrusion of Liquid Coal", B.E. Project Report, Department of Chemical Engineering, University of Canterbury.

15. Wiles, P.G., 1973, "A study of the carbon air arc", B.E. Project Report, Dept. of Chemical Engineering, University of Canterbury.

16. Finkelnburg, Wolfgang, "The high current carbon arc", Fiat Final Report No. 1052, Field Information Agency Technical.

17. Wiles, P.G., 1978, Postgraduate student in Dept. of Chemical Engineering, University of Canterbury, Private communication.

18. Anon, 1971, "Arc acetylene process", Hydrocarbon Processing, June, p.153.

19. Null, M.R. and Lozier, W.W., 1962, "Carbon arc as a radiation standard" Jnl. of the Optical Society of America, 52, No. 10, pp.1156-1162.

20. Kreith, Frank, 1973, "Principles of heat transfer", Third edition, Intext Educational Publishers, New York.

21. Anon, "Physical Properties of Carbon", Xeroxed information supplied by Union Carbide New Zealand Ltd.

THE VAPORISATION OF CARBON IN A HIGH INTENSITY ELECTRIC ARC

PART II

THEORETICAL

BY

C.E. DAVIES

Department of Chemical Engineering,
University of Canterbury,
Christchurch,
New Zealand

6 November 1978

....., why, it appears no other thing to me but a foul and pestilent congregation of vapours!

Hamlet Act II, Scene ii, 321.

CONTENTS

ACKNOWLEDGEMENT

I have had many interesting and useful discussions with Dr R.M. Allen of the Department of Chemical Engineering, and Drs Graham Wood and Bill Barit of the Mathematics Department, and am grateful for their comments and criticisms.

Dr John Abrahamson, whose enthusiasm has been a continuous and welcome spur, has been closely associated with most aspects of this work, and I acknowledge with thanks the advice and assistance he has given.

ABSTRACT

It is proposed that the vaporisation of carbon in an electric arc is a thermal process only, and a one dimensional mathematical model based on this assumption is derived to predict the rate of vaporisation of a carbon anode.

Although a one dimensional model may give an adequate description of the carbon vaporisation process, it is shown that the reality of a radial temperature gradient in a current carrying anode imposes a limit on the current that an anode of specified diameter and resistivity can carry. Further consideration of the behaviour of anodes at maximum current has indicated that for anode material of specified resistivity, there exists a maximum (absolute) rate for carbon vaporisation.

The energy required for the vaporisation of unit mass of carbon is shown to be a minimum (circa 25 kWh kg^{-1}) for anodes of small diameter and low resistivity.

NOTATION

The S.I. units for the symbols used in this report are given alongside the meaning, though for convenience and expediency in retaining the units adopted for practical reasons, strict adherence to S.I. units has not been followed.

Table of Basic and Derived S.I. units used in this work

Physical Quantity	Unit	Symbol
length	metre	m
mass	kilogram	kg
time	second	s
electric current	ampere	A
work, energy, heat	joule	J
power	watt	W
potential difference	volt	V
resistance	ohm	Ω

Symbol	Meaning	S.I. Units
c_p	Heat capacity of anode	$J\ kg^{-1}\ K^{-1}$
c_{pg}	Heat capacity of gas	$J\ kg^{-1}\ K^{-1}$
d_e	Electrode separation	m
D	anode diameter	m
D*	anode diameter at maximum ablation	m
E_a	anode voltage drop	V
E_a^h	anode voltage drop for hissing arc	V
E_{total}	total voltage drop	V
f	scale factor	-
g	acceleration due to gravity	ms^{-2}
G	mass velocity	$kg\ m^{-2}\ s^{-1}$
Gr	Grashof number	-

Symbol	Meaning	S.I. Units
h_c	Convective heat transfer coefficient	$W\ m^{-2}\ K^{-1}$
$\bar{h}_c$	mean heat transfer coefficient	$W\ m^{-2}\ K^{-1}$
I	current	A
I_ℓ	limiting current at which the centreline temperature of an electrode of specified diameter reaches the sublimation temperature of graphite	A
I^*_ℓ	Limiting current for which ablation rate is a maximum	A
k	thermal conductivity	$W\ m^{-1}\ K^{-1}$
k_1, k_2, k_3, k_4	constants	-
l_1, l_2, l_3, l_4	constants	-
L	height of body	m
L_a	anode length	m
$\dot{m}$	ablation rate	$kg\ s^{-1}$, $kg\ s^{-1}m^{-2}$
$\dot{m}_1$	ablation rate at limiting current	$kg\ s^{-1}$
$\dot{m}^*_1$	maximum $\dot{m}_1$ at specified resistivity	$kg\ s^{-1}$
Nu	Nusselt number	-
P_C	convective power	W
P_K	conductive power	W
P_I	electrical power	W
P_M	sublimation power	W
P_R	radiation power	W
P_U	power associated with internal energy	W
P_{Rf}	radiation power from front face	W
P_S	power due to ohmic heating	W
P_V	power generation per unit volume	W
Pr	Prandtl number	-
r	radius - cylindrical coordinate	m
r_o	radius of anode	m
R	resistance	Ω

Symbol	Meaning	S.I. Units
$(SER)_c$	Specific Energy Requirement for carbon vaporisation	$J\ kg^{-1}$
T	temperature	K
$\bar{T}_a$	mean temperature of anode	K
T_b	temperature of surroundings	K
T_c	temperature of current contacts	K
T_d	measured temperature at specified point z_d on anode	K
$\bar{T}_g$	mean temperature of anode and surrounding gas	K
T_f	temperature of anode face	K
T_p	temperature at plane located at $z = z_p$	K
T_{PI}	temperature reached by anode due to ohmic heating	K
T_s	temperature at anode surface	K
T_z	temperature at point z	K
u^z	velocity	$m\ s^{-1}$
x	cartesian coordinate	m
y	cartesian coordinate	m
z	cartesian coordinate, cylindrical coordinate	m
z_c	distance between current contact and first point at which $T = T_{PI}$	m
z_d	point at which temperature is T_d	m
z_p	location of hypothetical planeon anode	m
z_{PI}	point at which anode with boundary temperature above T_{PI} has fallen to T_{PI} measured from the boundary temperature at $z = 0$	m

Greek letters

		Dimension
α	thermal diffusivity	$m^2\ s^{-1}$
β	volumetric coefficient of thermal expansion	K^{-1}
ε	emissivity	-
θ	time	s
λ	heat of vaporisation of anode	$J\ kg^{-1}$

Symbol	Meaning	Dimension
μ	viscosity	kg m^{-1} s^{-1}
μ_s	viscosity at surface temperature	kg m^{-1} s^{-1}
ρ	resistivity	Ωm
ρ_g	density of gas	kg m^{-3}
σ	Stefan-Boltzmann constant	W m^{-2} K^{-4}
ϕ	work function of graphite	V

Subscripts and Superscripts

e	refers to element in differential balance
in	in
meas.	measured
out	out
$\vert_{z \text{ or } r = \text{valve}}$	or $\vert_{z \text{ or } r}$ Symbol at specified or unspecified z or r
$\vert^{+}$ or $\vert^{-}$	Symbol has value greater than or less than required value.

LIST OF FIGURES

1. INTRODUCTION

In part I of this report, experiments were described in which carbon vaporisation rates were measured in an attempt to provide data suitable for use in reactor assessment and scale up. Although a large number of reliable results were obtained, they were necessarily confined to a limited range of anode diameters and current intensities, and to anodes of low resistivity.

A theoretical treatment of the carbon vaporisation process specific to the carbon arc is lacking, and in view of the somewhat limited range of experimental data, it is thought that a sound mathematical model, if shown to be consistent with experiment, is essential to the accurate assessment of the process and any further work involving scale-up of the reactor.

2. PHYSICAL CHARACTERISTICS OF COMMERCIAL GRAPHITE

Graphite is made from a 'green' carbon mix of filler carbon particles embedded in an organic binder. After treatment at temperatures up to 3300 K, the product may be seen to consist of graphitized particles of the filler material embedded in a graphitized matrix of binder. Macropores of diameter similar to that of the filler particles run throughout the filler/binder aggregate, and intercrystalline micropores can be identified between the filler crystallites. The crystallites of filler and binder are not completely ordered, accounting for the non-isotropic nature of bulk graphite. A short but concise presentation of the physical characteristics and microstructure of commercial graphite can be found in reference 1 (the authors of this reference cite reference 2, which is unfortunately not available to this author).

Graphite clearly is not a homogeneous material, and the composite nature of its microstructure might well be expected to influence its vaporisation characteristics. It is known that different carbons show different ablation characteristics, but to what extent this is the result of differences in micro-

structure is debatable, and no attempt has been made to take the micro-structure of the anode into account in the model proposed for carbon erosion from the anode tip.

3. OUTLINE OF MATHEMATICAL MODEL FOR CARBON VAPORISATION FROM ANODE TIP

The model assumes that the erosion of carbon from the face of an anode in an electric arc is a thermal process only, so that all mass loss is the result of carbon vaporisation. The rate at which material is lost from a bulk mass can be found if its heat of vaporisation is known, and an accurate power balance can be made over closed boundaries drawn to include all surfaces from which vaporisation is occurring. In Part I, Section 3.4 it was noted that vaporisation occurred from the front face of the anode only, and Fig. 1A shows a schematic representation of power fluxes in and around an anode.

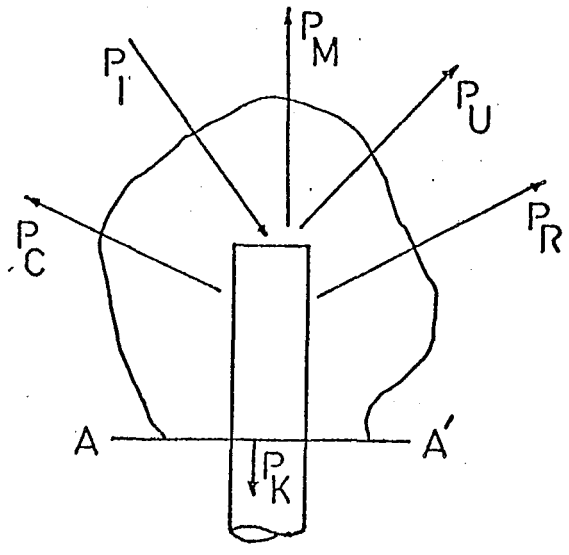

Fig. 1A
Power fluxes round anode

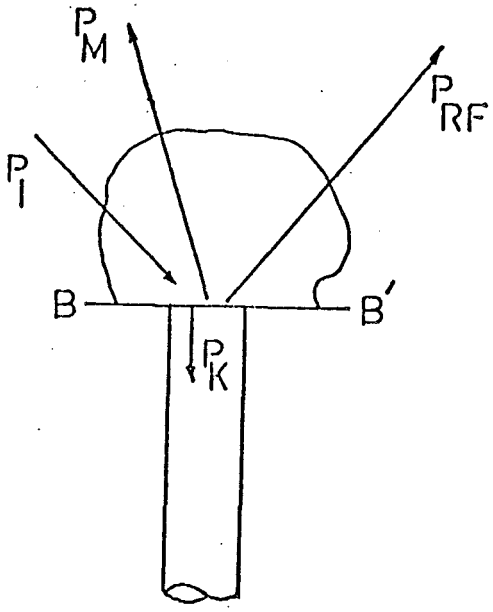

Fig. 1B
Power fluxes at anode face

Power is supplied to the anode by several mechanisms:-

(i) From electrons in the arc current accelerating through the anode voltage drop and then 'condensing' on the anode surface;

(ii) By ohmic heating due to the electric resistance of the anode material;

and depending on the local anode temperature, the temperature of the surroundings and the temperature of the gas in contact with the anode,

(iii) By radiation from the surroundings;

(iv) By convection from the gas surrounding the anode.

Of this energy, some is used to raise the anode temperature to that of the vaporising tip, and some is lost:-

(i) via vaporisation of material from the tip;

(ii) by conduction;

(iii) by radiation;

(iv) by convection.

Referring to Fig. 1A, we can write the following equation linking the net quantities shown.

$$P_I = P_M + P_R + P_C + P_U + P_K \qquad (1)$$

where:-

P_I = electrical power input to anode

P_M = power lost via vaporisation

P_R = power lost by radiation

P_C = power lost by convection

P_U = power lost as sensible heat

P_K = power lost by conduction.

P_M is the product of the rate of mass loss $\dot{m}$, and the heat of vaporisation of the anode material, λ, so provided P_I, P_R, P_C, P_U and P_K can be estimated, $\dot{m}$ can be found.

The plane AA' is arbitrary and equation 1 can be simplified if the balance is taken at the anode face BB', see Fig. 1B. Then:

$$P_I = P_M + P_{Rf} + P_K \qquad (2)$$

where P_{Rf} = power loss by radiation from the front face of the anode.

3.1 Power input from electrons incident on the front face of the anode

The incoming electrons are accelerated through a voltage drop E_a, the anode drop, so a current I, supplies energy $E_a I$ per unit time to the anode. In addition, in condensing on the anode surface, further power equal to the product of the current and the anode work function ϕ (ϕ = 4.5 V) is given to the anode. The total power input is:

$$P_I = E_a I + \phi I = I(E_a + \phi) \qquad (3)$$

3.2 Radiation from the anode face

If the temperatures of the front face and the surroundings are uniform and known, and the front face is assumed to be plane and at right angles to the longitudinal axis of the anode, P_{Rf} may be found from the equation:

$$P_{Rf} = \sigma \frac{\pi D^2}{4} \varepsilon (T_f^4 - T_b^4) \qquad (4)$$

where:

T_f = temperature of front face, which for a carbon anode is the vaporisation temperature of carbon = 3950 K (see Part I, Section 4.2.

T_b = temperature of surroundings

D = anode diameter

σ = Stefan-Boltzmann constant

ε = emissivity

3.3 Conduction loss from anode face

The rate of heat conduction away from the front face of the anode is given by:

$$P_K = -\kappa \frac{\pi D^2}{4} \frac{dT}{dz}\Big|_{\text{anode face}} \qquad (5)$$

where:

k = thermal conductivity of anode

A differential equation describing the temperature profile along the anode can be derived from a power balance taken over a small element, and solution of this equation provides access to $\frac{dT}{dz}\Big|_{\text{anode face}}$, which enables P_K to be found.

3.4 Derivation of the equation for the anode temperature profile

In the following analysis for a cylindrical anode, radial temperature gradients are taken to be negligible, and angular symmetry is assumed. The problem is thus reduced to one dimension.

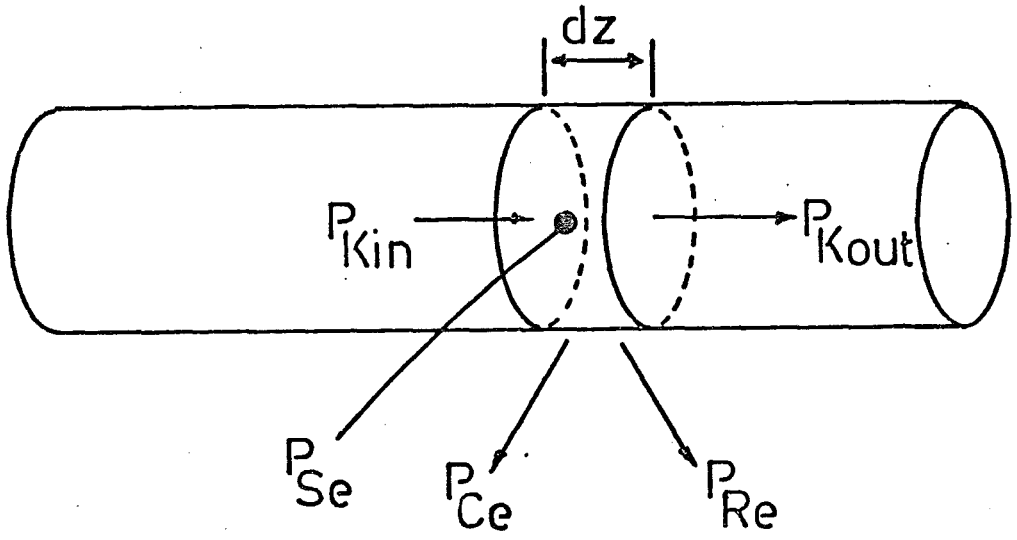

Fig. 2: Power balance in cylindrical rod

Referring to Fig. 2 and remembering that:

Rate of heat in flow	+	Rate of heat generation by internal sources	=	Rate of heat out flow	+	Rate of change of internal Energy

we can write:

$$P_{Kin} + P_{Se} = P_{Kout} + P_{Re} + P_U + P_{Ce} \qquad (6)$$

where:

P_{Kin} = rate of heat in flow into element by conduction

$$= \{-k \frac{\pi D^2}{4} \frac{dT}{dz}\}$$

P_{Se} = rate of heat generation by ohmic heating

$$= I^2 R$$

$$= \frac{4I^2 \rho dz}{\pi D^2}$$

P_{Kout} = rate of heat flow out of element by conduction

$$= \{-k \frac{dT}{dz} + \frac{d}{dz}(-k \frac{dT}{dz})dz\}\frac{\pi D^2}{4}$$

P_{Re} = net rate of heat loss from surface of element by radiation.

$$= \sigma \varepsilon \pi D \, dz \, (T^4 - T_b^4)$$

P_{Ce} = rate of heat loss from surface of element by convection.

P_U = rate of change of internal energy

$$= -\dot{m} c_p dT$$

(the subscript e refers to the element over which the differential balance is being made.)

c_p = heat capacity of anode material

R = resistance of element

ρ = resistivity of element material

Substituting each full term into equation 6 and rearranging:

$$\frac{d^2T}{dz^2} + \frac{4\dot{m}c_p}{k\pi D^2} \frac{dT}{dz} - \frac{4\sigma\varepsilon}{kD}(T^4 - T_b^4) + \frac{16 I^2 \rho}{\pi^2 D^4 k} - \frac{4P_{Ce}}{k\pi D^2} = 0 \qquad (7)$$

The magnitude of each term in equation 7 will vary greatly with distance, z, from the front face, (i.e. with temperature), but with the exception of P_{Ce}, can be accurately evaluated. The convective loss from the anode surface is difficult to calculate, as the velocity and also temperature of the gas surrounding the anode is not known. Fortunately, it can be shown that the convective term in equation 7 can be neglected.

3.4.1 Convection from the anode surface: In Appendix I, heat transfer coefficients are calculated for both free and forced convection from the anode. Free convection is quite obviously unimportant, but the heat transfer coefficient estimated for forced convection is of the order of

$200\,W\,m^{-2}\,K^{-1}$. Using this value, the appropriate mass vaporisation rates and temperature profiles were determined in the manner described in Section 3.5 for a current of 220 amps, and a background temperature of 2000 K. It was found that inclusion of the convective term in equation 7 had an almost undetectable effect on the temperature profile (see also Section 4.2.3), and lowered the vaporisation rate by only 1.2%. Thus, convective heat transfer from the anode surface may be safely neglected, and equation 7 becomes:

$$\frac{d^2T}{dz^2} + \frac{4\dot{m}c_p}{k\pi D^2}\frac{dT}{dz} - \frac{4\sigma\varepsilon}{kD}(T^4 - T_b^4) + \frac{16I^2\rho}{\pi^2 D^4 k} = 0 \qquad (8)$$

This equation is a particular case of the equation for heat flow by conduction in a solid, e.g. see Kreith (3) p.82-85, and was also derived in similar form by Abrahamson (4). For convenience, it will be sometimes referred to in subsequent parts of the text as the 'temperature profile equation'.

3.4.2 Boundary conditions: Equation 8 is a second order non-linear differential equation, and no exact analytical solution has been found, but it can be solved numerically. With two degrees of freedom, two appropriate boundary conditions must be satisfied.

The temperature at the anode face is the sublimation temperature of the anode material, and has been measured at 3950 K. Putting z = 0 at the anode face we can state b.c. No. 1: $z = 0$, $T = T_f = 3950$ K.

We do not have a second boundary condition as such, since we do not have any further information on T or its derivatives at SPECIFIED z. But, provided certain conditions are met, a solution which can be used in the estimation of $\dot{m}$ can be found. A physical argument that justifies the selection of this solution is first presented.

Solutions to equation 8 can be obtained for any pair of boundary conditions. So if a heat sink or source of arbitrary strength:-

$$\left(-k\,\frac{\pi D^2}{4}\,\frac{dT}{dz}\Big|_{z\,=\,z_p}\right)$$

is placed on the anode at some arbitrary distance z_p very close to the anode face such that at $z = z_p$, $T = T_p$, a solution can be found. Alternatively we can state that for $T|_{z=0} = T_f$, there exists a value of $\frac{dT}{dz}|_{z=0}$ such that at $z = z_p$, $T = T_p$. Now inspection of the temperature profile equation shows that at large values of z, $T = T_{PI}$ where T_{PI} is the particular integral $\{T_b^4 + \frac{4I^2\rho}{\pi^2 D^3 \sigma\varepsilon}\}^{\frac{1}{4}}$, which is the temperature of the current carrying rod (in equilibrium with its surroundings) heated from within by ohmic power dissipation.

Let us now find $\frac{dT}{dz}|_{z=0}$ such that at $z = z_p$, $T = T_{PI}$. z_p is gradually increased, and in each case, the strength of the sink/source i.e. $-k\,\frac{\pi D^2}{4}\,\frac{dT}{dz}|_{z\,=\,z_p}$ is noted. At some distance $z = z_{PI}$, equation 8 is satisfied with the conditions:

$$z = 0 \qquad T = T_f$$

$$z = z_{PI} \qquad T = T_{PI}$$

and

$$\frac{dT}{dz}\Big|_{z=z_{PI}} = 0$$

this is the required solution. Provided the conditions given in Section 3.4.3 are met it will be called the required model solution, and can be used to estimate $\dot{m}$.

Strictly speaking it may be necessary to qualify the above analysis, by restating the boundary conditions, since z_{PI} may tend to infinity. Then:

$$z = 0, \qquad T = T_f$$

$$z = z_{PIf}, \qquad T = T_{PI}(1 \pm f)$$

where f is a factor less than 1 that determines the accuracy of the solution.

As a first corollary of the above argument, it can be stated that: The required solution to equation 8 is found by rejecting all values of $\frac{dT}{dz}|_{z=0}$ that allow $\frac{dT}{dz}|_z = 0$ for $T > T_{PI}$, and all values of $\frac{dT}{dz}|_{z=0}$ that allow $T < T_{PI}$. Or more simply, the required solution is obtained with that value

of $\frac{dT}{dz}|_{z=0}$ which gives a non-oscillatory* temperature profile asymptotic to $T = T_{PI}$.

In practice it was found that small changes in $\frac{dT}{dz}|_{z=0}$ had a significant effect on $\frac{dT}{dz}|_{z=z_p}$ for $\frac{dT}{dz}|_{z \doteqdot z_{ss}}$ and solutions were adopted once

$$\frac{\frac{dT}{dz}|^{+}_{z=0} - \frac{dT}{dz}|^{-}_{z=0}}{\frac{dT}{dz}|^{+}_{z=0}} < \sim 0.1\%$$

where $\frac{dT}{dz}|^{+}_{z=0}$ = trial value of $\frac{dT}{dz}|_{z=0}$ too large, i.e. $T_z < T_{ss}$

$\frac{dT}{dz}|^{-}_{z=0}$ = trial value of $\frac{dT}{dz}|_{z=0}$ too small, i.e. $\frac{dT}{dz}|_{z} = 0$, $T_z > T_{PI}$

3.4.3. Conditions for required model solution: In the arc reactor, the anode projects a distance L_a from the current contacts which in practice will be maintained at a temperature $T_c << T_{PI}$ (for T_b = 2000 K, $T_{PI} > 2000$ K). There will thus be a heat flux from the anode to the contacts. By following a similar argument to that presented in Section 3.4.2. it can be seen that the temperature of the anode will fall from T_{PI} to T_c over a distance z_c. Now provided $L_a > (z_c + z_{PI})$ the current contacts can have no influence on the behaviour of the temperature profile for $z < (L_a - z_c)$. In the arc reactor used for experimental studies, $L_a \simeq 80$ mm. The behaviour of $z_c = z_c(I, T_c)$ and $z_{PI} = z_{PI}(I)$ for P, D constant is discussed in Section 4.2.1., and it is shown that for the currents of interest in this work $(z_{PI} + z_c) < L_a$, so the required solution as found by the method given in section 3.4.2. can be adopted as the required model solution.

---

* A complete investigation of the behaviour of equation 8 for conditions excluded by the first corollary has not been undertaken, and the nature of the oscillations is not yet known.

3.5 Estimation of rate of vaporisation from anode face

Substituting for P_I, P_M, P_{Rf} and P_K, in equation 2, and writing $\left.\frac{dT}{dz}\right|_{\text{anode face}} = \left.\frac{dT}{dz}\right|_{z=0}$

$$\dot{m} = \frac{I(E_a + \phi) - \frac{\sigma \varepsilon \pi D^2}{4}(T_f^4 - T_b^4) - \frac{k \pi D^2}{4}\left.\frac{dT}{dz}\right|_{z=0}}{\lambda} \qquad (9)$$

In the temperature profile equation, $\dot{m}$ is a parameter that is defined by $\left.\frac{dT}{dz}\right|_{z=0}$, so using a trial and error method, it must be recalculated at each trial from equation 9, using the current trial value of $\left.\frac{dT}{dz}\right|_{z=0}$. In this way, when $\left.\frac{dT}{dz}\right|_{z=0}$ that satisfies equation 8 to the required accuracy is found, $\dot{m}$ is simultaneously defined at the required value.

Numerical solutions to equations were successfully obtained using a 4th order Runge-Kutta method. The Runge-Kutta technique is described in most advanced mathematical texts, e.g. see ref. 5, and is outlined in Appendix II for the integration of a second order differential equation. In this Appendix, some observations are also recorded on the sensitivity of solutions to the step size used in this particular application.

3.6 Determination of coefficients in equations 8 and 9

The solution of equation 6 and 8 for a rod of specified diameter requires the heat of vaporisation, the emissivity, the heat capacity, thermal conductivity and electrical resistivity of graphite. The last three are known to vary with temperature, and as a consequence of the complex microstructure of commercial graphite, will vary slightly from product to product. In addition, we require the anode drop and the temperature of the surroundings. The anode drop is a characteristic of the arc, and the temperature of the surroundings is determined by the design of the reactor.

3.6.1. Resistivity and thermal conductivity: Some data are available on Union Carbide products (6), but these are incomplete, as they are not specific to the particular grade of carbon used and only cover the lower part of the temperature range for which they are required. Extrapolation was therefore necessary when values at high temperatures were needed. In the case of electrical resistivity, the Union Carbide data were given as a percentage change in the room temperature value, which in turn was presented as falling within a range of values, rather than as an exact figure. Thus, before extrapolating the Union Carbide data, resistivity and conductivity data from other published sources were examined.

This exercise indicated that extrapolation to higher temperatures would give values consistent with published high-temperature measurements, so the Union Carbide data was confidently adopted (and extrapolated), and for convenience was represented by a number of continuous linear functions, each specific to a stated temperature range. Data plots are shown in Appendix IIIA, and the expressions for $\rho = \rho(T)$, $k = k(T)$ are listed in Appendix IIIB.

3.6.2. Heat capacity: A limited range of heat capacity data are given in reference 6, but for convenience all heat capacities were taken from a plot of JANAF (17) data which covered the complete temperature range required. Several continuous linear functions each covering a part of the whole range were used to obtain $c_p = c_p(T)$. See Appendix IIIA, IIIB.

3.6.3. Heat of vaporisation: To the knowledge of this author, λ has not been directly measured, and must be computed from thermodynamic data. The vapour in equilibrium with the solid carbon surface contains many different carbon species, and ideally, all of these should be taken into account when estimating λ. Kratsch et. al. (1) have discussed the problems associated with the computation of λ, and included thirty carbon species (C_1 - C_{30}) in their calculations. Abrahamson (8) considered C_1 - C_5

only, yet reports a value of 23.3 MJ/kg at 4100 K, which is very close to the figure of approximately 20.9 MJ/kg computed by Kratsch et. al. for this temperature. Mentel (9) quotes 30 MJ/kg at 4000 K. There is therefore some uncertainty surrounding the "correct" value of λ, but the good agreement between the results of Abrahamson, and Kratsch et. al. does support the choice of a value of $\lambda \simeq 23$ MJ/kg at temperatures circa the face temperature of 3950 K.

3.6.4. Anode drop: This is an important parameter in the model as it determines the energy input to the vaporising surface. It is also an elusive quantity and difficult to measure. Cobine (10) gives two values, one of 20 volts due to Mason (11), and one of 10 volts obtained by applying a very simple (and incomplete) energy balance to the anode tip. Abrahamson (4) has discussed the Anode Drop in considerable detail, and estimates 17 volts. Accordingly, this author has exercised a certain arbitrariness in selecting a value of E_a, particularly as it is shown that the mathematical model presented in this report can be applied to its estimation.

3.6.5. Background temperature: The production of acetylene demands that the electric arc is enclosed so that the carbon vapour can be reacted with hydrogen. The reactor walls will be heated mainly by radiation from the anode and plasma, and under equilibrium conditions will attain a steady temperature which will be determined by the reactor design.

The temperature of the reactor walls was not measured experimentally, and in the illustrative calculations presented in this report, an (arbitrary) value of $T_b = 2000$ K was used.

3.6.6. Mechanics of solution: Equation 8 was solved on a PDP11 computer using an interactive program written in BASIC. Successive values of $\left.\frac{dT}{dz}\right|_{z=0}$ were tried together with the known starting value of T at $z = 0$, ($T_f = 3950$), until satisfactory convergence to T_{II} was obtained.

4. RESULTS

It has been stressed in earlier parts of this report that there is some uncertainty surrounding the values of the parameters in equation 8 and one term (convection) has been omitted. We must also observe that the model is stated in its simplest form and the conditions in the arc chamber differ (albeit only slightly) from those which the model describes. For instance, in close proximity to the anode tip is a cathode whose surface is at or close to the vaporisation temperature of carbon.

Equation 8 was solved for the range of conditions covered by our experimental work, so that theoretical and experimental results could be compared. In obtaining these solutions, no methodical attempt to find a best fit of the experimental data by adjusting E_a and λ was made. (E_a and λ are the dominant parameters of the model, and also those surrounded by the most uncertainty.) However, in the course of obtaining solutions, different values of E_a and λ were used, over various ranges of current and for different diameters, and some of these solutions have been used to illustrate certain features of the model. Numerical data used in compiling the plots illustrating the text are listed in Appendix IV.

4.1 Ablation Rate

Fig. 3 shows computed ablation rates for anodes 3.3, 7.94 and 9.53 mm diameter, and indicates that at a given current intensity, the ablation rate per unit area increases as anode diameter increases. This result is consistent with qualitative arguments advanced by Abrahamson (8) and Ward (12), and is important because it highlights the dangers inherent in plotting specific ablation rate against current intensity.

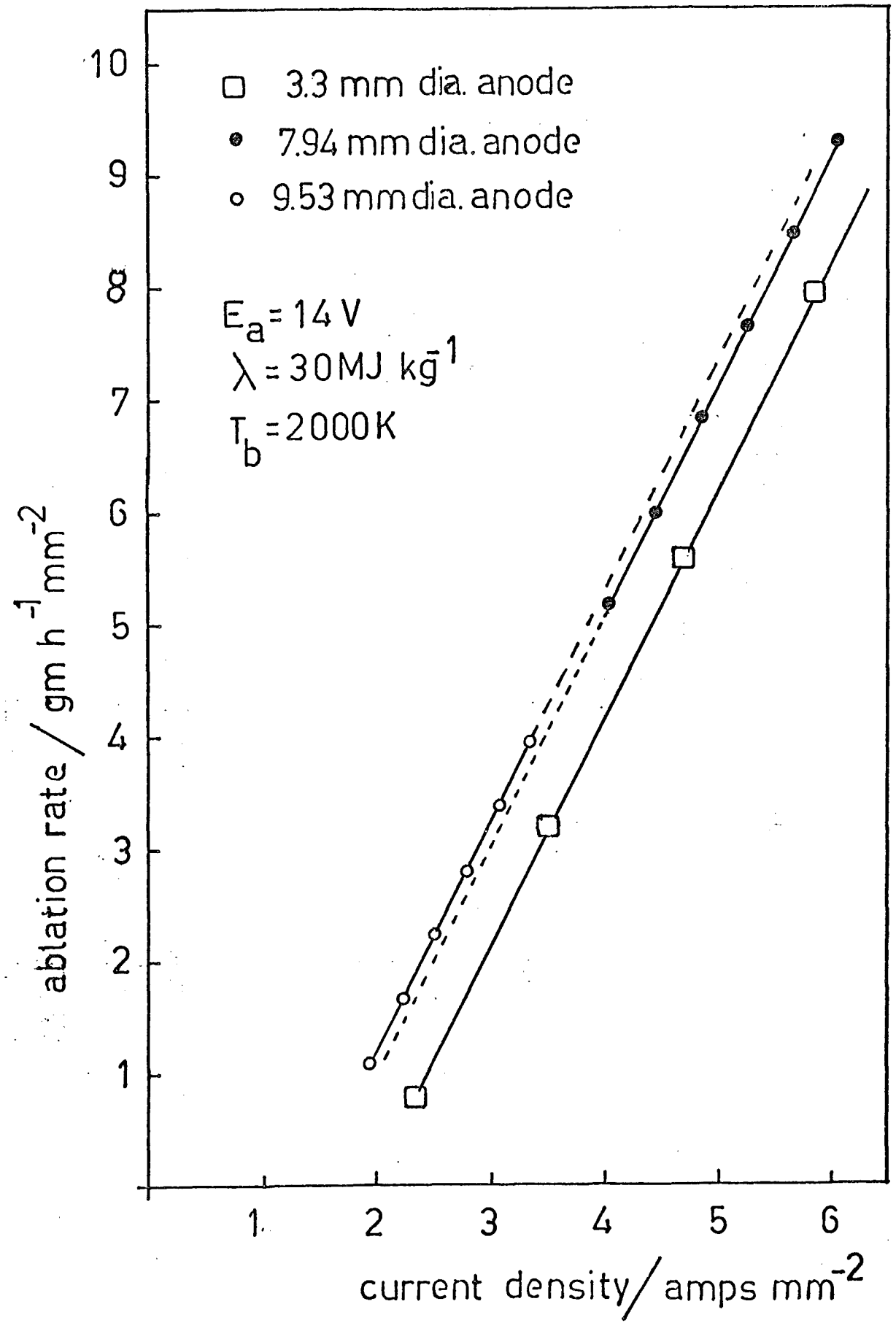

FIG. 3: ABLATION RATE AS FUNCTION OF CURRENT INTENSITY AND DIAMETER

Fig. 4 is a plot of ablation rate vs. current for a current range of 1 order of magnitude, i.e. 100-1000 amps. Ablation is linear for currents up to ~400 amps, and then increases more rapidly. This ablation curve reflects the behaviour of P_K which increases linearly with I, and then begins to decrease at I ≃ 400 amps (for D = 7.94 mm), falling to zero at that current for which ohmic heating raises the whole anode to the temperature of the tip, T_f. P_K is plotted vs. current in Fig. 5.

In Fig. 6 and Fig. 7, experimental and computed data for anodes 7.94 and 9.53 mm diameter are compared, and in Fig. 8 results for different diameters are shown on the same plot. Of all the computed results obtained, a value of E_a = 10.87 volts*, taken with λ = 23.3 J/kg, gave values of $\dot{m}$ closest to the experimental values, (though again it is stressed that no concerted attempt has yet been made to find a value of E_a that best fits the experimental data).

4.2 Temperature profile

The temperature profile along the anode is of practical importance in as much that the current contacts will act as a heat sink and will, under certain conditions, influence the value of P_K and hence the ablation rate. Computed profiles of course can also be compared with experimental measurements, as a further test of the applicability of the model to the vaporising carbon rod.

---

* The figure of 10.87 volts was obtained when selecting a trial value for E_a for use in conjunction with λ = 23.3 MJ/kg on the basis of values used in previous runs. In a previous trial, λ = 30 MJ/kg and E_a = 14 volts had been used, and a thumbnail scaling gave a trial value of $E_a = 10.87$ ($\frac{14}{30}$ x 23.3) which was used in the remainder of computer trials.

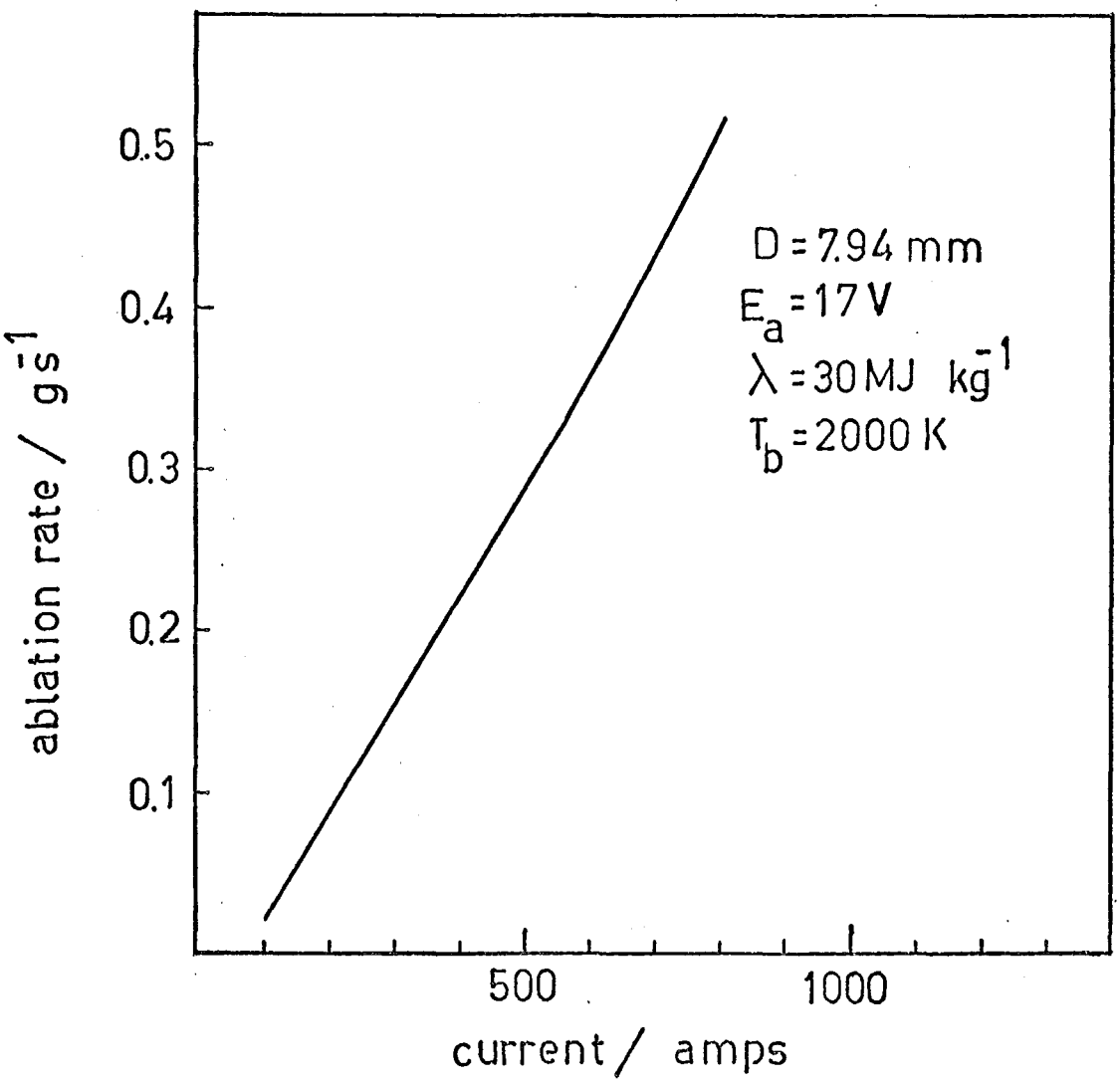

FIG. 4: ABLATION RATE AS FUNCTION OF CURRENT TO MAXIMUM ANODE CURRENT

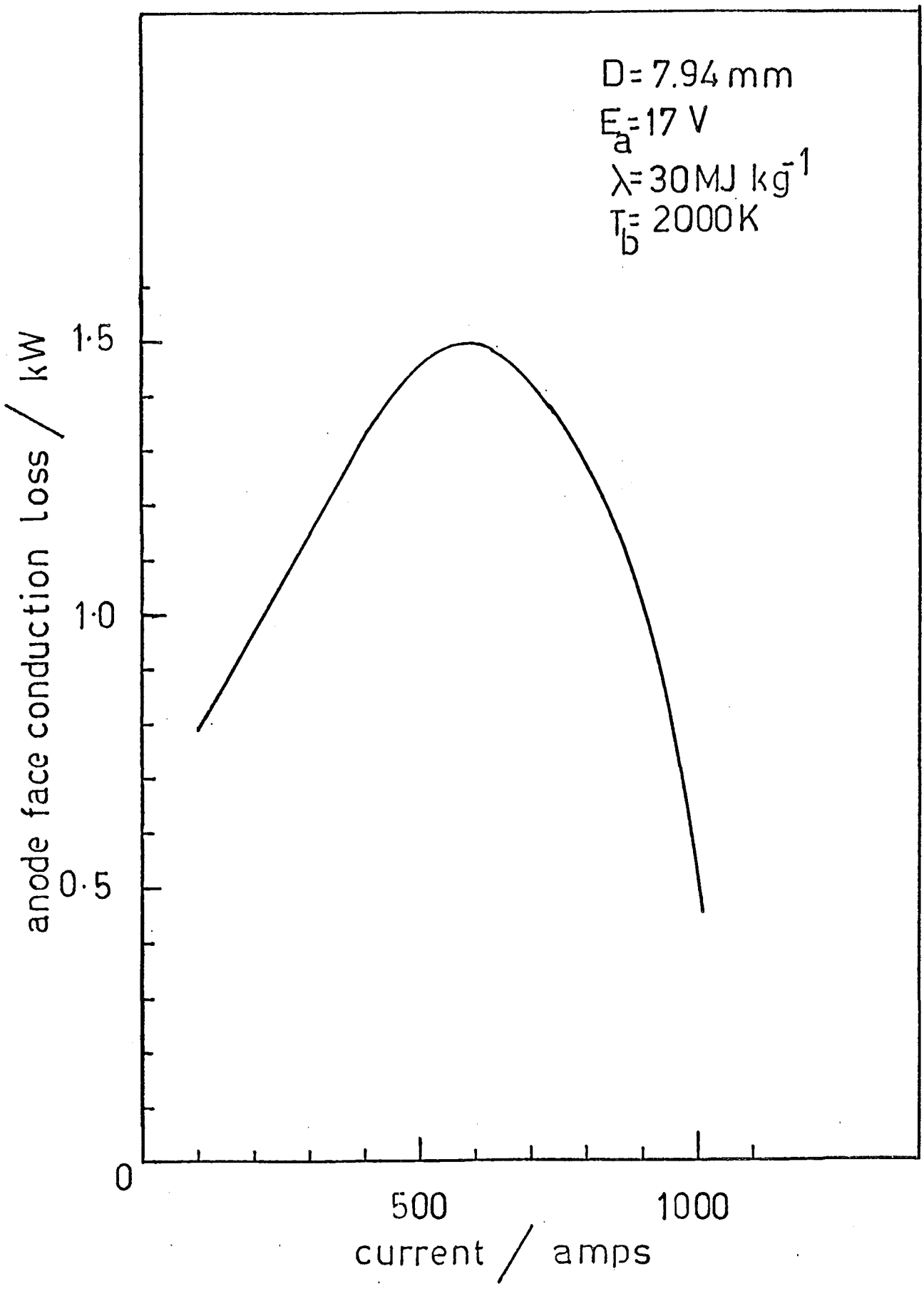

FIG. 5: VARIATION OF ANODE FACE CONDUCTION LOSS (P_K) WITH CURRENT

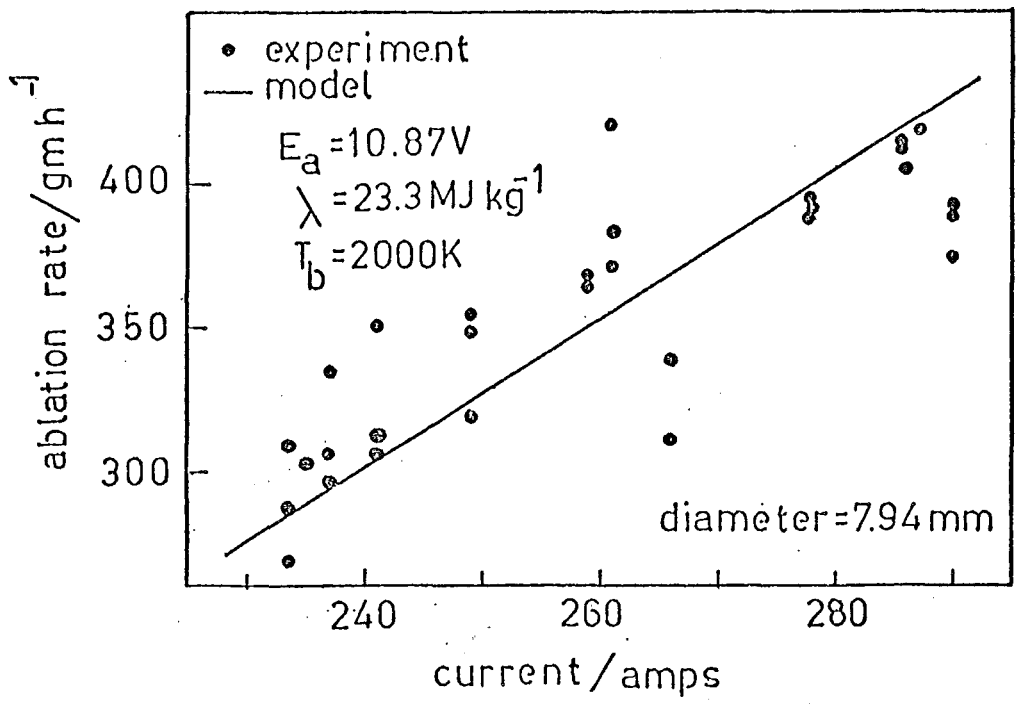

FIG. 6: COMPARISON OF MODEL & EXPERIMENTAL ABLATION RATES, 7.94 MM DIAMETER ANODE

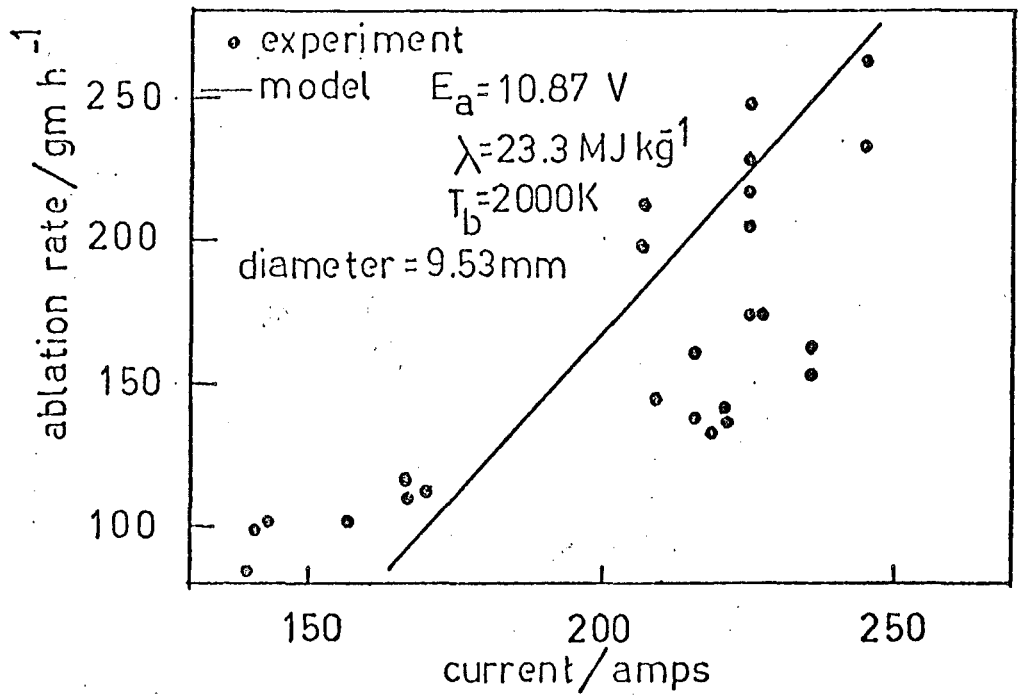

FIG. 7: COMPARISON OF MODEL & EXPERIMENTAL ABLATION RATES, 9.53 MM DIAMETER ANODE

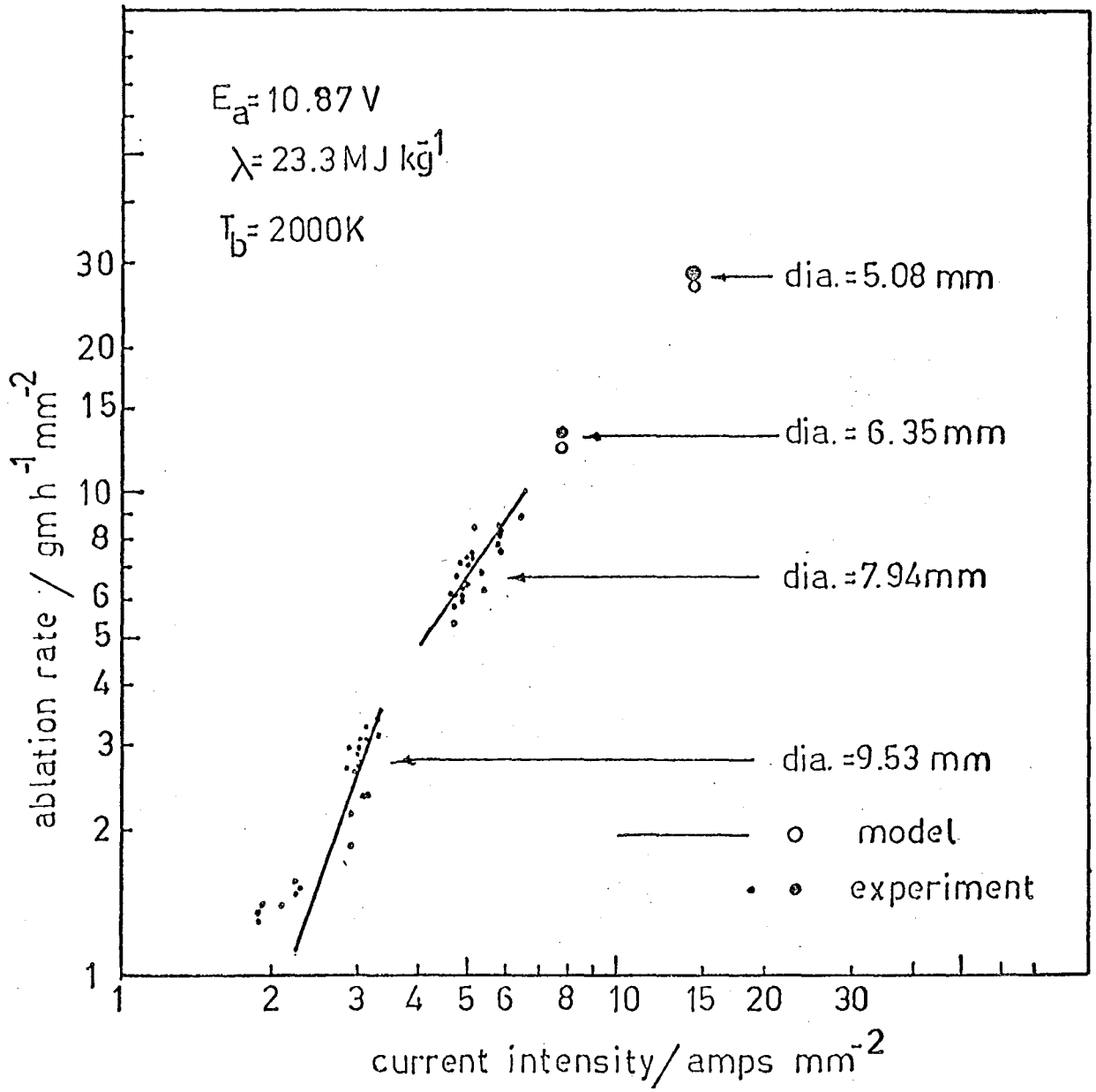

FIG. 8: COMPARISON OF MODEL AND EXPERIMENTAL ABLATION RATES OVER CURRENT INTENSITY RANGE 2 - 14 AMPS $_{MM}^{2}$

4.2.1. Influence of current contacts: Profiles in the region of the anode face were computed in the course of obtaining solutions to equations 8 and 9. Several profiles were also found for that part of the anode close to the current contacts, for a 7.94 mm diameter anode. These contact profiles were computed with the arbitrary boundary condition that the temperature at the current contact was 300 K or 700 K. The complete temperature profile along an anode is shown schematically in Fig. 9.

The distance along the anode for which the anode temperature is affected by the vaporising tip, z_{PI}, decreases with increasing current, see Fig. 10. The corresponding region close to the current contacts, z_c, decreases with increasing current, and also increasing contact temperature T_c, see Fig. 11. The anode projects approximately 80 mm into the reactor, and even for a current of 200 amps and T_c = 300 K, $(z_{PI} + z_c) < 80$ mm. In practice, $T_c > 300$ K and I is usually greater than 200 amps (for a 7.94 mm diameter anode).

So (referring to Figs. 10 and 11) $L_a > (z_{PI} + z_c)$ for all conditions of interest, we can be confident that the current contacts will not affect the vaporisation of carbon from the anode tip. However, at small ablation rates, viz. small currents, z_{PI} increases rapidly and under these conditions, the current contacts will exert some influence over the behaviour of the anode tip.

4.2.2. Comparison of experimental and computed profiles: A temperature profile measured for a current of 220 amps and 7.94 mm diameter anode, shows that T is approximately constant for a short distance from the anode tip, and then appears to decrease linearly with distance, whereas computed profiles are all non linear. It is interesting to note that the profiles for I = 220 amps ($\dot{m}$ = 0.0775 g s^{-1}) and $\dot{m}$ = 0 are very similar, see Fig. 12A. In Fig. 12B, the z-axis of the computed data has been shifted so that the temperatures of the measured and computed profiles are both the same at z = 0, and it is seen that better, but not entirely satisfactory

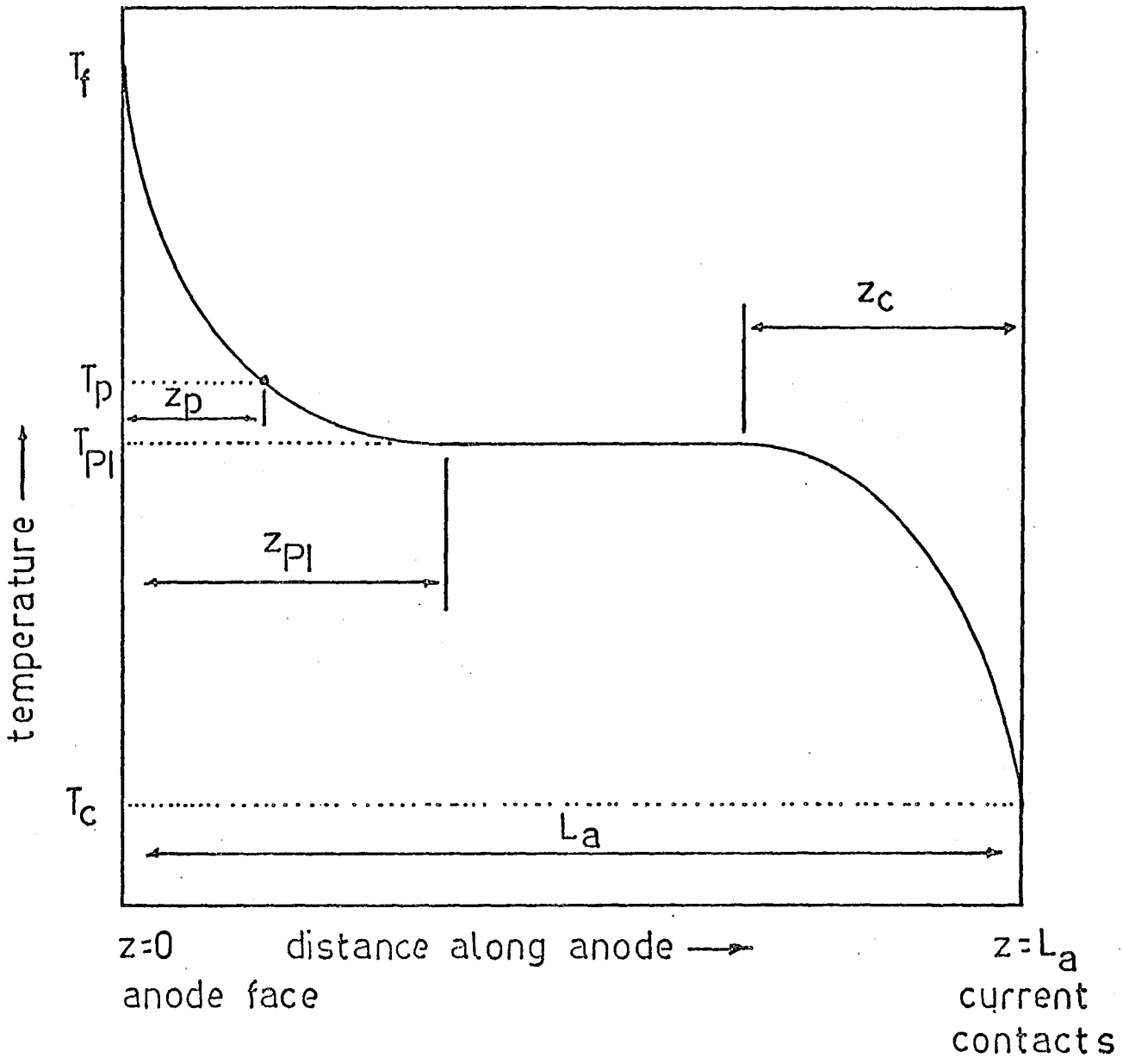

FIG. 9: SCHEMATIC DIAGRAM OF TEMPERATURE DISTRIBUTION IN ANODE

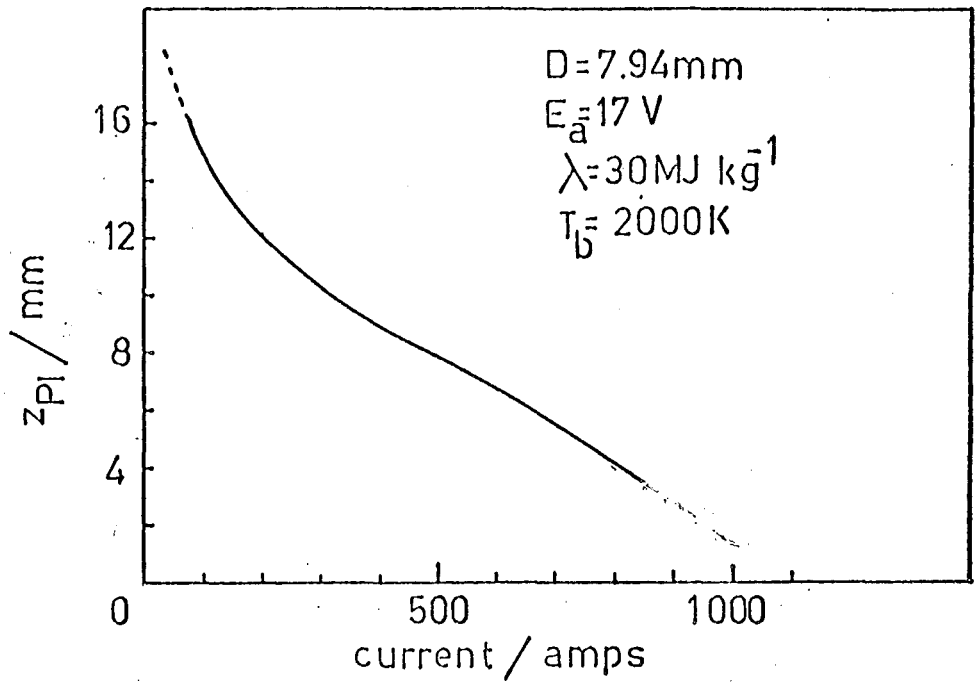

FIG. 10: BEHAVIOUR OF z_{PI} AS FUNCTION OF CURRENT

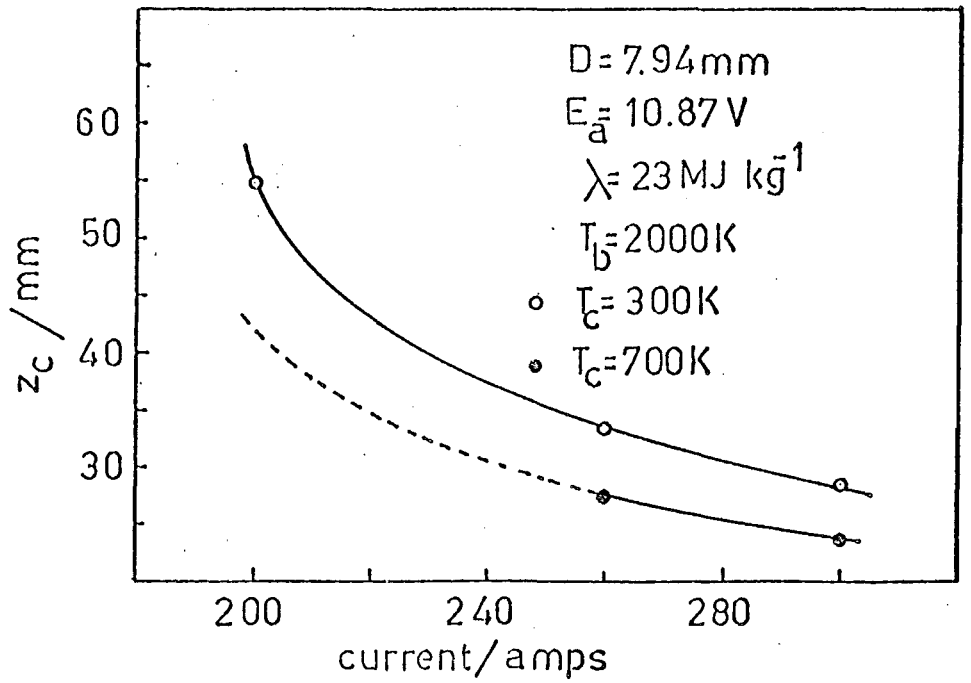

FIG. 11: VARIATION OF z_c WITH CURRENT AND T_c

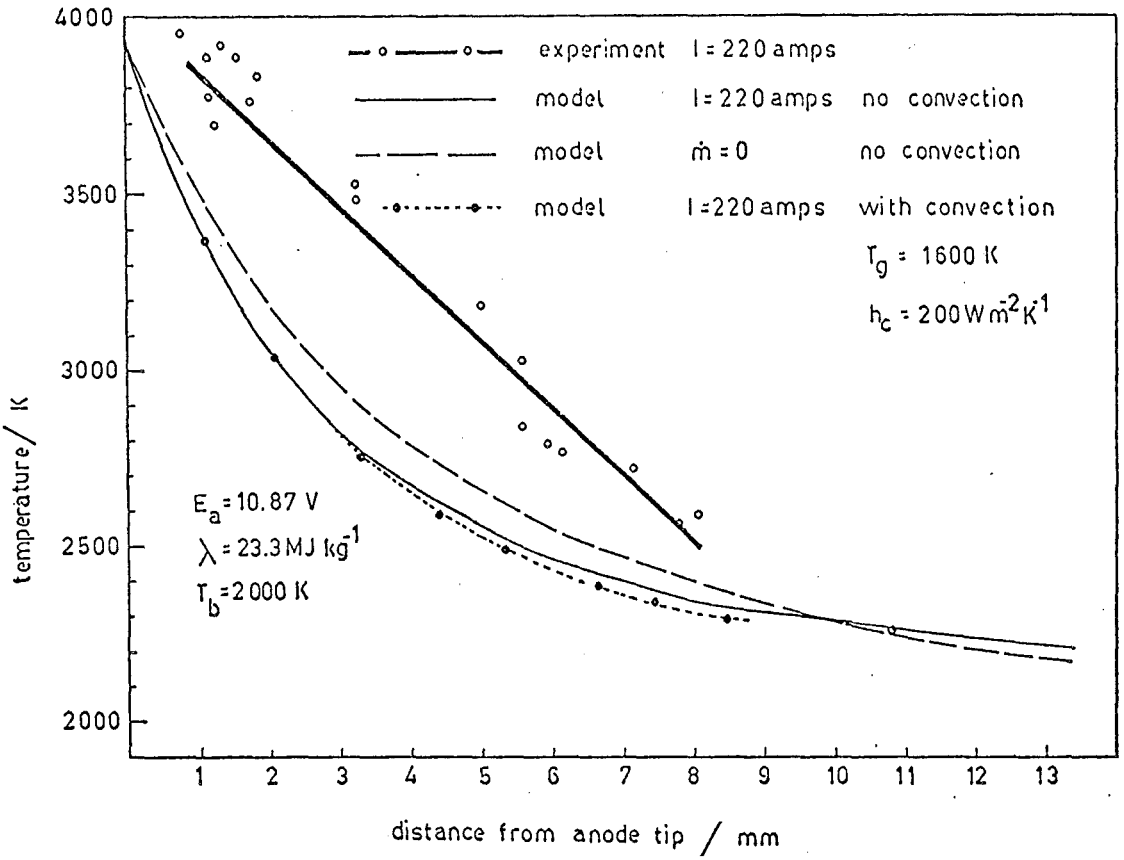
4000
3500
3000
2500
2000
temperature / K
experiment I = 220 amps
model I = 220 amps no convection
model ṁ = 0 no convection
model I = 220 amps with convection
T_g = 1600 K
h_c = 200 W m^{-2} K^{-1}
E_a = 10.87 V
λ = 23.3 MJ kg^{-1}
T_b = 2000 K
1 2 3 4 5 6 7 8 9 10 11 12 13
distance from anode tip / mm

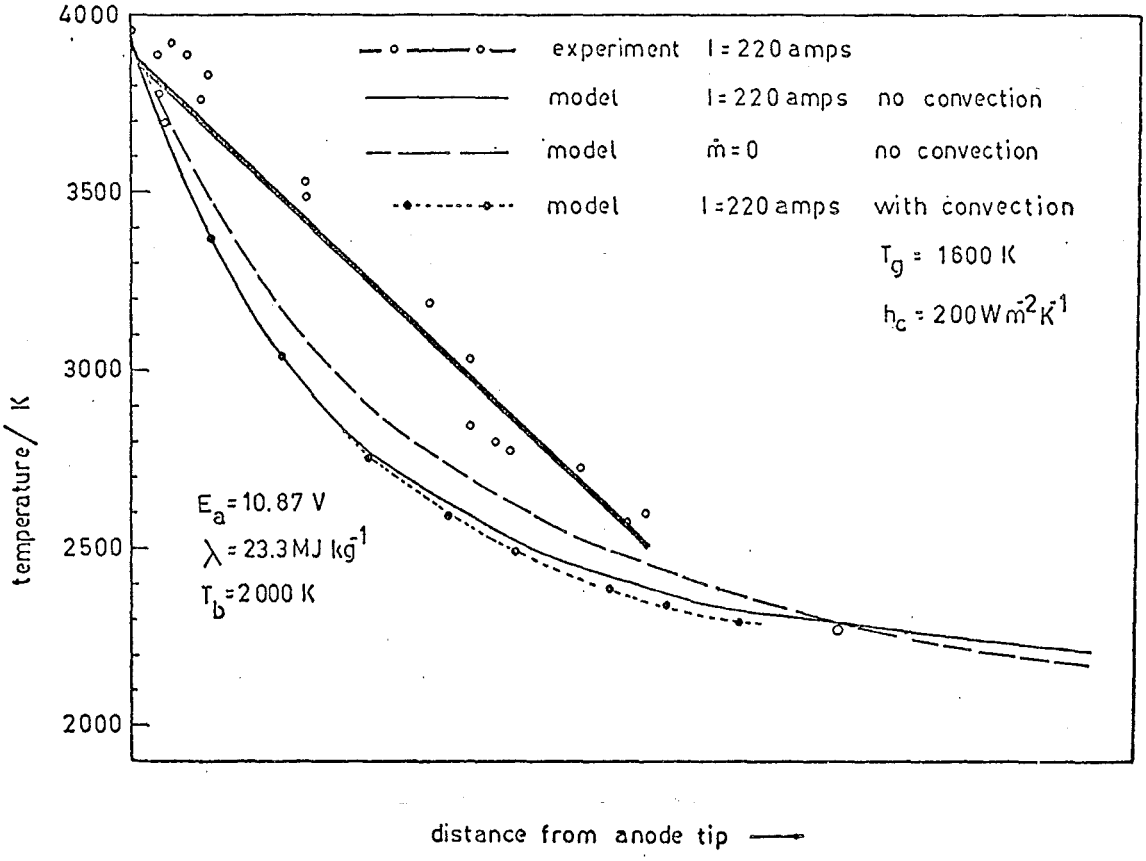
4000
3500
3000
2500
2000
temperature / K
experiment I = 220 amps
model I = 220 amps no convection
model ṁ = 0 no convection
model I = 220 amps with convection
T_g = 1600 K
h_c = 200 W m^{-2} K^{-1}
E_a = 10.87 V
λ = 23.3 MJ kg^{-1}
T_b = 2000 K
distance from anode tip

agreement is obtained. The discrepancies in measured and predicted profiles could be due to several factors which are briefly listed below:

(i) Non-uniform surroundings, e.g. a hot cathode in close proximity to the anode face.

(ii) The anode face in practice is not plane, but is angled with respect to the longitudinal axis of the anode.

(iii) Errors in the functions used to describe the temperature dependence of the parameters in equation 8.

(iv) In all calculations, emissivity was assumed to be constant and equal to 1. It is possible that $\varepsilon = \varepsilon(T)$.

(v) Errors in experimental measurements.

(vi) The system is not adequately described by a one dimensional model.

4.2.3. Convection: Equations 8 and 9 were solved with an extra term included to allow for convection. $T_{p.I}$ with convection was calculated to be 2127 K, and without convection 2176 K, but it is seen from Fig. 12A that the inclusion of the convective term has an almost undetectable effect on the temperature profile, and as mentioned in Section 3.4.1., a negligible effect on the ablation rate.

5. RADIAL TEMPERATURE GRADIENTS

The existence of a radial temperature gradient in the anode could undermine the validity of the assumption of a one dimensional model for carbon vaporisation, and has other implications that are probably more far-reaching. Consequently the radial temperature profile within a current carrying anode is examined in some detail.

5.1 Derivation of the equation for the radial temperature profile

The general heat conduction equation for a cylindrical body with angular symmetry (see ref. 3, p.85) is given by:

$$\frac{\partial^2 T}{\partial r^2} + \frac{1}{r}\frac{\partial T}{\partial r} + \frac{\partial^2 T}{\partial z^2} + \frac{P_V}{k} = \frac{1}{\alpha}\frac{\partial T}{\partial \theta} \qquad (10)$$

where

P_V = rate of heat generation per unit volume of the body

α = thermal diffusivity of body.

For a rod of radius r_o in which there are no longitudinal temperature gradients, which is at steady state, and which is carrying a current I,

$$\frac{\partial^2 T}{\partial z^2} = 0, \quad \frac{\partial T}{\partial \theta} = 0, \quad P_V = \frac{I^2 \rho}{\pi^2 r_o^4}$$

and equation 10 reduces to:

$$\frac{d^2 T}{dr^2} + \frac{1}{r}\frac{dT}{dr} + \frac{I^2 \rho}{k\pi^2 r_o^4} = 0 \qquad (11)$$

At the rod surface, the temperature is T_s, and at the centre, $\frac{dT}{dr} = 0$.

Thus we can state two boundary conditions:

$$r = r_o, \qquad T = T_s$$

$$r = 0, \qquad \frac{dT}{dr} = 0$$

Writing equation 11 in the form:

$$\frac{1}{r}\frac{d}{dr}\left(r\frac{dT}{dr}\right) = \frac{-I^2 \rho}{k\pi^2 r_o^4} \qquad (12)$$

and integrating twice with respect to r,

$$T = \frac{-I^2 \rho}{k\pi^2 r_o^4}\frac{r^2}{4} + A \ln r + B \qquad (13)$$

Using the two boundary conditions,

$$A = 0, \ \& \ B = T_s + \frac{I^2 \rho}{4k\pi^2 r_o^2}$$

T_s is found by equating the heat generation within the element to the nett loss from the surface. Neglecting convection:

$$2\pi r_o (dz)\ \varepsilon\ \sigma (T_s^4 - T_b^4) = \frac{I^2\ \rho\ dz}{\pi\ r_o^2} \tag{14}$$

and

$$T_s = \{\frac{I^2 \rho}{2\pi^2\ r_o^3 \varepsilon\sigma} + T_b^4\}^{\frac{1}{4}} \tag{15}$$

Substituting into equation 13,

$$T = \{\frac{I^2 \rho}{2\pi^2\ r_o^3\ \varepsilon\sigma} + T_b^4\}^{\frac{1}{4}} + \frac{I^2 \rho}{4\pi^2\ r_o^2\ k}\{1 - \frac{r^2}{r_o^2}\} \tag{16}$$

Inspection of equation 16 reveals that the temperature within the rod is always greater than the surface temperature, being greatest at the centre.

5.2 Consequences of radial temperature gradient

The presence of a radial temperature gradient demands that the assumption of a one dimensional model be closely scrutinised, and that due consideration be given to the ramifications of a centreline temperature greater than that at the anode surface.

5.2.1. Applicability of one dimensional model to carbon vaporisation

Although a one dimensional model is not strictly applicable to the description of the temperature profile along an anode, for moderate currents, the difference between the surface temperature and the temperature at the rod centre (ΔT) is very small when the background temperature is high. For instance for:

$I = 400$ amps, $D = 7.94$ mm, $T_z = 2000$ K

$\rho = .00001326\ \Omega m$, $k = 27.12\ W\ m^{-1}\ K^{-1}$

ΔT is only 117 K. For $I = 300$ amps, $\Delta T = 65$ K.

The good agreement between measured and predicted ablation rates has already been noted, and the above result confirms that the assumption of a one dimensional model is not unreasonable at moderate currents. At large currents, P_K is small anyway, and errors in P_K will have little effect on

the estimated value of $\dot{m}$.

5.2.2. Limiting behaviour: At high currents, the sublimation temperature of the carbon will be reached, and since this will occur first at the rod centre, the anode will explode. This effect was observed in trials conducted at Alloy Steel Ltd (see Part I, Section 5). Solution of equation 16 with $T_{r=0}$ = 3950 K will thus provide the maximum theoretical current I_ℓ that can be carried by an anode of specified diameter.

6. ABLATION AT LIMITING CURRENT

When an anode is carrying the limiting current, the term P_K in equation 9 is approximately zero†, and equation 9 can then be written as:

$$\dot{m}_\ell = I_\ell\left(\frac{E_a + \phi}{\lambda}\right) - \frac{\sigma\varepsilon\pi D^2}{4\lambda}\left(T_f^4 - T_b^4\right) \qquad (17)$$

where I_ℓ is obtained by solving Equation 16 for I with r = 0, T = T_f.

As might be expected from inspecting equations 16 and 17, for a specified resistivity, there is a diameter D* at which the ablation rate at the limiting current is a maximum, $\dot{m}^*_\ell$. If D is increased beyond D*, the energy input to the anode due to the increase in I_ℓ is insufficient to compensate for the increased radiation loss from the front face, and $\dot{m}_\ell$ falls. This is clearly seen in Fig. 13 which presents $\dot{m}_\ell = \dot{m}_\ell(\rho,D)$ computed for T_b = 2000 K.

---

† P_k will not be exactly zero, because although for z > 0, $T_{r=0} = T_f$, for z > 0, $T_{r>0} < T_f$ (see equation 16), and as a result there will be a (small) heat flux away from the anode face.

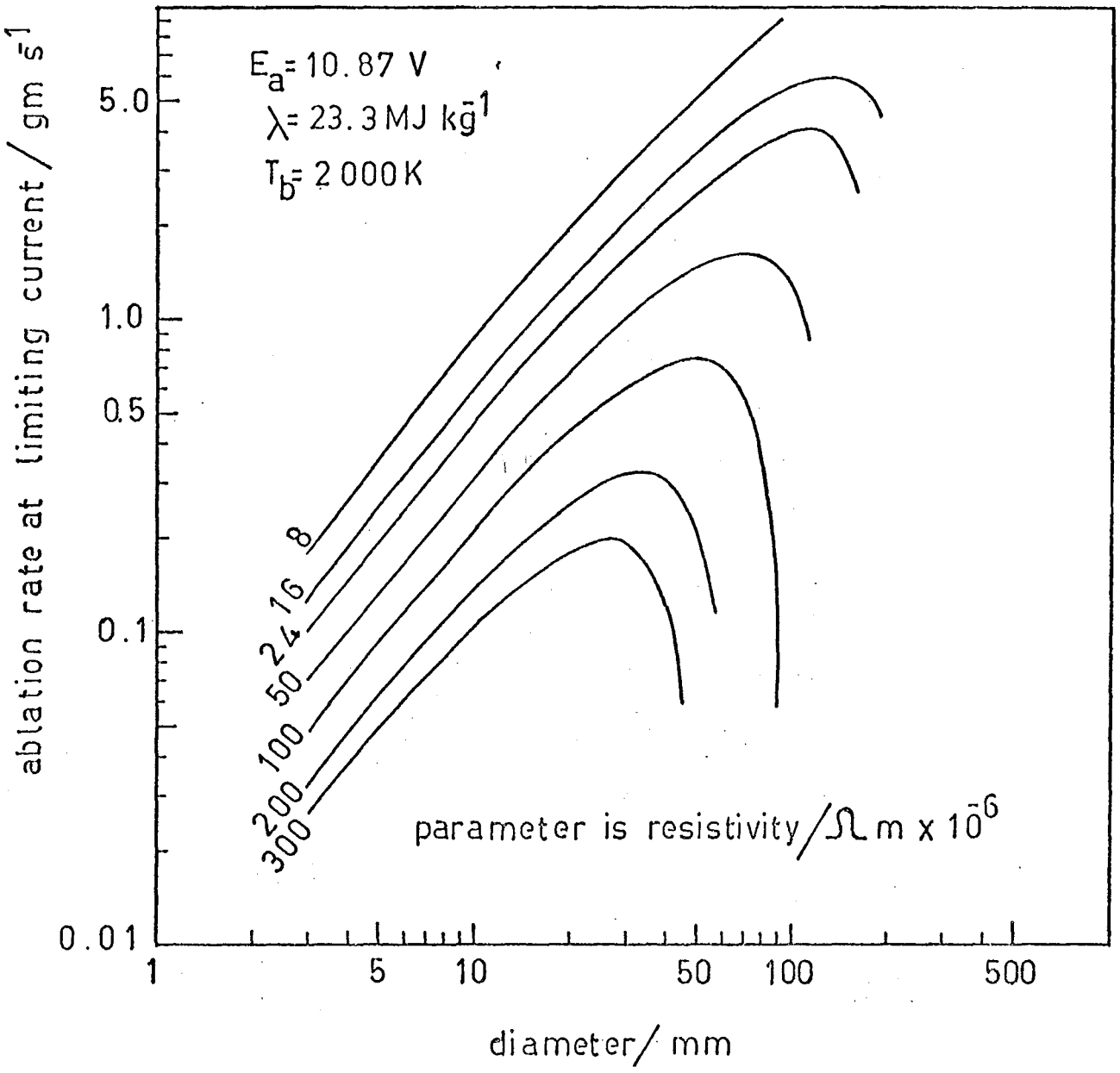

FIG. 13: VARIATION OF ABLATION RATE AT LIMITING CURRENT WITH DIAMETER AND RESISTIVITY

Fig. 14 shows $D^* = D^*(\rho)$. These data were obtained graphically from the locus of the maxima on Fig. 13. On the same figure (with a different scale), I^*_ℓ, the value of I_ℓ at maximum ablation rate, is shown as $I^*_\ell(\rho)$. $\dot{m}^*_\ell$ is shown exclusively as a function of resistivity in figure 15.

The existence of a maximum vaporisation rate has gross implications in arc reactor scale up, as together with carbon conversion factors† it defines the MINIMUM number of ablating anodes, viz. arc reactors, that are required to produce a specified amount of acetylene.

7. ENERGY REQUIREMENTS FOR CARBON VAPORISATION

When an electric arc is stuck between two electrodes, there is a voltage drop across the arc and also in the electrodes due to their resistance. The resistance of the electrodes will be determined by their resistivity, diameter and also length, which will be a function of reactor design. The following estimates of the energy requirement for carbon vaporisation omit the voltage drop in the electrodes which is difficult to determine for an unspecified reactor design. The energy required per unit mass of carbon vaporised so calculated for each case is thus a MINIMUM value which will never be achieved in practice, and because of this, a safe indicator of the trends expected from any real arc reactor.

The power dissipation in an arc reactor is fixed as the product of the current and the TOTAL voltage drop across the reactor, E_{total}. E_{total} has been observed to lie between 40 and 100 volts by a number of authors††(13), (14), (15). In part I of this work values obtained over a large number of

† Not all the carbon vaporised from an anode is converted to acetylene, and a carbon conversion factor may be defined as:

$$\frac{\text{mass carbon vaporised per unit time}}{\text{mass carbon fixed in acetylene per unit time}}$$

†† Graphite (i.e. very low resistance) electrodes of small diameter were used in all work reported in these references, thus $E_a \simeq E_{total}$.

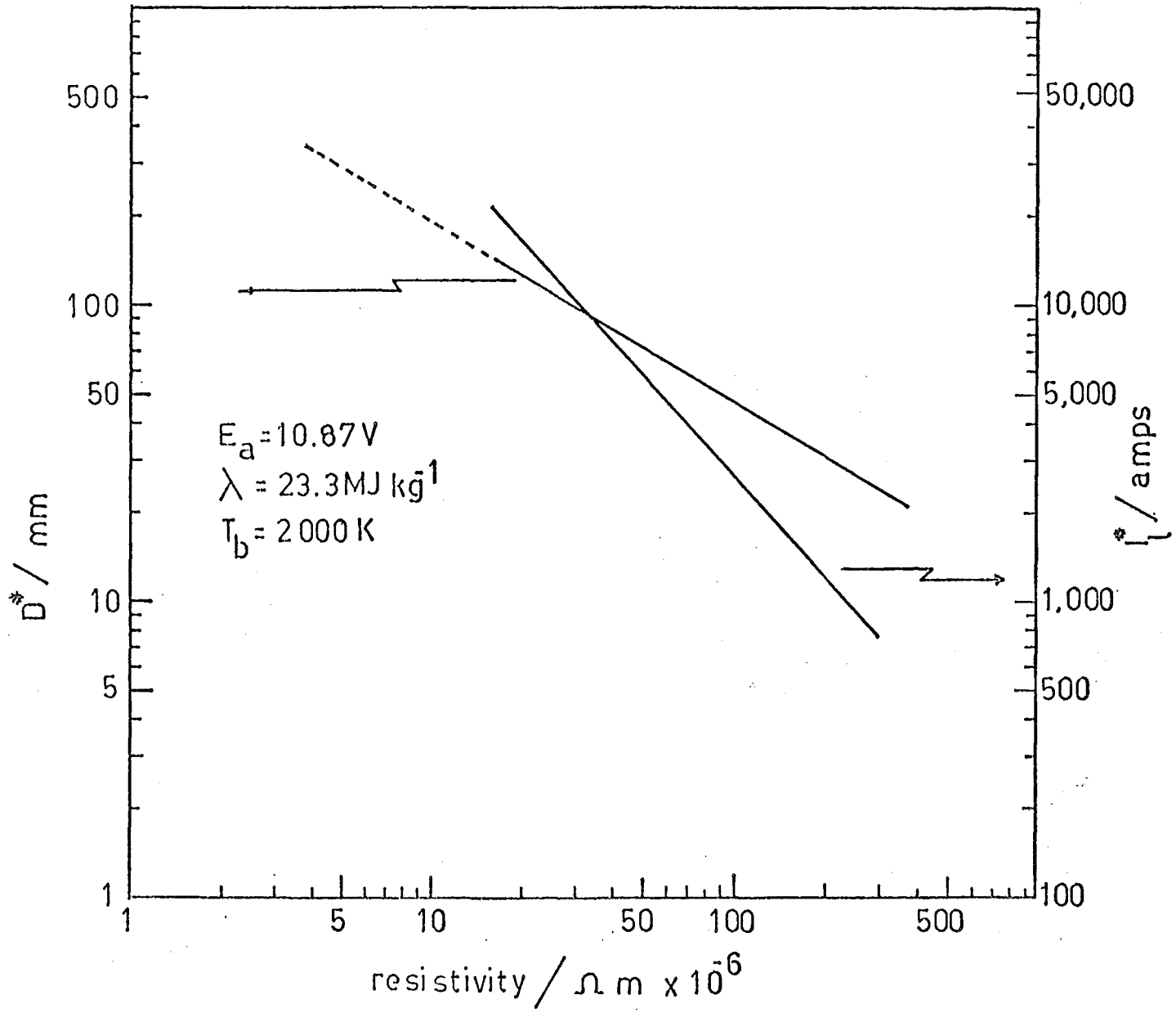

FIG. 14: DIAMETER AND LIMITING CURRENT FOR MAXIMUM ABLATION SHOWN AS FUNCTION OF RESISTIVITY

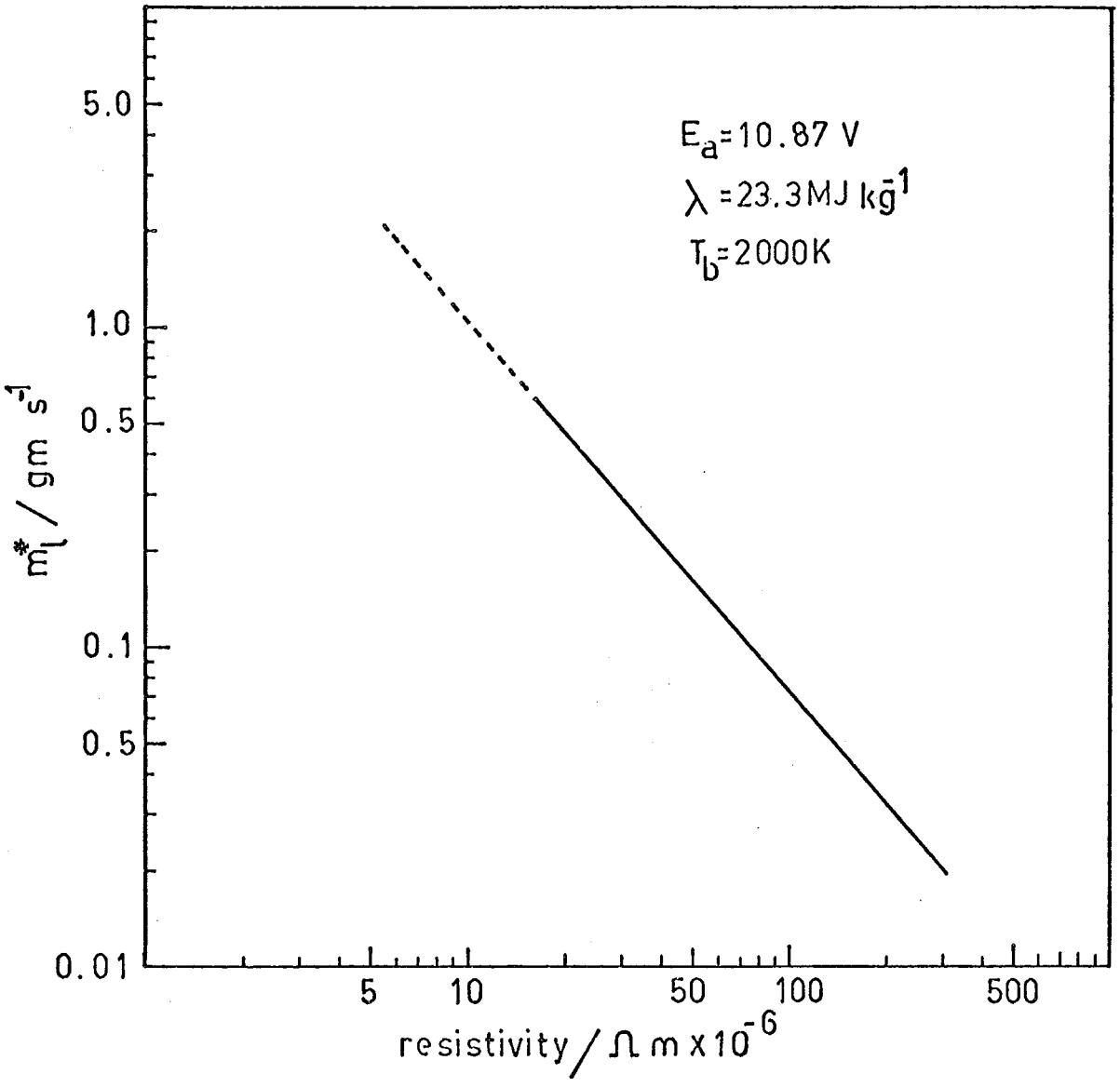

FIG. 15: MAXIMUM ABLATION RATE AS FUNCTION OF RESISTIVITY

runs were reported and generally were in excess of 60 volts, and a conservative value of E_{total} = 60 volts has been adopted in this work for estimating the power input to the arc.

In the literature on the subject of acetylene production, the energy required to produce one kg acetylene is usually quoted in the units kWh kg^{-1}, and these units have been used in calculating the Specific Energy Requirement for carbon vaporisation, $(SER)_c$ thus:

$$(SER)_c = \frac{I\ E_{total}}{3.6 \times 10^6\ \dot{m}} \text{ kWh } kg^{-1} \qquad (18)$$

where $\dot{m}$ has units kg s^{-1}.

Abrahamson (8) and Ward (12) have advanced qualitative arguments to the effect that at a specified ablation rate, $(SER)_c$ will decrease as diameter increases, and Fig. 3 can be used to show that this is indeed so. However, in the light of the observation that for anode material of specified resistance, $(SER)_c$ decreases until the limiting current (I_ℓ) is reached (see Fig. 16) (i.e. $(SER)_c$ is minimum at I_ℓ for specified D), and that current intensity at limiting current decreases with increasing diameter (see Fig. 17), the concept of relating $(SER)_c$ to current intensity is of restricted usefulness and should be abandoned. Instead, it is instructive to examine $(SER)_c$ at I_ℓ as a function of diameter and resistivity. In Fig. 18 we see that as diameter is increased, $(SER)_c$ for any anode running at its limiting current remains approximately constant circa 25-30 kWh kg^{-1} then increases rapidly and at D = D*, is more than double the values found at smaller diameters.

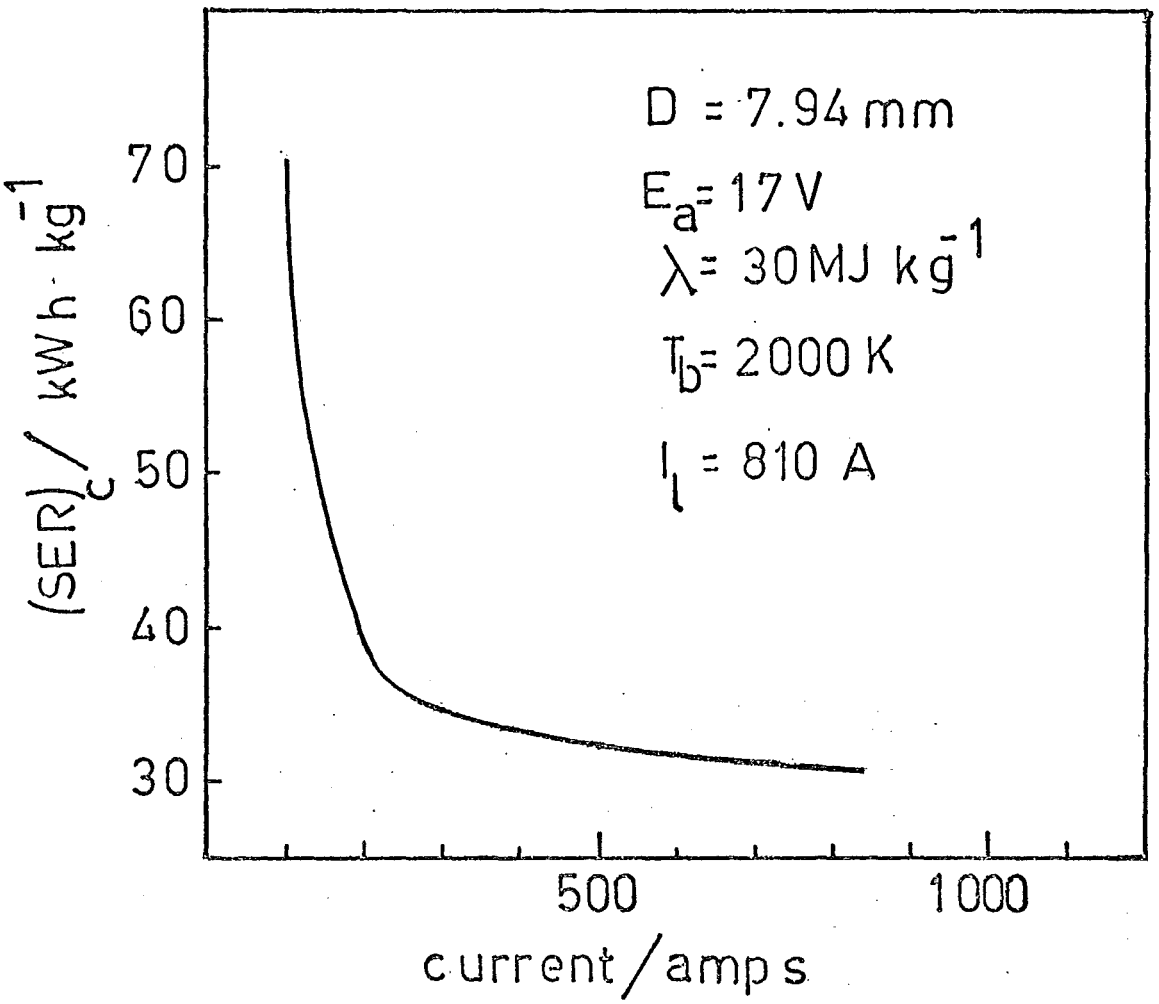

FIG. 16: VARIATION OF $(SER)_c$ WITH CURRENT

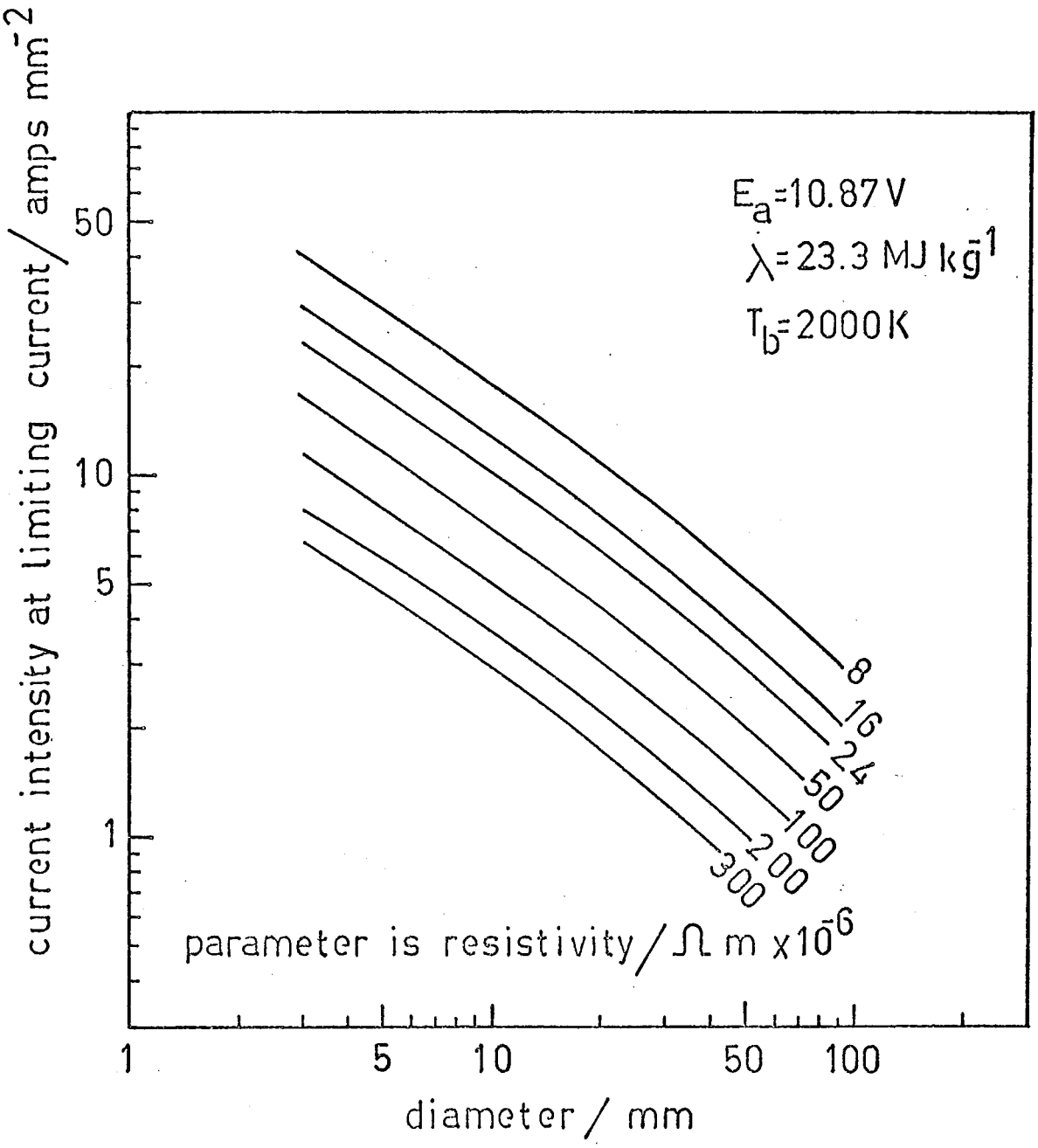

FIG. 17: VARIATION OF CURRENT INTENSITY AT LIMITING CURRENT WITH DIAMETER AND RESISTIVITY

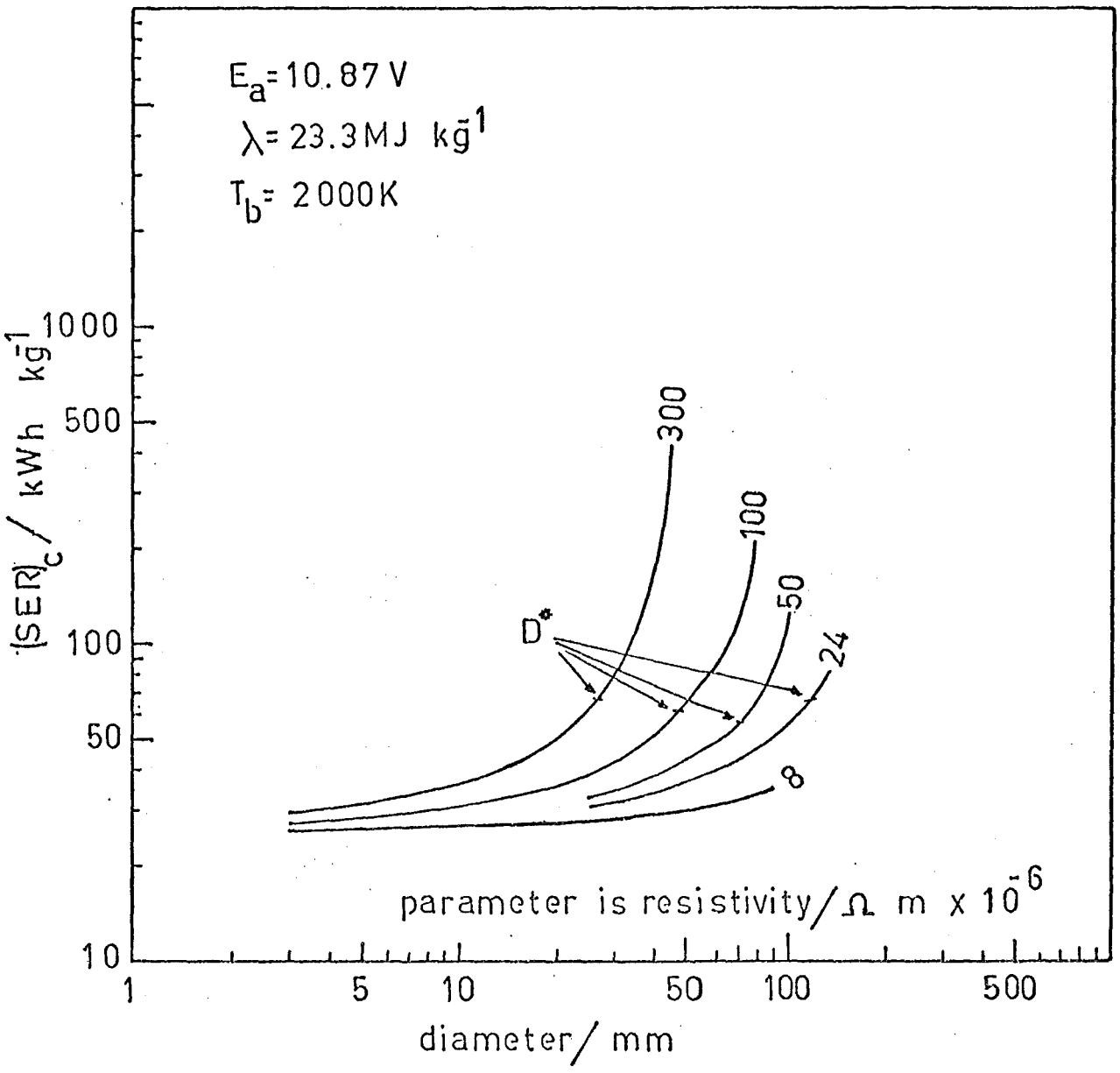

FIG. 18: VARIATION OF $(SER)_c$ WITH DIAMETER AND RESISTIVITY AT LIMITING CURRENT

8. FURTHER APPLICATIONS

The model used for carbon vaporisation cannot be used to predict arc phenomena, as it is not derived from arc physics and is merely a statement of heat-transfer occurring in the anode. However, in conjunction with experimental data obtained under controlled conditions, it can be used to refine estimates of the physical parameters upon which carbon vaporisation is dependent.

8.1 Anode Drop

Electric arcs can operate in one of two modes. At low current densities, the arc is silent and arc voltage decreases with increasing current, while at higher currents, the arc hisses and the arc voltage is constant or possibly increases slightly with arc current. At zero, or nearly zero ablation rates, equation 9 is independent (or nearly independent) of λ, and this suggests that this equation could be used to estimate E_a, independently of λ.

A controlled experiment using apparatus designed to provide a constant and known background temperature and also constructed so that the effect of radiation from the cathode is minimised is suggested. It would also be necessary to measure T_d, the temperature at some distance z_d from the anode, as it has been shown that for small currents, z_{PI} is large, and in this case, a specified boundary condition will be required for the correct solution of equation 8.

The experiment would be conducted as follows:

Ablation rates would be monitored to check that $\dot{m} \simeq 0$, for a number of currents chosen so that both silent and hissing areas were studied. In each experiment, at a constant electrode separation d_e, I, T_f^{meas}, T_d, z_d and d_e would be recorded.

$\left.\frac{dT}{dz}\right|_{z=0}$ is obtained by solving equation 8 with the boundary conditions:

$$z = 0, \qquad T = T_f^{meas}$$

$$z = z_d, \qquad T = T_d$$

thus, if different anode diameters and electrode separations were used, $E_a = E_a(I,D,d_e)$ could be determined.

8.2 Heat of Vaporisation

If a value of E_a^h for a hissing arc could be determined, this could then be used in conjunction with experimental data on $\dot{m} > 0$ (and of course the assumption that E_a^h = const.) to estimate λ.

9. SUMMARY

(i) A one dimensional model which treats the loss of carbon from the face of an anode in an electric arc as a thermal process only has been derived. Predicted and measured vaporisation rates are in close agreement over a wide range of currents and diameters. The model is also useful in the examination of longitudinal temperature gradients in the anode.

(ii) The model can be applied to the estimation of the anode voltage drop, a physical parameter of fundamental importance in electric arc systems, and can be used for the estimation of the heat of vaporisation of the anode.

(iii) The solution to the equation for the radial temperature distribution in a cylindrical rod provides a method of assessing the limiting current that can be carried by a carbon conductor.

(iv) It has been shown that for a carbonaceous anode of specified resistivity there will exist a maximum anode vaporisation rate.

(v) The energy required to produce unit mass of acetylene, $(SER)_c$, is shown to be a minimum when an anode is carrying the maximum permissible current, I_ℓ. As anode diameter increases, $(SER)_c$ also increases,

APPENDIX I

Convective Heat Transfer from the Anode Surface

The precise calculation of convective heat transfer coefficients is difficult and the following analyses are carried out to determine whether convection is expected to play a significant role in the heat transfer processes occurring at the anode surface.

The temperature profile along the anode was measured for a 7.94 mm diameter anode and a current of 220 amps. The temperature at the tip was 3950 K and fell to 2200 K 11 mm away. In the ensuing analyses the anode is divided into two regions. At distances greater than 11 mm from the tip, the temperature is assumed to be constant at 2200 K, and a mean temperature, $\overline{T}_a$ of $\frac{(3950 + 2200)}{2}$ K is assumed for the tip region, see Fig. 19. Both free and forced convection are considered.

1. Free Convection

The heat transfer coefficient at the anode surface may be found from the following expressions for vertical surfaces (ref. 3, p.393):

$$Nu = 0.555\ (Gr\ Pr)^{1/4} \qquad Gr < 10^8 \qquad \text{A.1}$$

$$Nu = 0.0210\ (Gr\ Pr)^{2/5} \qquad Gr > 10^9 \qquad \text{A.2}$$

where,

Nu = Nusselt number based on the height of the body

$$= \frac{\overline{h}_c\ L}{k}$$

Gr = Grashof number

$$= \frac{\rho_g^2\ \beta\ g\ \Delta T\ L^3}{\mu^2}$$

Pr = Prandtl number

$$= \frac{C_{pg}\ \mu}{k}$$

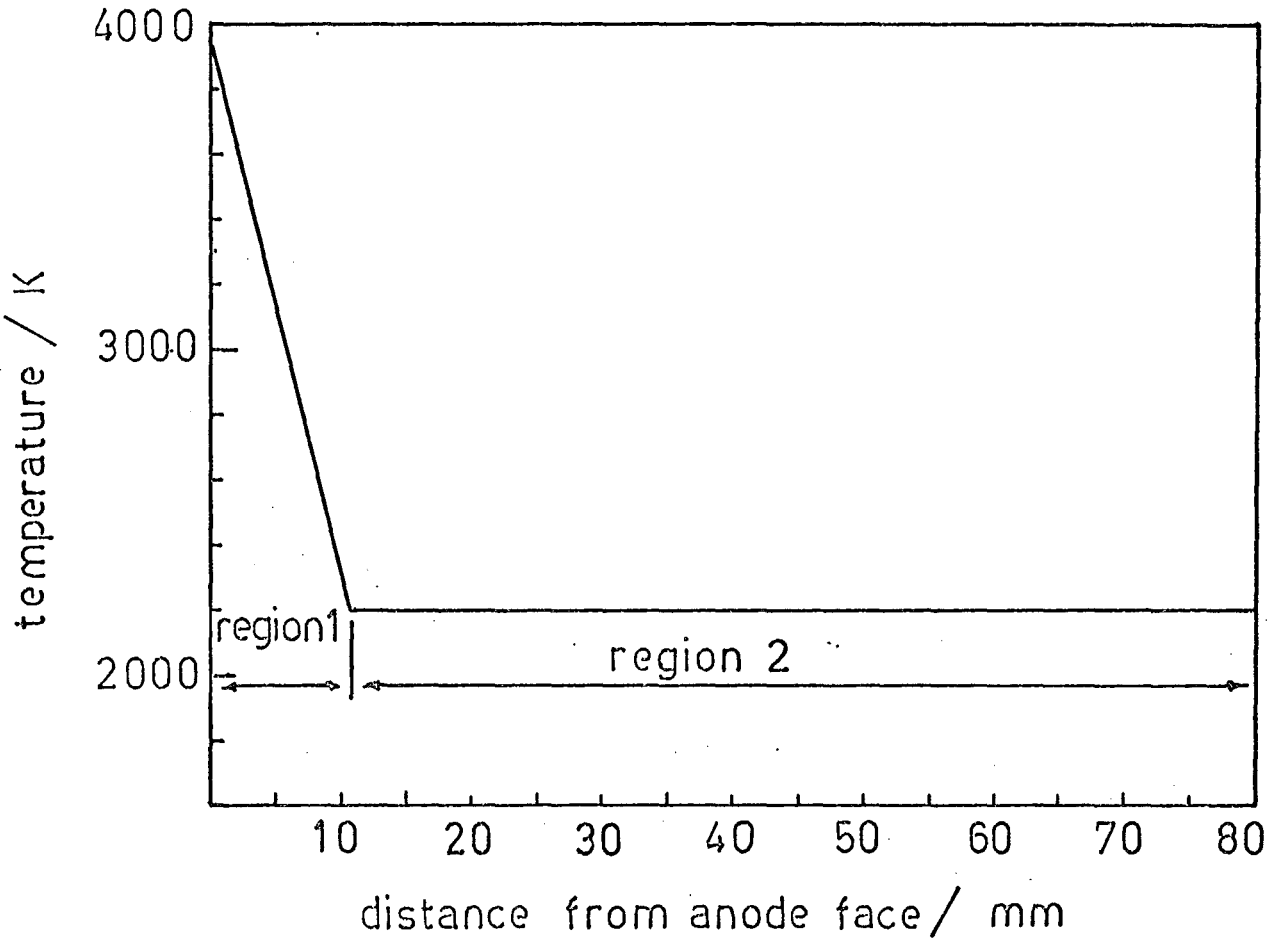

FIG. 19: SCHEMATIC REPRESENTATION OF TEMPEPATURE DISTRIBUTION IN AN ANODE FOR FREE AND FORCED CONVECTION

and,

ρ_g = density of surrounding gas

β = volumetric coefficient of thermal expansion

g = acceleration due to gravity

L = height of body

ΔT = difference in temperature between the body and surrounding gas

$\bar{h}_c$ = mean heat transfer coefficient

μ = viscosity of the surrounding fluid

c_{pg} = heat capacity of surrounding fluid

The physical properties are evaluated at the arithmetic mean temperature of the fluid and the body surface. Let us consider the following extreme situation in which the gas surrounding the anode is hydrogen at 0 K.

First of all region 1 (see Fig. 19):

$\bar{T}_a$ = 3075 K, $\therefore$ the mean temperature of the gas and anode surface

$$\bar{T}_g = \frac{(3075 + 0)}{2} = 1537.5 \text{ K.}$$

At 1537.5 K, the physical properties of hydrogen are:

		Source
ρ_g	= 0.016 kg m^{-3}	Ref. 16
β	= 3659 x 10^{-6}	Ref. 17
μ	= 247 x 10^{-7} kg m^{-1} s^{-1}	(Sutherland's formula)
C_{pg}	= 16.35 kJ kg^{-1}	Ref. 7
k	= 0.6 W m^{-1} K^{-1}	Ref. 18
L	= .01 m	

$$(Gr\ Pr) = \frac{C_{pg}\ \rho_g^2\ \beta\ g\ \Delta T\ L^3}{\mu k} \qquad A.3$$

and substituting the values of the physical properties of hydrogen at $\bar{T}_g$,

$$Gr = 3.17$$

So, $Nu = 0.555\ (Gr\ Pr)^{\frac{1}{4}}$

$\bar{h}_c$ = 44.5 W m^{-2} K^{-1}

In region 2, T_a = 2200 K, $\bar{T}_g$ = 1100 K. At 1100 K, the physical properties of hydrogen are:

		Source
ρ_g	= .0223 kg m^{-3}	Ref. 16
β	= 3659 x 10^{-6}	Ref. 17
μ	= 205 x 10^{-7} kg m^{-1} s^{-1}	Sutherland's formula
C_{pg}	= 15.257 kJ kg^{-1}	Ref. 7
k	= 0.51 W m^{-1} K^{-1}	Ref. 18
L	= .07 m	

$\bar{h}_c$ is calculated to be 27 W m^{-2} K^{-1}

The total power transferred away from the surface of a 7.94 mm diameter rod for the conditions shown in Fig. 19, is given by:

$$P_C = \bar{h}_c A \Delta T|_{\text{region 1}} + \bar{h}_c A \Delta T|_{\text{region 2}} \qquad \text{A.4}$$

$$= 34.1 + 103$$

$$= 137.1 \text{ Watts}$$

(A = surface area)

The radiation loss is given very approximately as:

$$P_R = A \varepsilon \sigma \bar{T}_a^4|_{\text{region 1}} + A \varepsilon \sigma T_a^4|_{\text{region 2}} \qquad \text{A.5}$$

$$= 1264 + 2300$$

$$= 3564 \text{ Watts}$$

It is clear that the rate of heat loss in free convection is very small in comparison to the radiation loss from the tip region (and so the total loss) and may be neglected.

2. Forced Convection

Evaluation of the heat transfer coefficient in forced convection requires the velocity of the fluid surrounding the anode. The circulation patterns in the arc chamber are not well established, though Wiles (19) has estimated the velocity of the gas sweeping past the anode in the region close to the anode tip at ~ 1 m/s. This figure was obtained from high speed movie films of the motion of very small particles of carbon entrained in the gas stream.

The heat transfer coefficient in forced convection for flow parallel to a tube is given by the expression (see Ref. 19):

$$\frac{\bar{h}_c}{k}\left(\frac{\mu_s}{\mu}\right)^{.14} = 1.86\left(\frac{DG}{\mu}\frac{C_p\mu}{k}\frac{D}{L}\right)^{1/3} \qquad \text{A.6}$$

where

μ_s = viscosity at surface

G = mass velocity

In this calculation we will take $\mu_w \simeq \mu$.

Taking an extreme case, it was shown that if convective loss from the anode surface was by free convection it could be neglected. A calculation for the case of forced convection, again using the extreme case of a cold surrounding gas gives a heat transfer coefficient an order of magnitude higher than for free convection, so it is prudent to examine this case more closely using more realistic values of the relevant parameters.

Ward (12) has presented enthalpy/composition data for the gases leaving the arc reactor, and these indicate that the temperature of the gases leaving the reactor lie between 1600 K and 3100 K. Let us assume that the temperature of the hydrogen surrounding the anode is 1600 K. Then for the tip region, calculating the physical properties at the temperature of the surrounding gas,

$$k_{1600} \doteqdot k_{1537.5} = 0.6 \text{ W m}^{-2}\text{K}^{-1}$$

$$C_{p1600} \doteqdot C_{p1537.5} = 16.35 \text{ kJ kg}^{-1}$$

$$\rho_{g1600} \doteqdot \rho_{g1537.5} = 0.016 \text{ kg m}^{-3}$$

$$u = 1 \text{ m s}^{-1}$$

$$G = .016 \times 1 = .016 \text{ kg m}^{-2}\text{s}^{-1}$$

$$L = .01 \text{ m}$$

Substituting into A.6 we find:

$$\bar{h}_c = 197 \text{ W m}^{-2} \text{ K}^{-1}$$

For region 2, L = .07m and $\bar{h}_c = 103 W m^{-2} K^{-1}$. It was considered that these values for convective heat transfer coefficients are sufficiently high to warrant an examination of the effect of convective heat loss from the anode on the ablation rate and anode temperature profile. This was done using a value of $h_c = 200 W m^{-2} K^{-1}$ and a gas temperature of 1600 K, and the results are discussed in sections 3.4.1 and 4.2.3.

APPENDIX II

The Runge-Kutta Method

In the solution of a first order equation, increments in the dependent variable are computed by the repeated application of prescribed formulae to the equation in question. Equations of a higher order are first reduced to an equivalent set of first order equations, which are then treated in a similar manner.

We can write:

$$\frac{dy}{dx} = f_1(x, y, z) \qquad \text{A.7}$$

$$\frac{dz}{dx} = f_2(x, y, z) \qquad \text{A.8}$$

Starting at x_0, y_0, z_0, the increments in y and z for the first increment in x are computed by the formulae:

$$k_1 = f_1(x_0, y_0, z_o)\,\Delta x \qquad \text{A.9}$$

$$k_2 = f_1\left(x_0 + \frac{\Delta x}{2}, y_0 + \frac{k_1}{2}, z_0 + \frac{\ell_1}{2}\right) \qquad \text{A.10}$$

$$k_3 = f_1\left(x_0 + \frac{\Delta x}{2}, y_0 + \frac{k_2}{2}, z_0 + \frac{\ell_2}{2}\right) \qquad \text{A.11}$$

$$k_4 = f_1(x_0 + \Delta x, y_0 + k_3, z_0 + \ell_3) \qquad \text{A.12}$$

$$\Delta y = \frac{1}{6}(k_1 + 2k_2 + 2k_3 + k_4) \qquad \text{A.13}$$

$$\ell_1 = f_2(x_0, y_0, z_0)\Delta x \qquad \text{A.14}$$

$$\ell_2 = f_2\left(x_0 + \frac{\Delta x}{2}, y_0 + \frac{k_1}{2}, z_0 + \frac{\ell_1}{2}\right) \qquad \text{A.15}$$

$$\ell_3 = f_2\left(x_0 + \frac{\Delta x}{2}, y_0 + \frac{k_2}{2}, z_0 + \frac{\ell_2}{2}\right. \qquad \text{A.16}$$

$$\ell_4 = f_2(x_0 + \Delta x, y_0 + k_3, z_0 + \ell_3) \qquad \text{A.17}$$

$$\Delta z = \frac{1}{6}(\ell_1 + 2\ell_2 + 2\ell_3 + \ell_4) \qquad \text{A.18}$$

The next increment is computed by replacing x_0, y_0, z_0, by x_1, y_1, z_1, in equations A.9 - A.18, and repeated application of the above formulae enables $y = \sum_{1}^{n} \Delta y_i$ to be found at $x = \sum_{1}^{n} \Delta x_i$.

In most of the computer runs for solving equation 8, Δx was varied in size on each iteration. In the majority of calculations (Δx), was made 0.1 mm with subsequent values calculated from the expression:

$$(\Delta x)_{i+1} = \frac{60x\ (\Delta x)_i}{-(\Delta T)_i} \qquad \text{A.19}$$

Equation A.19 gives values of $(\Delta T)_{i+1}$ approximately equal to 60 K. It was observed that choosing $(\Delta x)_{i+1}$ so that $(\Delta T)_{i+1} << 60$ K (using an expression of the form,

$$(\Delta x)_{i+1} = \frac{\text{Constant x } (\Delta x)_i}{-(\Delta T)_i} \qquad \text{A.20}$$

where constant << 60 K) had a negligible effect on the solutions obtained, even when $(\Delta T)_{i+1} \simeq 2$ K.

Values of $(\Delta x)_1 < 0.1$ mm had a negligible effect on solutions

No attempt was made to obtain solutions with $(\Delta x)_1 > 0.1$ mm o $(\Delta x)_{i+1}$ chosen so that $(\Delta T)_{i+1} > 60$ K.

APPENDIX III

Physical Properties of Graphite

III A. Comparison of Published Data

In solving equations 8 and 9, continuous functions were required to describe the temperature dependence of resistivity, thermal conductivity and heat capacity.

Resistivity

Bapat (20) and Bapat and Nickel (21) have measured the resistivity and thermal conductivity of different commercial graphites at temperatures up to 3500 K, and their results were compared with Union Carbide data which was available for temperatures up to 2200 K. Above ~ 1000 K it was observed that the data in refs. 6, 20 and 21 for electrical resistivity increased linearly with temperature. It is seen from Fig. 20 that the Union Carbide data (scaled from a value of 8×10^{-6} Ωm at 293 K) falls within the range covered by the data of Bapat and Nickel, so a linear extrapolation was confidently adopted. In order to cover temperatures from room temperature upwards, four other linear functions were fitted to a plot of the Union Carbide data (see Fig. 21).

Thermal Conductivity

Fig. 22 shows a plot of thermal conductivity vs. reciprocal temperature. The fit of a function of the form

$$k = \frac{\text{constant}}{T} + \text{constant} \qquad \text{A.21}$$

though not excellent, is good, and certainly adequate for this work.

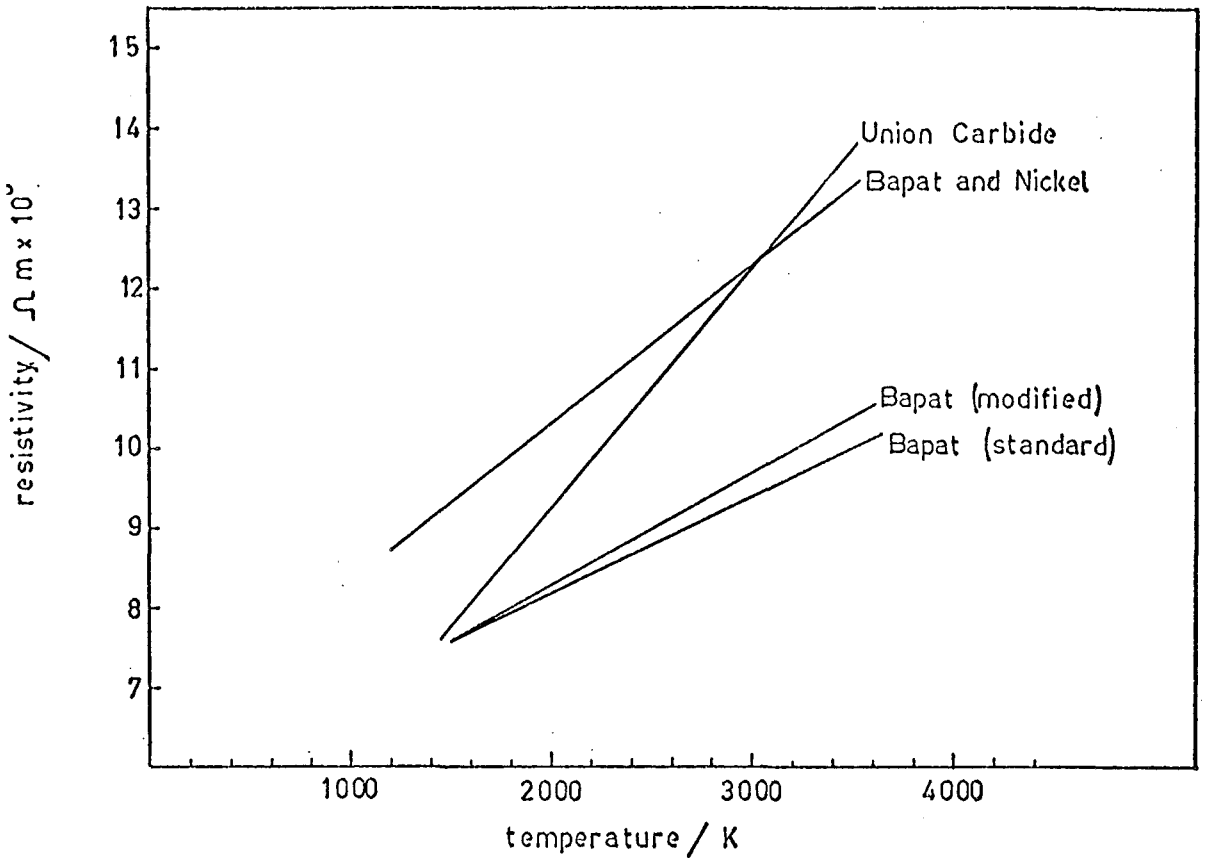

FIG. 20: COMPARISON OF PUBLISHED DATA ON ELECTRICAL RESISTIVITY OF GRAPHITE AT ELEVATED TEMPERATURES

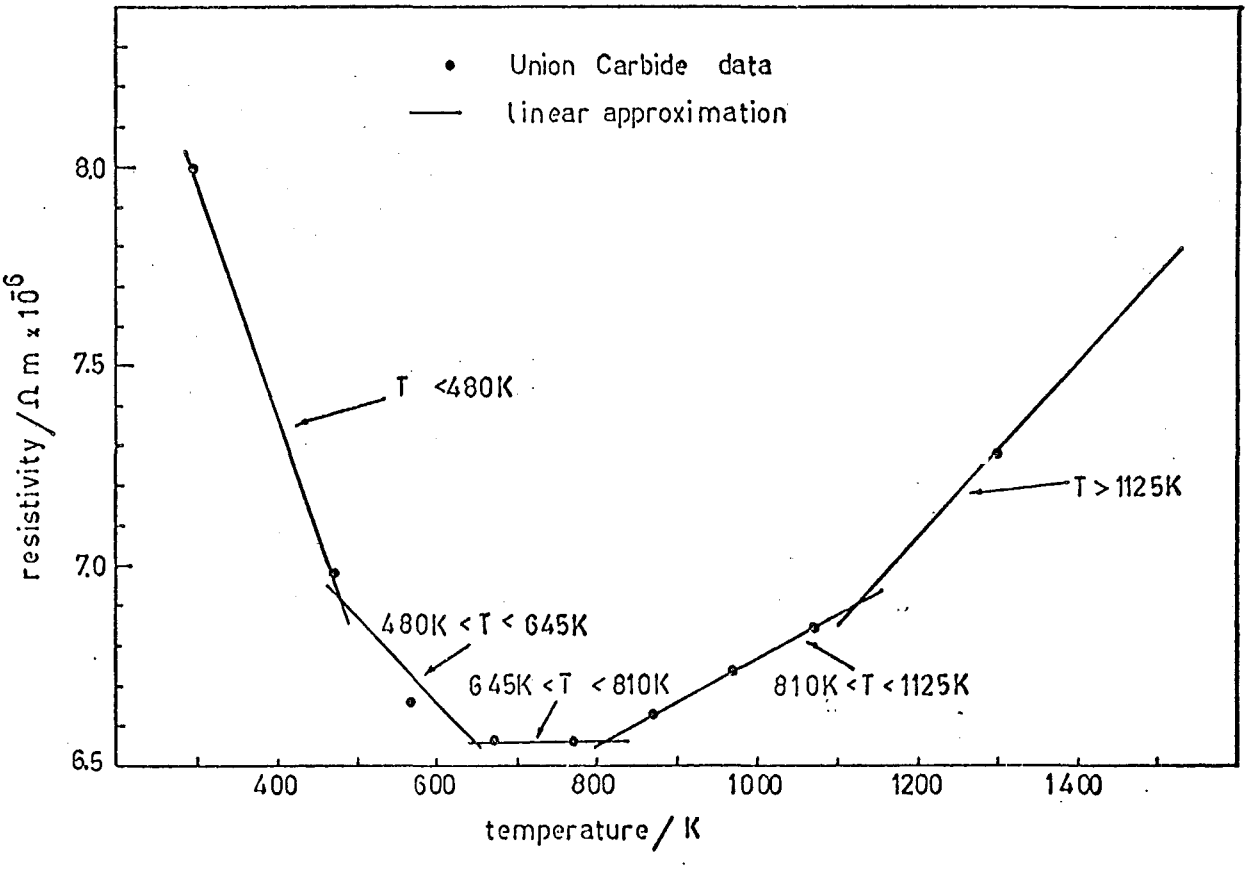

FIG. 21: TEMPERATURE DEPENDENCE TO ELECTRICAL RESISTIVITY OF GRAPHITE

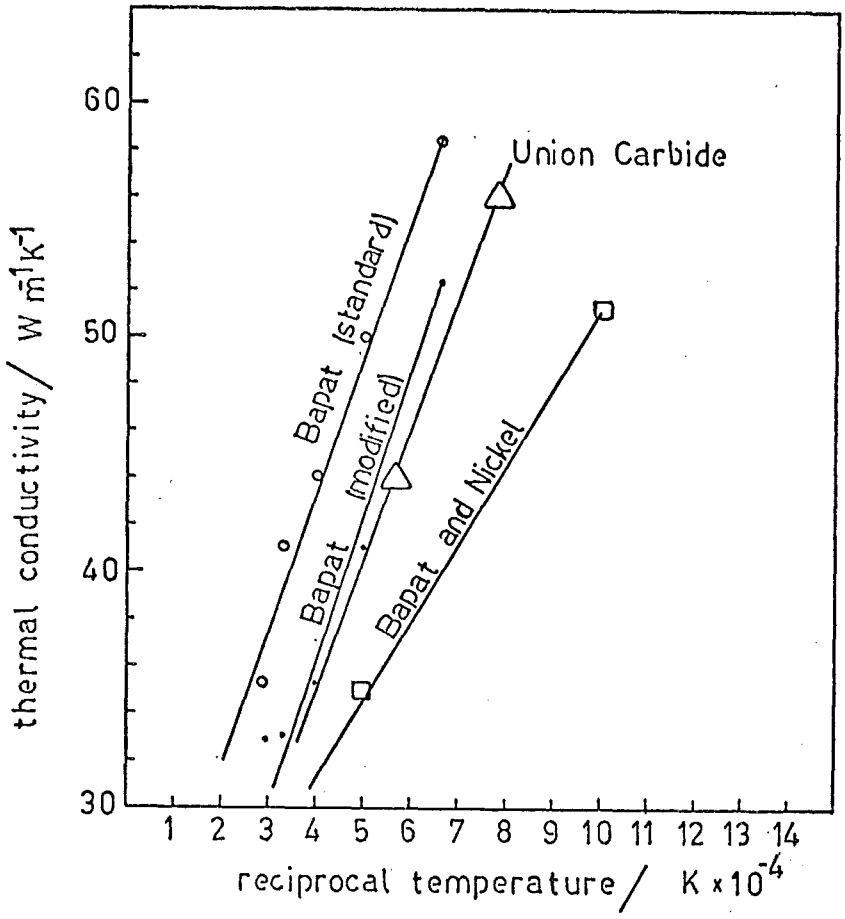

FIG. 22: COMPARISON OF PUBLISHED DATA ON THERMAL CONDUCTIVITY OF GRAPHITE AT ELEVATED TEMPERATURES

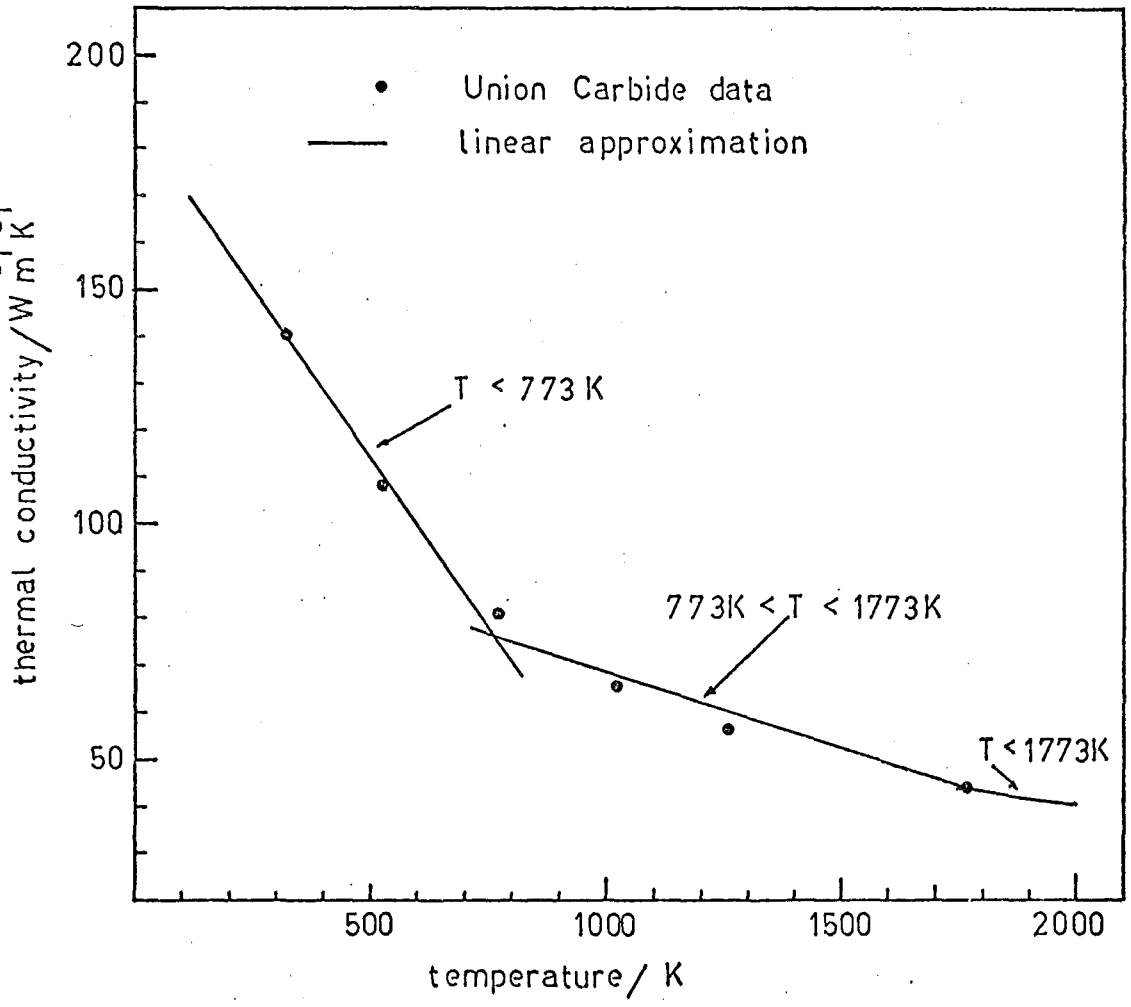

FIG. 23: THERMAL CONDUCTIVITY OF GRAPHITE AS FUNCTION OF TEMPERATURE

Fig. 22 also shows that the available Union Carbide data are within the same range as the results of Bapat (20) and Bapat and Nickel (21), so for T > 1773 K, an extrapolation of the form of equation A.21 was used. Conductivity below 1773 K was represented by two linear functions, (see Fig. 23).

Heat Capacity

Heat capacity data were taken from JANAF tables. Fig. 24 shows a plot of c_p vs. temperature. Three linear functions were selected to cover temperatures between 600 K and 4000 K.

Appendix IIIB.

Functions used for temperature dependence of physical properties of graphite.

1. Electrical Resistivity

$T < 480$ K; $\rho = 10^{-6} \times (-5.8289 \times 10^{-3} \times T + 9.70787)$ Ωm

$480 \text{ K} < T < 645$ K; $\rho = 10^{-6} \times (-2.1212 \times 10^{-3} \times T + 7.92818)$ Ωm

$645 \text{ K} < T < 810$ K; $\rho = 6.56 \times 10^{-6}$ Ωm

$810 \text{ K} < T < 1125$K; $\rho = 10^{-6} \times (1.07936 \times 10^{-3} \times T + 5.68571)$ Ωm

$1125 \text{ K} < T$; $\rho = 10^{-6} \times (2.256 \times 10^{-3} \times T + 4.349)$ Ωm

2. Thermal Conductivity

$T < 773$ K ; $k = (-0.1450 \times T + 188.14)$ W m^{-1} K^{-1}

$773 \text{ K} < T < 1773$ K; $k = (-0.031885 \times T + 100.647)$ W m^{-1} K^{-1}

$1773 \text{ K} < T$; $k = \left(\frac{54672.7}{T} + 13.28\right)$ W m^{-1} K^{-1}

3. Heat Capacity

$600 \text{ K} < T < 1100$ K; $C_p = (0.82128 \times T + 947.952)$ J kg^{-1} K^{-1}

$1100 \text{ K} < T < 1800$ K; $C_p = (0.2585292 \times T + 1566.9744)$ J kg^{-1} K^{-1}

$1800 \text{ K} < T$; $C_p = (0.0569328 \times T + 1929.66)$ J kg^{-1} K^{-1}

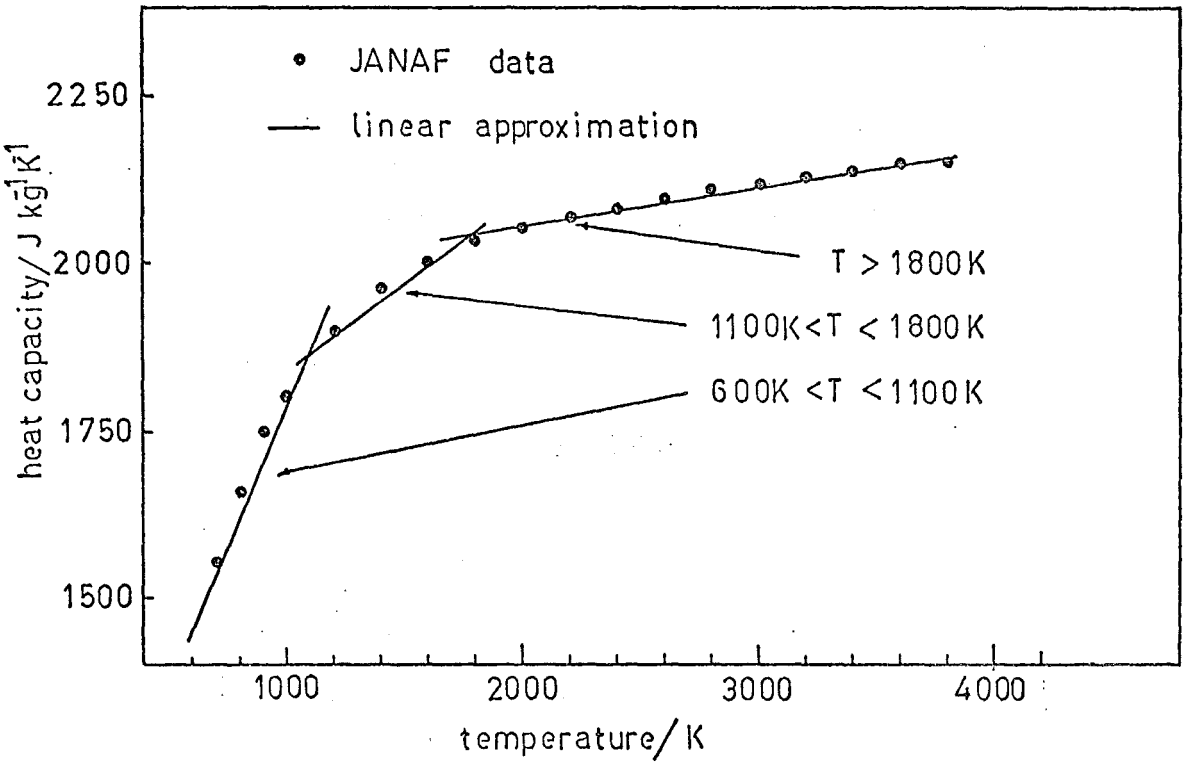

FIG. 24: HEAT CAPACITY OF GRAPHITE AS A FUNCTION OF TEMPEPATURE

APPENDIX IV

Data for figures used in text.

Table 1. Data for Fig. 3

Diameter mm	Current Amps	Current density Amps mm^{-2}	Ablation rate gm h^{-1} mm^{-2}
3.3	20	2.34	.81
3.3	30	3.51	3.19
3.3	40	4.68	5.58
3.3	50	5.85	7.95
7.94	200	4.04	5.18
7.94	220	4.43	6.0
7.94	240	4.85	6.83
7.94	260	5.25	7.64
7.94	280	5.65	8.47
7.94	300	6.06	9.31
9.53	140	1.96	1.1
9.53	160	2.24	1.67
9.53	180	2.52	2.24
9.53	200	2.80	2.80
9.53	220	3.08	3.38
9.53	240	3.36	3.95

E_a = 14 V; λ = 23.3 MJ kg^{-1}; T_b = 2000 K

Table 2: Data for Fig. 4, Fig. 5, Fig. 10 and Fig. 16

Current amps	Ablation Rate $g\ s^{-1}$	P_k W	$(SER)_c$ $kW\ hr\ kg^{-1}$	z_{pI} mm
100	0.2388	795	69.8	14.98
200	0.8938	980	37.3	12.22
300	1.55	1150	32.25	10.23
400	2.21	1335	30.2	-
500	2 89	1437	28.84	8.3
600	3.59	1500	27.86	6.78
800	5.1	1275	26.2	~4.00
1000	6.77	550	24.6	~1.40

D = 7.94 mm; E_a = 17 V; I_ℓ = 810 A; λ = 30 MJ kg^{-1}; T_b = 2000 K

Table 3: Model data for Fig. 6, Fig. 7 and Fig. 8

Diameter mm	Current A	Current Intensity $A\ mm^{-2}$	Ablation Rate $gm\ hr^{-1}\ mm^{-2}$	Ablation Rate $g\ hr^{-1}$
5.08	290	14.31	26.77	-
6.35	245	7.74	12.41	-
7.94	200	4.04	4.84	239.5
	220	4.43	5.63	278.8
	240	4.85	6.5	321.7
	260	5.25	7.35	363.9
	280	5.65	8.21	406.4
	300	6.06	9.08	449.6
9.53	140	1.96	0.528	37.7
	160	2.24	1.129	80.6
	180	2.52	1.73	123.1
	200	2.80	2.32	165.8
	220	3.08	2.92	208.5
	240	3.36	3.52	250.9

E_a = 10.87 V; λ = 23.3 MJ kg^{-1}; T_b = 2000 K.

Table 4: Experimental data for Fig. 6, Fig. 7, Fig. 8

Diameter mm	Current A	Current Density $A\ mm^{-2}$	Ablation Rate $gm\ h^{-1}\ mm^{-2}$	Ablation Rate $g\ h^{-1}$
5.08	290	14.31	28.63	-
6.35	245	7.74	13.36	-
7.94	233	4.69	5.8	287.9
"	233	4.69	6.24	309.8
"	233	4.69	5.42	269.0
"	235	4.73	6.11	303.3
"	237	4.77	5.98	296.8
"	237	4.77	6.17	306.3
"	237	4.77	6.75	335.1
"	241	4.85	6.31	313.2
"	241	4.85	7.08	351.5
"	241	4.85	6.17	306.3
"	249	5.02	7.16	355.4
"	249	5.02	7.03	349.0
"	249	5.02	6.45	320.2
"	259	5.22	7.37	365.8
"	259	5.22	7.44	369.3
"	261	5.26	7.74	384.2
"	261	5.26	7.5	372.3
"	261	5.26	8.49	421.4
"	266	5.35	6.27	339.0
"	266	5.35	6.83	311.2
"	277	5.58	7.82	388.2
"	277	5.58	7.98	396.1
"	277	5.58	7.91	392.6
"	286	5.76	8.17	405.6
"	286	5.76	8.37	415.5
"	287.5	5.79	8.29	411.5
"	289	5.82	8.45	419.5
"	290	5.84	7.82	388.2
"	290	5.84	7.91	392.6
"	290	5.84	7.57	375.7
9.53	140	1.88	1.29	95.83
"	141	1.89	1.34	99.55
"	143	1.91	1.38	102.5
"	157	2.11	1.38	102.5
"	167	2.25	1.48	109.9
"	167.5	2.25	1.57	116.3
"	170.5	2.30	1.51	112.2

Table 4 contd.

Diameter mm	Current A	Current Density A mm^{-2}	Ablation Rate gm h^{-1} mm^{-2}	Ablation Rate g h^{-1}
9.53	207	2.79	2.86	212.5
"	207	2.79	2.67	198.4
"	209	2.81	1.95	144.9
"	216	2.91	2.17	161.2
"	216	2.91	1.86	138.2
"	218	2.93	2.67	132.5
"	223	3.00	2.76	137.0
"	223	3.00	2.86	142.0
"	225	3.03	2.93	217.7
"	225	3.03	3.08	228.8
"	225	3.03	3.34	248.1
"	225	3.03	2.76	205.0
"	226	3.04	2.36	175.3
"	227	3.06	2.36	175.3
"	236	3.18	3.23	153.0
"	236	3.18	3.08	160.3
"	245	3.30	3.41	223.3
"	245	3.30	3.14	253.3

Table 5: Data for Fig. 11

Current A	Contact Temperature K	z_c mm
260	300	33.3
260	700	27.4
300	700	23.6
300	300	28.4
300	300	54.8

E_a = 10.87 V; λ = 23.3 MJ kg^{-1}; T_b = 2000 K

Table 6: Data for Fig. 12A

(i) Experiment

z / mm	Temperature / K
0.77	3950
1.15	3777
1.15	3887
1.25	3693
1.35	3920
1.54	3884
1.73	3758
1.83	3831
3.27	3481
3.27	3526
5.00	3184
5.58	3029
5.67	2837
5.96	2792
6.15	2767
7.12	2720
7.79	2561
8.08	2591
10.77	2265

D = 7.94 mm

I = 220 amps

(ii) Model 220 amps no convection

z / mm	Temperature / K
0.18	3825
0.38	3711
0.59	3597
0.83	3484
1.09	3371
2.12	3035
3.11	2815
4.14	2653
5.06	2548
6.27	2446
7.05	2397
7.99	2350
9.19	2304
10.76	2262
12.98	2223
16.5	2191
23.03	2165

D = 7.94 mm

E_a = 10.87 V

λ = 23.3 MJ kg^{-1}

T_b = 2000 K

$\dot{m}$ = 0.0775 kg s^{-1}

(iii) Model 220 amps with convection

z / mm	Temperature / K
0.19	3824
0.28	3766
0.58	3595
0.81	3481
1.06	3368
2.05	3032
3.29	2757
4.36	2596
5.32	2491
6.61	2390
7.45	2342
8.48	2295
9.81	2251
11.63	2212
14.4	2180
19.56	2166

$D = 7.94$ mm

$E_a = 10.87$ V

$\lambda = 23.3$ MJ kg^{-1}

$T_b = 2000$ K

$T_g = 1600$ K

$\bar{h}_c = 200$ W m^{-2} K^{-1}

$\dot{m} = 0.0765$ kg s^{-1}

(iv) Model small current, $\dot{m} = 0$

z / mm	Temperature / K
0.21	3839
0.45	3724
0.72	3611
0.85	3554
1.01	3497
2.12	3158
3.14	2934
4.12	2769
5.40	2605
6.50	2498
7.89	2393
8.74	2392
9.73	2291
10.90	2242
12.33	2194
14.12	2147
16.44	2103
19.60	2061
24.07	2017

$D = 7.94$ mm

$E_a = 10.87$ V

$\lambda = 23.3$ MJ kg^{-1}

$T_b = 2000$ K

$\dot{m} = 0$

The profile calculated for $\dot{m} = 0$ was found with I (estimated) at 70 amps. P_K is nearly constant at small currents at 735 Watts, (for $D = 7.94$ mm, $T_b = 2000$ K), and using this value, $I|_{\dot{m}=0} \doteqdot 89$ amps.

Table 7: Data for Fig. 13, Fig. 17, Fig. 18

Resistivity	Diameter	Limiting current	Current intensity	Ablation rate	$(SER)_c$
$\Omega m \times 10^{-6}$	mm	A	$A\ mm^{-2}$	$gm\ s^{-1}$	$kW\ h\ kg^{-1}$
8	3	282	39.9	0.182	25.8
	5	565	28.8	0.362	26.0
	10	1401	17.8	0.881	26.5
	25	4360	8.9	2.604	27.9
	40	7610	6.1	4.324	29.33
	50	9860	5.0	5.42	30.3
	60	12160	4.3	6.456	31.4
	70	14480	3.8	7.422	32.5
	80	16840	3.4	8.33	33.7
	90	19200	3.0	9.14	35.0
16	3	200	28.3	0.128	26.0
	5	400	20.4	0.253	26.4
	10	989	12.6	0.609	27.1
	25	3082	6.3	1.76	29.2
	40	5380	4.3	2.85	31.5
	50	6970	3.5	3.51	33.1
	60	8600	3.0	4.11	35.0
	70	10240	2.7	4.62	36.9
	80	11900	2.4	5.07	39.14
	90	13580	2.1	5.44	41.6
	150	23870	1.35	5.97	66.7
	200	32600	1.03	4.12	132.0
	250	41400	0.84	0.142	4872.0
24	3	163	23.1	0.103	26.2
	5	326.5	16.6	0.205	26.6
	10	809	10.3	0.49	27.5
	25	2515	5.1	1.387	30.22
	40	4395	3.5	2.204	33.25
	50	5690	2.9	2.667	35.6
	70	8360	2.2	3.384	41.2
	80	9720	1.9	3.63	44.64
	90	11090	1.7	3.795	48.8
	130	16670	1.25	3.65	76.1
	140	18070	1.2	3.4	88.6
	150	19490	1.1	3.08	106.0
	160	20900	1.0	2.66	121.0

Table 7 contd.

Resistivity	Diameter	Limiting current	Current intensity	Ablation rate	$(SER)_c$
50	3	113	16	0.103	26.2
	5	226	11.5	0.138	27.25
	10	561	7.1	0.327	28.6
	25	1745	3.6	0.879	33.1
	40	3045	2.42	1.313	38.7
	50	3940	2.00	1.512	43.43
	60	4860	1.7	1.641	49.4
	70	5790	1.5	1.689	57.1
	80	6730	1.3	1.657	67.7
	90	7680	1.2	1.545	82.8
100	3	80	11.3	0.0488	27.3
	5	160	8.15	0.0947	28.2
	10	395	5.0	0.217	30.33
	25	1235	2.5	0.543	37.9
	40	2150	1.71	0.723	49.6
	50	2790	1.42	0.754	61.7
	60	3440	1.2	0.704	81.4
	70	4100	1.1	0.575	119
	80	4760	.95	0.358	222
	90	5430	.85	0.0609	1485
200	3	56.5	8.0	0.0334	28.3
	5	113	5.75	0.0637	29.6
	10	280	3.6	0.141	33.1
	25	870	1.8	0.302	48.0
	30	1085	1.53	0.325	55.7
	40	1520	1.2	0.307	82.5
	50	1970	1.00	0.213	154.4
	55	2200	0.9	0.136	269
300	3	46	6.5	0.0264	29
	5	92	4.7	0.0498	30.78
	10	229	2.9	0.1076	35.5
	20	543	1.72	0.184	49.2
	25	712	1.45	0.198	59.9
	30	882	1.24	0.191	77.2
	35	1063	1.1	0.169	105
	40	1240	1.0	0.122	168.7
	45	1424	0.9	0.059	402

E_a = 10.87 V; λ = 23.3 MJ kg^{-1}; T_b = 2000 K

Table 8: Data* for Fig. 14 and Fig. 15

Resistivity $\Omega m \times 10^{-6}$	D* mm	I_ℓ* A	$\dot{m}_\ell$* $g\ s^{-1}$
16	140	780	0.2
24	120	1,165	0.34
50	70	2,780	0.77
100	50	6,000	1.65
200	32	15,300	4.1
300	27	21,400	6.0

E_a = 10.87 V; λ = 23.3 MJ kg^{-1}; T_b = 2000 K

* Obtained graphically from Fig. 13.

10. REFERENCES

1. Kratsch, K.M., Martinez, M.R., Clayton, F.I., Greene, R.B. and Wuerer, J.E., 1968: "Graphite Ablation in High Pressure Environments" paper presented to AIAA Entry Vehicle Systems and Technology Conference, Williamsburg Convention Centre, Williamsburg, Virginia, 3-5 December.
2. Riley, W.C., 1967: "Graphite, High Temperature Materials and Technology", John Wiley & Sons Inc.
3. Kreith, Frank, 1973: "Principles of Heat Transfer", third edition, Intext Educational Publishers, New York.
4. Abrahamson, J., 1970: Unpublished report, Department of Chemical Engineering, University of Canterbury, Christchurch, New Zealand.
5. Mickley, Harold S., Sherwood, Thomas K., and Reed, Charles E., 1957: "Applied Mathematics in Chemical Engineering", McGraw Hill Book Company Inc., p.198.
6. Anon: "Physical Properties of Carbon", query source, date, and "Variation of the physical properties of carbon and graphite with respect to temperature", query source, date. Xeroxed information supplied by Union Carbide New Zealand Ltd.
7. J.A.N.A.F.: Thermochemical tables, 1965, U.S. Department of Commerce.
8. Abrahamson, J., 1971, "The reactions of coal in a high intensity arc" Ph.D. thesis, University of Canterbury, Christchurch, New Zealand, Appendix 2.
9. Mentel, J., 1977: "The influence of vaporisation upon the roots of a high current arc. I. Different forms of vaporisation in the arc roots", Applied Physics, 14, pp269-276.
10. Cobine, James Dillon, 1958: "Gaseous Conductors", Dover Publications Inc., New York, p330.
11. Mason, R.C., 1937: "Probe measurements on high pressure arcs", Phys. Rev., 51, p.28.

12. Ward, R.A., 1974: "The Production of Acetylene in a High Intensity Arc" Ph.D. thesis, University of Canterbury, Christchurch, New Zealand.

13. Baddour, Raymond F., and Blanchet, Jean L., 1964: "Reactions of carbon vapour with hydrogen and with methane in a high intensity arc", I. and E.C. Proc. Des. Dev., 3, No. 3, p.258.

14. Baddour, Raymond F., and Iwasyk, John M., 1962: "Reactions between elemental carbon and hydrogen at temperatures above 2800 K", I. & E.C. Proc. Des. Dev., 1, No. 3, p.169.

15. Finkelnburg, Wolfgang, "The high current carbon arc", Fiat Final Report No. 1052, Field Information Agency Technical.

16. Spiers, H.M., editor, 1950: "Technical Data on Fuel", 5th edition, British National Committee, London.

17. Perry, John H., 1963, ed. "Chemical Engineer's Handbook", McGraw-Hill.

18. Krinberg, I.A., 1965: "Calculation of the thermal conductivity of some gases at temperatures of 1000 - 20,000 K at atmospheric pressure", trans. from Teplofizika Vysokikh Temperatur, 3, No. 4, pp654-657.

19. Wiles, P.G., Ph.D. student, Department of Chemical Engineering, University of Canterbury (private communication).

20. Bapat, S.G., 1973: "Thermal conductivity and electrical resistivity of two types of ATJ-S graphite to 3500 K", Carbon, 11, pp511-514.

21. Bapat, S.G. and Nickel, H., 1973: "Thermal conductivity and electrical resistivity of Poco grade AXF-Q1 graphite to 3300 K", Carbon, 11, pp323-327

SUPPLEMENT

In Part 1, section 3.5.2, it was noted that the ablation rate of carbon grade GA was higher than for graphite at the same current intensity. This is readily explained by the model derived in this report.

Carbon grade GA has a thermal conductivity 1/20 to 1/100 that of graphite and is four to seven times higher in electrical resistivity. These factors will cause P_K (see Fig. 1A, equation 2, and also equation 9) to be lower than for graphite for a specified anode face temperature, i.e. T_f, and as a result, ablation rate will be higher.

The above observations stand in further support of the model presented in this report.